

Editor: Nikos Hatzianastassiou

Received and published: 18 Jun 2020

Thank the Editor very much for handling the manuscript We take into account all the comments from referees and make revisions. Please check the responses to the referees and the revised manuscript.

Anonymous Referee #1

Received and published: 13 May 2020

We are very grateful for the referee's critical comments. The followings are our point-by-point responses to the comments. Our responses start with "R:".

General comments

This paper presents a method for estimating the radiative forcing due to light-absorbing particles (LAPs) in snow (RFLS) using several data sources, which include MODIS albedos, snow grain size derived from MODIS data, snow depth from the ERA-Interim reanalysis, surface downwelling solar radiation from CERES, and finally, in situ measurements of BC in snow (used for computing correction factors for the algorithm). The proposed approach allows the estimation of RFLS in larger areas than would be possible with in situ measurements alone. It thus provides an additional data source complementing estimates from in situ data and climate models. As noted in the introduction, there are previous studies that utilized MODIS to retrieve the radiative forcing of LAPs in snow, but this might be the first one to consider the spatial variability in RFLS between different regions. The approach is further employed to analyze the factors underlying the spatial variation of RFLS, finding that the variations in LAP content, snow depth and geographical factors (e.g., latitude) are more important than those in snow grain size (Fig. 7). Furthermore the retrieved values of RFLS are compared with results from a few climate models (Figs. 8 and 9) and with previous studies (Fig. 10).

A practical limitation of the proposed approach is that it can only be applied in regions with no/very short vegetation. Also, judging by the correction factors needed to eliminate systematic differences to RFLS derived from in situ data, it appears that the approach works fairly well in heavily polluted regions, but for regions with relatively clean snow, the uncertainties are very large (Fig. S2b). So if one interpretes

“hemispherescale” values (p. 6, line 17) as “hemisphere-mean” values, they cannot yet be obtained with this approach.

There is certainly enough new material in this work to be published in ACP. The paper is reasonable well written especially as regards the description of the approach, but I think there are disturbingly many numerical values in the text towards the end, and possibly some apples-to-oranges comparisons.

R: Thank you very much for the positive comments, which will encourage us to do more in-depth research in the future. Moreover, the referee’s comments are quite significant that can help us to improve the paper quality substantially. We have addressed all of the comments carefully according to the suggestions. Especially, we have extended the study period from January-February to December-May, so that the snow cover area over the Arctic can be retrieved. We have replaced the clear-sky radiative forcing with all-sky radiative forcing, which makes more sense to the research community. We have recalculated the broadband snow albedo with wavelengths of 300-2500 nm. We have revised misleading descriptions and reduce some numerical values throughout the manuscript according to the suggestions. All of the detailed responses can be seen as follow.

1. It is not justified to “sell” the values averaged over all ISCAs as the Northern Hemisphere (NH) mean values (e.g., p.2, lines 11-13, and p. 34, lines 6-7) since they really represent only a small part of the NH land area. The approach samples only areas with (nearly) full snow cover and no/very short vegetation, which naturally results in a high bias in the computed “NH average” RF. The assumption of clear-sky conditions further increases the RF values, while the analysis of only January and February data decreases the RF in the Arctic, but perhaps increases it at midlatitudes, compared to annual-mean values. In general, you should avoid listing numerical values without explaining what they really mean, especially in the abstract.

R: The referee's opinions are very valuable. We have replaced "Northern Hemisphere (NH) averaged radiative forcing" with "radiative forcing averaged over mapped snow-covered area in Northern Hemisphere" and revised the similar issues throughout the manuscript. Moreover, we have recalculated the all-sky radiative forcing to replace the clear-sky radiative forcing and extended the study period of only January and February to December to May. In addition, we have revised the abstract and main text carefully to avoid the values without certain explanation.

2. Specifically, the abstract should state that these are clear-sky values, that the albedo reduction refers to wavelengths 300-1300 nm, and the RF values refer to areas with full snow cover and little/no vegetation above snow.

R: We have recalculated the broadband snow albedo with wavelengths of 300-2500 nm under all-sky condition. We have stated the "estimated radiative forcing" as "...radiative forcing except for midlatitude mountains in December-May for the period 2003–2018...over mapped snow-covered area in Northern Hemisphere" in the abstract and throughout the manuscript.

3. p. 6, lines 14-16, Section 2.4, and Section 4.6: Taking only two CMIP6 models, and calling them "CMIP6" or "CMIP6 ensemble mean" is misleading, especially as the two models (CESM2 and CESM2-WACCM) are very closely related and produce nearly identical results (Fig. S4). It would be advantageous to use data from more CMIP6 models, if data from more models has now become available. If not, just take CESM2 and call it CESM2! In addition, instead of a "Global climate model", you should use the specific model name for Flanner et al. (2009), that is CAM3.1. Incidentally, it is a predecessor of the atmospheric and land components of CESM2.

R: Thanks very much for the explanations and suggestions. Actually, we have limited knowledge of climate models and the referee's comments help us improve the

understanding about CESM2 and CAM3.1. We have removed the comparison about CAM3.1 because it is the predecessor of the atmospheric and land module of CESM2 as the referee mentioned. We have carefully revised the improper description throughout the manuscript.

4. p. 7, line 6 and elsewhere: Why do you only use data for January and February? The reason for this should be stated explicitly. Perhaps because the midlatitude snow cover is most extensive then? However, this choice screens out almost all of the Arctic, due to the low sun angles, so that the “Arctic” RFLS values in this work in practice only represent southern Greenland. Also, considering spring months would increase the Arctic RFLS values substantially

R: The referee’s comments are quite significant. We have updated the data from January-February to December-May, so that the study period can include winter and spring, and snow-covered areas over the Arctic have been mapped.

5. p. 9. A brief description of the in situ BC measurements employed to correct the RFLS values should be included in Section 2 (at least, regions and references), perhaps between current Sections 2.2 and 2.3. Do these measurements represent BC or LAPs in general?

R: We have added more details about in-situ measurements in Sect. 2.3. These measurements are equivalent BC, which can represent the all light absorption by LAPs. We have added a detailed explanation for “equivalent BC” in p. 9, lines 17-21.

6. p. 9, lines 7–10: What was the reason for converting SWE to snow depth? To my knowledge, this has no effect on the results (in the end, SNICAR cares of SWE only).

R: Actually, SNICAR cares of SWE only. However, the offline SNICAR requires both snow depth and snow density as input, so that we converted SWE to snow depth with an assumed snow density. Anyhow, as your say, this has no effect on the results.

7. p. 9, Section 2.3. It should be stated how/why these emission data were used. I get the impression that they were used just as background information (not in estimating the RFLS).

R: Indeed, BC emission and deposition data were used just as background information. So that we have moved Figure 4a and 4b to the supplements (Figure S2a, b).

8. p. 11, lines 11-16: You describe how SBDART has several options for defining the atmospheric properties. It would be more important to tell what was assumed in the present calculations (also regarding aerosols).

R: We have added the description about the options for defining the atmospheric properties in SBDART. Details can be seen in p. 11, lines 3-7:

“In our study, the subarctic and midlatitude winter standard atmospheric condition is performed as well as the tropospheric and stratospheric background aerosols are archived in SBDART (Tanre, D. et al., 1990). According to Dang et al. (2017), the cloud optical depth in high-latitude and mid-latitude was assumed as 11 and 20 under cloudy-sky condition, respectively.”

9. p. 12, line 11: You could add snow grain shape to this list.

R: We note that SNICAR only assumes a spherical snow grain. We have added the description about snow grain shape as “...and spherical grain shape.” in p. 11, line 20.

10. p. 12, lines 20-21: “previous studies have tended to assume a semi-infinite snowpack”. This is a good point, and I think it would be worth showing how much this influences the results. Consider adding a figure which shows the ratio of RFLS computed using the actual (ERA-Interim) snow depth vs. RFLS computed using semi-infinite snow.

R: As the referee’s suggestion, we have added Figure 7 to show the ratio of RFLS computed using the actual (ERA-Interim) snow depth vs. RFLS computed using semi-infinite snow and taken a discussion about the influence of snow depth on radiative forcing retrieval in Sect. 4.4.

11. p. 13, line 20: add “...for clear-sky conditions” at the end of the sentence.

R: We have replaced clear-sky radiative forcing with all-sky radiative forcing throughout the manuscript.

12. p. 16, Eq. (7): Please state explicitly that the impact of LAPs on snow albedo computed in this work refers to the spectral range 300-1300 nm only. There is a chance of misinterpretation here, as usually people think of broadband albedo integrated over the entire downwelling solar spectrum at the surface. (An alternative would be to calculate “real” broadband albedo changes, integrated over 0.3–4 μm or at least 0.3–2.5 μm). This choice should not matter for RFLS, however.

R: Thanks for the referee's suggestion. We have recalculated the broadband albedo with wavelengths of 300-2500 nm.

13. In Eq. (2), diffuse and direct spectral solar radiation are added as such ($E_{dif}(\lambda; \phi) + E_{dir}(\lambda; \phi)$), suggesting that they both are defined wrt. a horizontal surface, but in Eq. (7) (and Eqs. (10) and (11)) the direct radiation is weighted by the cosine of local solar zenith angle ($E_{dir,\lambda} \cos \beta + E_{dif,\lambda}$), which implies that the direct radiation is defined wrt. a surface perpendicular to Sun's direction. This seems inconsistent.

R: We have revised this inconsistency throughout the manuscript.

14. p. 17, line 7: “we assumed that the properties for snow and LAPs remain invariable throughout the day”. In fact, if you keep the snow physical properties and LAP concentration constant, the impact of LAPs on snow albedo decreases with increasing solar zenith angle, so the use of $\Delta\alpha_{MODIS,corrected}^{LAPs}$ evaluated at noon probably overestimates the daily-average impact of LAPs somewhat. (I would guess, perhaps of the order of 10%, but this is something that you could check with SNICAR.)

R: We have corrected the overestimates by further simulating the daily-average snow albedo by changing the solar zenith angle from sunrise to sunset using SNICAR model and SBDART model. Revisions are added in p. 16, lines 11-16 and as follow:

“Following Miller et al. (2016), we assumed that the properties for snow and LAPs remain invariable throughout the day. Based on calculated $\alpha_{snow,\lambda}^{mdl}$ and $\alpha_{snow,\lambda}^{MODIS}$ at noon, the diurnal variation of pure and polluted snow albedo can be simulated by SNICAR from sunrise to sunset. Then, daily-average snow albedo reduction ($\Delta\alpha_{MODIS,daily}^{LAPs}$) can be derived by integrating the diurnal snow albedo reduction, which is weighted by simultaneous solar irradiance from SBDART.”

15. In Eq. (11), is $\cos \beta$ the daytime mean value?

R: We have new algorithm. $\cos \beta$ is calculated based on the certain latitude and solar zenith (solar azimuth) from sunrise to sunset.

16. p. 22, lines 16-17: You should remind the reader that this result refers specifically to the months of January and February. In spring and early summer, much of the Arctic is still snow-covered and solar radiation is much more abundant, so RFLS is substantially larger than in January-February.

R: We have updated the data from January-February to December-May, so that the study period can include winter and spring, and snow-covered areas over the Arctic have been mapped.

17. p. 22, line 20. “In situ observations of snow albedo reduction” actually refer to the albedo reduction calculated using in-situ observed LAPs. Here, it should be noted what was the measure of LAPs used in the in situ observations? Was it BC (excluding dust) or equivalent BC (implicitly also including dust). I guess in-situ observations usually yield the latter?

R: We have revised “in situ observations of snow albedo reduction” as “Albedo reduction calculated using in-situ observed LAPs ($\Delta\alpha_{in-situ,daily}^{LAPs}$)...” in p. 22, line 15. Also, we have added a statement that the measure of LAPs was equivalent BC in p. 9, lines 17-21.

18. p. 22, line 11. These corrections deserve a bit more discussion. The value $c_{polluted} = 1:1$ suggests that the approach works rather well for heavily polluted snow. However, the value $c_{clean} = 5:6$ for “relatively pure” snow, along with the scatter of points in Fig.

S2, suggests that the method becomes quite inaccurate then. Can you comment on the possible reasons for that? Perhaps the limiting factor is simply the accuracy of albedo calculations and observations, and a possible systematic bias between the two? For example, for 100 ng/g of BC (which many would already consider not so clean snow!) the albedo reduction is only ~ 0.02 . So, if in Eq. (7) $\alpha_{\text{snow};\lambda}$ mdl is biased high and/or $\alpha_{\text{snow};\lambda}$ MODIS is biased low, this would result in $c > 1$, the more so the cleaner the snow.

R: We have added a discussion about the uncertainty of the snow albedo reduction retrieval, which is negative correlated to snow pollution condition, to demonstrate the low correction value for heavily polluted snow but high correction value for relatively pure snow. We also discussed the influence of in-situ observation on the correction factor as suggested. Details can be seen in p. 27, lines 18-21 and p. 28, lines 1-18.

19. p. 23–26: I think the large number of numerical values in the text is disrupting to the reader. Some concrete suggestions would be: 1) for p. 23, lines 14-20 provide the MAE and RMS statistics in the figure panels in Fig. 5, 2) in Section 4.4., put the numerical values in a table. If you prefer to keep them in the text, you could at least skip the instantaneous RF values.

R: We have simplified the number of numerical values in the text for avoiding to disrupt the reader throughout the manuscript and put the MAE and RMSE statistics in Table S1 in supplements as suggestions. We have put the general statistics of snow albedo reduction and radiative forcing in Sect. 4.4 in Table 1 and we prefer to keep the values in different regions in the text in detail. Finally, we removed the discussion of instantaneous RF values in the text.

20. p. 28, line 10 – p. 29, line 7: As noted above, the model used by Flanner et al. (2009) should be called “CAM3.1” rather than “GCM”. More importantly, you discuss

springtime RF for Flanner et al. Did you compute springtime values for the MODIS retrievals too? This should be made clear in the text. Comparing January–February values with springtime (March–May?) values would be meaningless.

R: We have removed the comparison about CAM3.1 because it is the predecessor of the atmospheric and land module of CESM2 as the referee mentioned.

21. p. 31-32 and Fig. 10. The comparison with previous radiative forcing estimates is interesting, but one should be careful not to compare apples with oranges let alone watermelons – or at least be explicit about when this is being done. In other words, I think you should provide more information about the previous studies considered here. The RF differences could arise from the consideration of different regions, different seasons, clear-sky vs. all-sky forcing etc., so these details should be mentioned. This information would probably best fit in a table.

R: As the referee’s suggestions, we have added a table (Table 2) about the detailed information of the previous studies and revised the discussion about the possible sources of the RF differences. Details can be seen in Sect. 5.

22. p. 31, line 21 – p. 32, line 1: “Miller et al. (2016) reported a daily RFLS of < 4 W m⁻²”. Figure 10b (2nd panel) shows much larger values.

R: We have replaced Figure 10 with Table 2. We have rechecked the reference and revised as follow:

“...Miller et al. (2016) reported a daily RFLS of ~ 35 -86 (37-100) W m⁻² based on in-situ measurements (remote sensing) in the San Juan Mountains in May 2010.”

23. p. 32, line 7: Should this be Qian et al. (2014) or Qian et al. (2009) (cf. Fig 10c, second panel).

R: Thank you for pointing out the mistake, it should be “Qian et al. (2009)”. We have rechecked all data in section 5.

24. p. 32, lines 16-17: It is stated that Wang et al. (2014a) reported a northern hemisphere RFLS value of 0.45 W m^{-2} . However, so far I can tell, that paper is concerned with the direct radiative forcing due to BC in air (not snow). Furthermore, Fig. 10c refers to Wang et al. (2004), which is not present in the reference list.

R: Thank you for pointing out the mistake. “Wang et al. (2004)” should be “Wang et al. (2014a)”. In addition, Wang et al. (2014a) only reported the RF due to BC in air actually and has nothing to do with snow. We have removed it and rechecked all data in section 5.

25. p. 32, lines 15–21. I think your explanation is in principle correct, although at least the values of Bond et al. (2013) and Hansen and Nazarenko (2004) are annual-mean values, not January-February. But the fundamental point here is that your approach cannot provide northern-hemisphere (NH) mean values, which the cited studies attempt to provide, uncertainties notwithstanding. It can only provide values for ISCAAs that are snow-covered and without much vegetation. For true NH mean values, you should also include forested regions and regions without snow, and even oceans and sea ice, and also consider the impact of clouds. It is obvious that your reported NH values are larger than the actual NH mean forcing.

R: We have revised the description of our RF as “radiative forcing averaged over mapped snow-covered area in Northern Hemisphere” and added a table about the detailed information of the RF from previous studies to demonstrate the difference.

26. p. 34, lines 5–6. Referring to the previous comment, I would much prefer the formulation “for the Northern Hemisphere ISCA as a whole ...”.

R: According to your suggestion, we have revised “For the Northern Hemisphere as a whole ...” as “For the Northern Hemisphere ISCA as a whole ...”.

27. p. 35, lines 11–13. Climate models cannot incorporate remote sensing retrievals directly. They could however be used for model validation and to guide model development.

R: This sentence has been revised as “We propose that climate models validated by these refined remote sensing retrievals should be able to capture the RFLS more accurately, thereby providing more reliable estimates of the future impacts of global climate change.”

28. p. 62, caption of Fig. 7. It should be indicated whether the lower panel refers to instantaneous or daily radiative forcing.

R: We have revised Figure 7. The attribution refers to daily RF.

29. p. 63, Fig. 8: A couple of things to be checked: 1) Are the Flanner et al. results allsky or clear-sky values; 2) do the $RF_{MODIS,daily}$ values represent January-February (as in the rest of the paper) or spring? It would not be meaningful to compare Jan-Feb vs. March-May.

R: We have removed the comparison about CAM3.1 because it is the predecessor of the atmospheric and land module of CESM2 as the referee pointed out.

30. Fig. S5: It is inconsistent to compare springtime radiative forcing in (a) with radiative forcing based on CMIP6 (i.e., CESM2) soot content in snow in January-February in (b).

R: We have revised Figure S5. We have removed the comparison about CAM3.1 because it is the predecessor of the atmospheric and land module of CESM2 as the referee pointed out. When comparing with CESM2, the MODIS retrievals are the averages of December-May.

1. p. 4, lines 2-3: This sentence is cumbersome. Suggestion: “As a result, persistent uncertainties remain in regional and global-scale RFLS estimates based on field measurements.”

R: We have revised this sentence as suggestion.

2. p. 4, line 7: add “explaining” before “approximately one quarter of observed global warming”.

R: Added as suggestion.

3. p. 6, line 18: replace “valuable parameters” with “valuable information”. (The reason is explained in the specific comment #27).

R: Revised as suggestion.

4. p. 7, line 18: replace “generated by” with “derived from”.³

R: Revised as suggestion.

5. p. 8, line 4: replace “solar radiation” with “solar radiances”.

R: Revised as suggestion.

6. p. 11, lines 11-12: “standard aerosol types”?

R: Thank you pointed out the grammatically wrong sentence. We have Revised.

7. p. 12, line 4: “indicent radiation, surface spectral distribution”. Do you mean “incident radiation at the surface and its spectral distribution”?

R: Revised as suggestion.

8. p. 14, line 5: I think this should be “both of which are required to exceed 0.6”.

R: Revised as suggestion.

9. p. 18, lines 4-6: I think this sentence should be moved after Eq. (15): “The spatial variability in snow albedo due to ILAPs can be expressed as Eq:(15) where R_{eff} , SD and G indicate spatial-mean values of R_{eff} , SD, and G, with G requiring spatially constant values for the solar zenith angle, surface topography, and solar radiation parameters”.

R: Revised as suggestion.

10. p. 22, line 5: “respectably” should be “respectively”.

R: Revised.

11. p. 35, line 3: It is not clear what “synthetically” means here.

R: We want to express “relatively comprehensive and systematically”. If the referee still consider “synthetically” in unreadable we will revise it in next version.

12. Figure 1 (and also Fig. S1) would be easier to read if the values given on the colour bars would match with the values used to draw the curves. Now it is difficult to say which LAP content, snow depth etc. each curve exactly represents. Also, in the caption of Fig. 1, “angel” should be “angle”.

R: Revised as suggestion.

13. In Fig. 3, “savannas” should probably be “tundra”?

R: Revised and Figure 3b has been replotted.

14. In Fig. 6 and also Fig. S5, the interpretation of the box-plots should be explained.

R: The interpretation of the box-plots had been added in this version.

15. In Fig. S3b, “confindence level” should be “confidence level”.

R: Revised.

References

- Dang, C., Warren, S. G., Fu, Q., Doherty, S. J., Sturm, M., and Su, J.: Measurements of light-absorbing particles in snow across the Arctic, North America, and China: Effects on surface albedo, *J Geophys Res-Atmos*, 122, 10149-10168, 2017.
- Miller, S. D., Wang, F., Burgess, A. B., Skiles, S. M., Rogers, M., and Painter, T. H.: Satellite-Based Estimation of Temporally Resolved Dust Radiative Forcing in Snow Cover, *Journal of Hydrometeorology*, 17, 1999-2011, 2016.
- Qian, Y., Gustafson, W. I., Leung, L. R., and Ghan, S. J.: Effects of soot-induced snow albedo change on snowpack and hydrological cycle in western United States based on Weather Research and Forecasting chemistry and regional climate simulations, *Journal of Geophysical Research*, 114, 10.1029/2008jd011039, 2009.
- Tanré, D., Deroo, C., Duhaut, P., Herman, M., Morcrette, J. J., Perbos, J., and Deschamps, P. Y.: Technical note Description of a computer code to simulate the satellite signal in the solar spectrum: the 5S code, *International Journal of Remote Sensing*, 11, 659-668, 10.1080/01431169008955048, 1990.

Edward Bair (Referee)

nbair@eri.ucsb.edu

Received and published: 20 May 2020

We are very grateful for the referee's critical comments. The followings are our point-by-point responses to the comments. Our responses start with "R:".

Aside from the Data Statement section, the authors responded to my comments, but did not make changes to the manuscript addressing my suggestions in my Access Review. Given the preliminary nature of the Access Review, that's fine with me, but during this formal review stage I ask that my comments be addressed in the manuscript. I have provided a copy of the Access Review below.

R: We are really sorry for making no changes to the manuscript addressing your suggestions aside from the Data Statement section. We really appreciate the reviewer's comments, which can help us to improve the paper quality substantially and encourage us to do more in-depth research in the future. We have addressed all the comments very carefully in this section as detailed below.

Limitations:

In the manuscript, the authors have not addressed the problem of distinguishing between absorbers in the air and on the snowpack as stated by Warren (2013). Some of the regions examined have extensive air pollution. The MCD43C3 albedo product used relies on MOD09 surface reflectance which masks out snow when estimating aerosol optical thickness. Snow is difficult to mask, and the "dark and dense vegetation technique" used to estimate aerosol optical thickness (Vermote & Saleous, 2006) has shown errors over snow cover in the past that have supposedly been addressed (Vermote et al., 2002). However, one can still find errors. For example, MOD09 surface spectra sometimes show strong hook features over relatively clean fully-snow covered pixels in the visible wavelengths that are not present in the top of atmosphere

reflectances and can only be ascribed to problems with atmospheric correction. I'm not suggesting that the MCD43C3 product is unsuitable, rather I'd like to see its limitations over snow discussed in the manuscript. Saying that "more [sic] in-situ observations and hyperspectral imagery are needed." is not a sufficient response.

R: The referee's opinions are very valuable. Indeed, the absorbers in the air can disturb the retrieval of MODIS surface reflectance. According to the MODIS Surface Reflectance User's Guide (Collection 6, <https://modis.gsfc.nasa.gov/data/dataproduct/mod09.php>), the accuracy of the atmospheric correction is typically: $\pm(0.005 + 0.05 \times \text{reflectance})$ under conditions that AOD is less than 5.0 and solar zenith angle is less than 75° . Therefore, we estimate the uncertainty of calculated radiative forcing based on the level of accuracy of the atmospheric correction in our study. Details could be found in Section 4.5.

MYD10C1 does not use spectral unmixing; it uses the 2-band NDSI which shows high scatter when converted to fractional snow cover using Equation 5. Thus, the fractional snow cover filter used is an undiscussed bias in the approach, where LAP could be mistaken for non-snow objects and vice-versa.

R: The referee's opinions are very valuable. We have added an estimation and discussion on the uncertainty of calculated radiative forcing from the uncertainty of converting NDSI to fractional snow cover. According to (Rittger et al., 2013) and Riggs et al. (2016), the converted percentage error assumed in this study was 10%. Details could be found in Section 4.5.

Note that MODIS is a multispectral, not a hyperspectral sensor.

R: We have revised the mistake.

Exclusion of midlatitude mountains and other vast snow-covered areas in the Northern Hemisphere is substantial and should be stated in the Abstract. As Referee #1 and #2 both point out, the domain (non-vegetated & non-mountainous areas) and time periods

(Jan-Feb) are limited. These limitations undermine global application (e.g. p3 l1 & p6 l2).

R: We have added a statement for exclusion of midlatitude mountains in the Abstract and an explanation for why we exclude midlatitude mountains in the main text in p. 20, lines 7-11. We have extended the study period from January-February to December-May, so that the snow cover area over the Arctic can be retrieved. Also, we have replaced the clear-sky radiative forcing with all-sky radiative forcing, which makes more sense to the research community.

Further discuss limitations

Consider addressing the challenges in measuring LAP stated in Warren (2013) directly, such as distinguishing between absorbers in the air and those in the snowpack. Equation 5 when applied in the MOD10A1 product shows an RMSE of 0.227 and a positive bias of 0.11 (Rittger et al., 2013). These errors and biases are important because darker objects at visible wavelength in mixed snow-covered pixels (e.g. shadows and vegetation) can be misidentified as LAP.

R: As mentioned above, we have added estimations and discussions about the uncertainty of calculated radiative forcing from converting NDSI to fractional snow cover in Section 4.5.

Section 3.2.3

This basis for the snow grain size retrievals cites studies (Nolin & Dozier, 2000; Painter et al., 2013; Seidel et al., 2016) which use hyperspectral imagery at an more than order magnitude greater spatial and spectral resolution than a multispectral instrument like MODIS. The authors are relying on the albedo retrieval from a single MODIS band at $1.24\ \mu\text{m}$ to estimate grain size. This approach has high uncertainty due to errors in albedo retrievals from MODIS. In a previous study, Pu et al. (2019) state the MAE is $71\ \mu\text{m}$ or 3 times greater than in the studies cited above using hyperspectral instruments. The previous two comments suggest why substantial correction factors for the remotely-sensed measurements (Section 4.3) are needed.

R: The referee's opinions are very valuable. We have added an estimation and discussion about the uncertainty of calculated radiative forcing from snow grain size retrieval. The percentage error of snow grain size retrieval assumed in this study is 30% according to the study of Wang et al. (2017) and Pu et al. (2019). Based on the discussion of the uncertainties from atmospheric correction, snow cover fraction calculation and snow grain size retrieval, we further demonstrate the necessity of substantial correction factors for the remotely-sensed measurements and why the correction factor is different over relatively polluted snow and relatively clean snow. Details could be found in Section 4.5.

Section 4.1

The study area does not include most of the midlatitude mountains in the northern hemisphere. Snow and ice melt in these areas provides a valuable water resource to over 1B people worldwide (Barnett et al., 2005) and studies cited by the authors in the Introduction (Painter et al., 2012; Seidel et al., 2016) show this snow is heavily affected by LAP.

R: In this study, the MODIS surface albedo data used is MCD43C3, which has a resolution of $0.05^\circ \times 0.05^\circ$. Usually, the snow cover fraction over midlatitude mountains at such a coarse resolution is low, which cause that most of midlatitude mountains are not mapped as snow-covered area. In addition, midlatitude mountains are characterized as complex terrain, which will cause high biases in radiative forcing retrieval at a coarse resolution of $0.05^\circ \times 0.05^\circ$ in spite of topographic correction. Therefore, we didn't report the results over midlatitude mountains in this study. We have added an explanation why midlatitude mountains are not included in Section 4.1 in p. 20, lines 7-11. However, we agreed with the referee that the radiative forcing over midlatitude mountains are quite important, so that we will focus on these areas using finer resolution MODIS data (MCD43A3, MOD/MYD09) or data from high resolution satellites (e.g. Sentinel-2 and Landsat 8) in the future.

Data availability

No data statement is provided. Please see the ACP Data Policy which requires a statement of how the data can be accessed.

R: We have added more descriptions about the data access referring to the ACP Data Policy in Data availability.

References:

- E. Vermote. (2015). MOD09A1 MODIS Surface Reflectance 8-Day L3 Global 500m SIN Grid V006. NASA EOSDIS Land Processes DAAC. <http://doi.org/10.5067/MODIS/MOD09A1.006>
- Pu, W., Cui, J., Shi, T., Zhang, X., He, C., and Wang, X.: The remote sensing of radiative forcing by light-absorbing particles (LAPs) in seasonal snow over northeastern China, *Atmospheric Chemistry and Physics*, 19, 9949-9968, 10.5194/acp-19-9949-2019, 2019.
- Riggs G A, Hall D K, Román M O. MODIS snow products collection 6 user guide. National Snow and Ice Data Center: Boulder, CO, USA, 2016.
- Rittger, K., Painter, T. H., and Dozier, J.: Assessment of methods for mapping snow cover from MODIS, *Advances in Water Resources*, 51, 367-380, 10.1016/j.advwatres.2012.03.002, 2013.
- Wang, X., Pu, W., Ren, Y., Zhang, X., Zhang, X., Shi, J., Jin, H., Dai, M., and Chen, Q.: Observations and model simulations of snow albedo reduction in seasonal snow due to insoluble light-absorbing particles during 2014 Chinese survey, *Atmospheric Chemistry and Physics*, 17, 2279-2296, 10.5194/acp-17-2279-2017, 2017.

1 Satellite-based radiative forcing by light-absorbing particles in snow across the
2 Northern Hemisphere

3

4 Jiecan Cui¹, Tenglong Shi¹, Yue Zhou¹, Dongyou Wu¹, Xin Wang^{1, 2} and Wei Pu¹

5 ¹Key Laboratory for Semi-Arid Climate Change of the Ministry of Education, College

6 of Atmospheric Sciences, Lanzhou University, Lanzhou 730000, China

7 ²Institute of Surface-Earth System Science, Tianjin University, Tianjin 300072, China

8

9 Corresponding author: Wei Pu (puw09@lzu.edu.cn) ~~and Xin Wang (wxin@lzu.edu.cn)~~

10

Abstract. Snow is the most reflective natural surface on Earth and consequently plays an important role in Earth's climate. Light-absorbing particles (LAPs) deposited on the snow surface can effectively decrease snow albedo, resulting in positive radiative forcing. In this study, we used remote sensing data from NASA's Moderate Resolution Imaging Spectroradiometer (MODIS) and the Snow, Ice, and Aerosol Radiative (SNICAR) model to quantify the reduction in snow albedo due to LAPs, before validating and correcting the data against ~~in-in~~-situ observations. We then incorporated these corrected albedo-reduction data in the Santa Barbara DISORT Atmospheric Radiative Transfer (SBDART) model to estimate Northern Hemisphere radiative forcing except for midlatitude mountains in December-May~~in January and February~~ for the period 2003–2018. Our analysis reveals an average corrected reduction in snow albedo ($\Delta\alpha_{MODIS,corrected}^{LAPs}$) of ~ 0.021 under all-sky condition ~~~ 0.0246~~ , with ~~instantaneous radiative forcing ($RF_{MODIS,ins}^{LAPs}$) and~~ daily radiative forcing ($RF_{MODIS,daily}^{LAPs}$) values of $\sim 2.9 \text{ W m}^{-2}$, respectively, over mapped snow-covered area in Northern Hemisphere~~of ~ 5.9 and $\sim 1.7 \text{ W m}^{-2}$, respectively~~. We also observed significant spatial variations in $\Delta\alpha_{MODIS,corrected}^{LAPs}$ ~~, $RF_{MODIS,ins}^{LAPs}$~~ and $RF_{MODIS,daily}^{LAPs}$ ~~throughout the Northern Hemisphere~~, with the lowest respective values (~ 0.016 and ~ 2.6 ~~~ 0.0123 , $\sim 1.4 \text{ W m}^{-2}$, and $\sim 0.29 \text{ W m}^{-2}$~~) occurring in the Arctic and the highest (~ 0.11 and $\sim 12 \text{ W m}^{-2}$ ~~~ 0.1669 , $\sim 36 \text{ W m}^{-2}$, and $\sim 11 \text{ W m}^{-2}$~~) in northeastern China. From MODIS retrievals, we determined that the LAP content of snow accounts for 84% and 70%~~57.6% and 37.2%~~ of the spatial variability in ~~Northern Hemisphere~~-albedo reduction and radiative forcing, respectively. We also compared retrieved radiative forcing values with those of

earlier studies, including local-scale observations, remote-sensing retrievals, and model-based estimates. Ultimately, estimates of radiative forcing based on satellite-retrieved data are shown to represent true conditions on both regional and global scales.

1. Introduction

Seasonal snow cover affects 30% of Earth's land surface and exerts a cooling influence on global climate through its direct interaction with the surface ~~radiation~~radiances budget (Painter et al., 1998; Flanner et al., 2011). However, snow surface darkening due to light-absorbing particles (LAPs) such as black carbon (BC), organic carbon (OC), dust, and algae, can significantly alter the reflective properties of snow (Warren, 1982, 1984; Hadley and Kirchstetter, 2012). When deposited on the snow surface, LAPs increase the absorption of solar ~~radiation~~radiances (Painter et al., 2012a; Liou et al., 2014; Dang et al., 2017), thereby reducing the snow albedo (Warren and Brandt, 2008; Kaspari et al., 2014). As a result, radiative forcing of LAPs in snow (RFLS) plays a critical role in snow-cover decline on both regional and global scales (Warren and Wiscombe, 1980), perturbing the climate system and impacting hydrological cycles (Qian et al., 2011).

One of the primary LAPs, BC, is derived from the incomplete combustion of fossil fuels and biomass (Bond et al., 2013; Dang et al., 2015) and is second only to CO₂ in its contribution to climate forcing (Hansen and Nazarenko, 2004; Ramanathan and Carmichael, 2008; Bond et al., 2013). Yet, despite considerable efforts to measure the

1 BC content of Northern Hemisphere snow and ice (Doherty et al., 2010, 2014; Huang
2 et al., 2011; Ye et al., 2012; Wang et al., 2013b, 2017), the inherent challenges presented
3 by a temporospatially variable snow cover mean our understanding of LAPs in snow is
4 far from complete. As a result, persistent uncertainties remain in regional and global-
5 scale RFLS estimates based on field measurements~~As a result, RFLS estimate based on~~
6 ~~field measurements remains a persistent uncertainty in regional and global scale~~ (Zhao
7 et al., 2014).

8 Several previous investigations have utilized numerical models to estimate RFLS,
9 including that of Hansen and Nazarenko (2004), who concluded that BC in snow and
10 ice exerts a positive climate forcing throughout the Northern Hemisphere of $+0.3 \text{ W m}^{-2}$,
11 or explaining approximately one quarter of observed global warming. More recently,
12 Flanner et al. (2007) employed an aerosol/chemical-transport general-circulation model,
13 coupled with the Snow, Ice, and Aerosol Radiative (SNICAR) model (Flanner et al.,
14 2007; 2009), to estimate globally averaged radiative forcing values of $+0.054$ (range
15 $0.007\text{--}0.13$) and $+0.049$ ($0.007\text{--}0.12$) W m^{-2} for a strong (1998) and weak (2001) boreal
16 fire year, respectively. Using the Weather Research and Forecasting (WRF) model
17 (Skamarock et al., 2008) coupled with a chemistry component (Chem) (Grell et al.,
18 2005) and SNICAR modeling, Zhao et al. (2014) demonstrated that RFLS over northern
19 China in January–February ~~December–May~~ 2010 was $\sim 10 \text{ W m}^{-2}$. However, despite
20 their potentially valuable contribution, climate models contain significant uncertainties
21 in representations of LAP emissions, transport, deposition, and post-depositional

1 processes that can propagate into simulations of LAP concentrations and their climate
2 forcing (Qian et al., 2015; Lee et al., 2016). Zhao et al. (2014) also confirmed that,
3 relative to observational data, modeled LAPs and radiative forcing estimates exhibit
4 biases that are difficult to explain and quantify. These shortcomings underscore the need
5 for a refined approach to estimating real-time RFLS that minimizes the mismatch
6 between field observations and model simulations.

7 In addition to modeling, remote sensing has been used to assess the physical
8 characteristics of snow cover (Nolin and Dozier, 1993, 2000; Painter et al., 2009, 2012a,
9 2013; Miller et al., 2016). Nolin and Dozier (2000), for example, retrieved grain-size
10 data from satellite-derived reflectance at near-infrared (NIR) wavelengths, following
11 the rationale that snow-grain size, in conjunction with solar zenith angle, dictates the
12 path-length of penetrating photons (Wiscombe and Warren, 1980) and thus influences
13 albedo in the NIR. Similarly, recent studies have attempted to employ satellite-derived
14 snow albedo at visible (VIS) wavelengths to retrieve RFLS data (Seidel et al., 2016; Pu
15 et al., 2019). Briefly, this retrieval method exploits the imaginary component of the
16 complex refractive index for ice (K_{ice}), which is very low at VIS wavelengths and
17 results in the extremely high VIS albedo for pure snow. In contrast, the imaginary
18 component of the complex refractive index for LAPs (K_{LAPs}) at VIS wavelengths is
19 orders of magnitude greater, resulting in the reduction in VIS snow albedo (Wiscombe
20 and Warren, 1980). Moreover, albedo variability at VIS wavelengths is dominated by
21 even minor concentrations of LAPs (Brandt et al., 2011; Painter et al., 2012b).

1 Painter et al. (2012a) employed surface-reflectance data provided by NASA's Moderate
2 Resolution Imaging Spectroradiometer (MODIS) for the Upper Colorado River Basin
3 and Hindu Kush-Himalaya (HKH) to make the first quantitative, remote-sensing-based
4 retrievals of instantaneous surface radiative forcing (RF) due to LAPs. Relative to the
5 Western Energy Balance of Snow (WEBS) network (Painter et al., 2007), that study
6 established that MODIS-derived radiative forcing exhibits a positive bias at lower RF
7 values and a slightly negative bias at higher values. A more recent study by Seidel et al.
8 (2016) used remote sensing to constrain instantaneous melt-season RFLS values of 20–
9 200 W m⁻² for the Sierra Nevada and Rocky Mountains, while Pu et al. (2019) reported
10 MODIS-derived values of 22–65 W m⁻² for northern China in January–
11 February ~~December–May~~ (regional average ~45 W m⁻²). Acknowledging this
12 demonstrated efficacy of remote sensing retrievals for establishing RFLS on regional
13 scales, we note this approach has so far not captured spatial variability in RFLS on a
14 global scale.

15 In this study, we employed MODIS data to determine the reduction in Northern
16 Hemisphere snow albedo due to LAPs. Retrievals were validated and corrected
17 according to ground-based snow observations, after which spatial variability in albedo
18 reduction and radiative forcing over mapped snow-covered area in Northern
19 Hemisphere were assessed quantitatively. Finally, we compared our satellite-derived
20 radiative forcing values with the modeling results of ~~a Global Climate Model (GCM)~~
21 ~~(Flanner et al., 2009) and the Coupled Model Intercomparison Project Phase 6 (CMIP6)~~

CESM2 (Eyring et al., 2016; Danabasoglu et al., 2020). Despite the persistence of non-negligible uncertainties and biases, our satellite-based retrievals constitute the first hemisphere-scale assessment of RFLS and provide valuable information parameters for improving climate model simulations.

2. Data

2.1. Remote-sensing data

To investigate the impact of LAPs on snow albedo, we utilized the following MODIS data sets: surface albedo (MCD43C3; $0.05^\circ \times 0.05^\circ$ resolution), snow cover (MYD10C1; $0.05^\circ \times 0.05^\circ$ resolution), land cover type (MCD12C1; $0.05^\circ \times 0.05^\circ$ resolution), and atmospheric parameters (MYD08_D3; $1^\circ \times 1^\circ$ resolution). Each data set corresponds to ~~January–February~~December–May for the period 2003–2018 (<https://earthdata.nasa.gov>, last access: 20 January 2019). MCD43C3 is the daily combined MODIS output derived from both the Terra and Aqua satellites, and provides black-sky albedo (directional hemispherical reflectance, DHF) and white-sky albedo (bi-hemispherical reflectance, BHF) at local solar noon for bands 1–7 (band 1, 620–670 nm; band 2, 841–876 nm; band 3, 459–479 nm; band 4, 545–565 nm; band 5, 1230–1250 nm; band 6, 1628–1652 nm; band 7, 2105–2155 nm), as well as values for quality control, local noon solar zenith angle, and associated parameters. MCD43C3 observations are weighted to estimate albedo on the 9th day of each 16-day period and have been corrected for the influence of local slope and aspect, atmospheric gases, and

1 aerosols.

2 Snow-cover data are provided daily by MYD10C1 as a report of the snow-cover
3 fraction (SCF), ~~derived from~~generated by the Normalized Difference Snow Index
4 (NDSI). MCD12C1 provides a spatially aggregated and reprojected land-cover type,
5 which is derived from the supervised classification of MODIS reflectance data, while
6 MODIS MYD08_D3 reports values of solar azimuth angle.

7 Average-daily solar ~~radiation~~radiances ~~and cloud fraction were~~ was obtained from
8 NASA's Clouds and the Earth's Radiant Energy System (CERES:
9 <https://ceres.larc.nasa.gov>, last access: 12 April 2019), part of the Earth Observing
10 System comprising the Aqua, Terra, and S-NPP satellites. CERES provides
11 instantaneous measurements of solar ~~radiation~~radiances, which are then converted to
12 average-daily flux by angular dependence and empirical diurnal albedo modeling as the
13 satellite passes through the point of descent (Doelling et al., 2013; Su et al., 2015; Loeb
14 et al., 2018). We used the total downward shortwave flux and cloud fraction at the
15 surface, provided by the "CERES Single Scanner Footprint 1.08 (SSF1deg)" product,
16 to estimate average-daily RFLS under ~~clear~~all-sky conditions.

17 Shuttle Radar Topography Mission (SRTM) digital elevation data are provided by the
18 US Geological Survey (<https://www.usgs.gov/>, last access: 9 December 2018) to adjust
19 slope- and aspect-induced changes of surface solar ~~irradiation~~radiance in complex
20 terrain. The spatial resolution of SRTM data for the Northern Hemisphere is 30 m.

1

2 **2.2. Snow depth data**

3 Estimates of snow depth were obtained from the European Centre for Medium-Range
4 Weather Forecasts (ECMWF) Interim Re-Analysis (ERA-Interim)
5 (<https://www.ecmwf.int>, last access: 15 January 2019). ERA-Interim is a new
6 generation of reanalysis based on a 12-hourly and 4-dimensional variational data
7 assimilation (4D-Var) covering the period 1979–present. ERA-Interim performs better
8 in model physics frameworks, data quality control, and background error criteria than
9 previous versions (Berrisford et al., 2011; Brun et al., 2013). In this study, we used
10 snow-water equivalent (SWE) data for ~~January–February~~December–May covering the
11 period 2003–2018. These data were generated by forecast models and updated
12 according to a Cressman analysis of snow observations (Drusch et al., 2004; Dee et al.,
13 2011). We note that the previous occurrence of false snow-free patches, arising from
14 application of Cressman analysis in regions of sparse ground control, has been
15 mitigated by ECMWF upgrades (Dee et al., 2011). Finally, SWE is converted to snow
16 depth by assuming that average ~~January–February~~December–May snow density is ~~~200~~
17 300 kg m⁻³, consistent with snow-depth estimates by the Canadian Meteorological
18 Centre (CMC) (Sturm et al., 1995; Brown and Mote, 2009).

19 —

20 ~~2.3. BC emission and deposition data~~

21 ~~We used the PKU BC 2007 (EPKU: <http://inventory.pku.edu.cn>, last access: 5 June~~

2019) global inventory, with a spatial resolution of $0.1^{\circ} \times 0.1^{\circ}$, to obtain BC emissions data for the period 2003–2014. PKU-BC-2007 was developed using a bottom-up method based on sub-national fuel combustion data (Wang et al., 2013a, 2014b) and an updated set of BC emission factors (Wang et al., 2012). To constrain BC deposition fluxes during our study period, we applied the Modern Era Retrospective Analysis for Research and Applications, version 2 (MERRA-2: <https://gmao.gsfc.nasa.gov/reanalysis/MERRA-2/>, last access: 5 June 2019), which simulates BC via a radiatively coupled version of the Goddard Chemistry, Aerosol, Radiation, and Transport model (GOCART; Chin et al. 2002; Colarco et al. 2010). The efficacy of the GOCART aerosol module in simulating observable aerosol characteristics has been verified by a wealth of previous studies (e.g., Nowottnick et al. 2010, 2011; Bian et al. 2013; Randles et al., 2017).

2.3. In-situ measurements of LAPs in snow

To correct the satellite retrievals, we collected a comprehensive set of in-situ measurements of BC concentrations from the field campaigns in the Arctic in spring of 2005–2009 (Doherty et al., 2010), North America in January–March of 2013 (Doherty et al., 2014), Northern China in January–February of 2010, 2012 and 2014 (Ye et al., 2012; Wang et al., 2013; Wang et al., 2017). The BC concentrations are measured by the two-sphere integrating-sandwich (TSI) spectrophotometer in the Arctic, North America, and Northern China (Grenfell et al., 2011; Wang et al., 2020). Briefly, TSI produces a diffuse radiation field when the white light illumination is transmitted into

1 an integrating sphere; then the diffuse radiation passes through the filter and is detected
2 by a spectrometer. The TSI technique acquires the light attenuation spectrum due to the
3 LAPs loaded on the sample filter (Grenfell et al., 2011). Then, the light attenuation
4 spectrum of the sample filter is transformed into an equivalent BC mass (unit: g cm^{-2})
5 loading by comparing against the standard filters. The equivalent BC has been defined
6 by Doherty et al. (2010) which briefly as the amount of BC in the snow to account for
7 the wavelength-integrated total light absorption in the wavelengths of 300-750 nm by
8 all particulate constituents. In this study, we used BC_{equiv} for all LAPs to calculate the
9 in-situ snow albedo reduction and radiative forcing (Fig. S3).

10 **2.4. Climate model simulations**

11 We compared our remotely sensed retrievals of ~~snow BC~~ daily-average RFLS for the
12 2003–2014 study period with simulated ~~concentrations~~ results derived from ~~CMIP6~~
13 CESM2 (<https://esgf-node.llnl.gov/>, last access: 15 July 2019), ~~which coordinates the~~
14 ~~design and distribution of GCM simulations of past, present, and future climate. To date,~~
15 ~~only two CMIP participants, CESM2 and CESM2-WACCM, have provided simulations~~
16 ~~of snow BC concentrations. Therefore, In this study,~~ we employed simulations of snow
17 BC concentrations derived from the CESM2 data derived from the CESM2 and
18 ~~CESM2-WACCM~~ historical experiments, in conjunction with ERA-Interim SWE,
19 MODIS-retrieved snow grain-size, and CERES total downward shortwave flux data
20 under all-sky condition, to model daily-average RFLS for the study period. Simulations
21 were performed using the Snow, Ice, and Aerosol Radiative (SNICAR) and Santa

Barbara DISORT Atmospheric Radiative Transfer (SBDART) models, and the modeled output was compared ~~to-with~~ satellite-based retrievals. ~~We also compared our retrieval-based estimates of RFLS to values simulated by the SNICAR model coupled with a GCM (Flanner et al., 2007, 2009).~~

3. Methods

3.1. Radiative transfer model

In this study, we used the Santa Barbara DISORT Atmospheric Radiative Transfer (SBDART) model to calculate spectral surface solar irradiance. Constituting one of the most widely applied models for calculating the atmospheric radiative transfer at Earth's surface, under both clear- and cloudy-sky conditions (Ricchiazzi et al., 1998), SBDART combines a low-resolution atmospheric transmission model, Discrete Ordinate Radiative Transfer (DISORT) module, and Mie scattering output for the scattering of light by ice crystals and water droplets (Stamnes et al., 1988; Fu et al., 2017). Radiative transfer equations for a vertically inhomogeneous, non-isothermal, plane-parallel atmosphere are integrated numerically using the DISORT module. SBDART comprises multiple standard atmospheric profiles, cloud models, basic surface types, ~~standard types,~~ as well as vertical distribution models for aerosols and gas absorption, and enables users to specify these input parameters in real values. In our study, the subarctic and midlatitude winter standard atmospheric condition is performed as well as the tropospheric and stratospheric background aerosols are archived in SBDART (Tanre,

D. et al., 1990). According to Dang et al. (2017), the cloud optical depth in high-latitude and mid-latitude was assumed as 11 and 20 under cloudy-sky condition, respectively. The spectral irradiance from SBDART is only used for integrating the spectral MODIS albedo to achieve broadband albedo, thus the uncertainty of solar irradiance from the assumed atmospheric properties has limited influence on the retrieval of radiative forcing (see Section 3.2). we used SBDART to calculate the clear-sky spectral direct and diffuse solar radiation at local noon. Spectral radiation ranges from 0.3 to 1.3 μm , at 0.01 μm intervals, and with 1° latitude resolution. Average incident direct and diffuse solar spectra for ~~January–February~~December–May under clear/cloudy sky are shown in Fig. S1.

The Snow, Ice, and Aerosol Radiative (SNICAR) model is a two-stream multiple scattering radiative transfer model (Flanner et al., 2007, 2009) that has been used widely both to simulate the albedo, transmission, and vertical absorptivity of LAP-contaminated snowpack and to estimate RFLS (Painter et al., 2012a; Bryan et al., 2013; Miller et al., 2016). SNICAR employs the theory proposed by Wiscombe and Warren (1980) and Toon et al. (1989). Specifically, snow is considered to be composed of aggregated ice ~~spheres~~grains with optical effective radii (R_{eff}) of 50–1500 μm , and lognormal distribution, and spherical grain shape. SNICAR also accounts for the incident radiation at the surface and its spectral distribution~~incident radiation, surface spectral distribution~~, solar zenith angle, snow depth and density, snow layer number, and the type and concentration of LAPs in the snowpack. The model's ability to provide

realistic simulations of snow albedo has been verified by several previous studies (Hadley and Kirchstetter, 2012; Meinander et al., 2013; Zhong et al., 2017; Wang et al., 2017).

3.2. Retrieval of quantitative snow properties from remote sensing

The variability of spectral snow albedo depends on the LAP content, grain size, grain shape, and depth of the snowpack, in addition to solar zenith angle. ~~In this study, snow grain was assumed to be spherical according to SNICAR.~~ As shown in Fig. 1a, the deposition of BC (as representative of LAPs generally) serves to decrease the albedo of snow significantly, particularly in the ultraviolet (UV) and VIS wavelengths, which account for approximately half of all direct solar ~~irradiation~~radiance and the majority of diffuse solar ~~irradiation~~radiance (Fig. S1). In contrast, the impact of BC on albedo is considerably smaller in NIR wavelengths and can be negligible at $>\sim 1150$ ~~2500~~ nm. Snow depth plays a similar role to LAP content and primarily affects albedo in UV and VIS wavelengths (Fig. 1be).

Although snow albedo decreases with snow depth, previous studies have tended to assume a semi-infinite snowpack for which albedo is independent of depth. As a consequence, the role of LAPs in albedo reduction has been overestimated for those areas where the snowpack is thin (Warren, 2013). In this study, we incorporated ERA-Interim SWE data in our SNICAR model simulations to correct for the snow-depth overestimation effect. In contrast, snow grain-size and solar zenith angle influence the

snow albedo chiefly in NIR wavelengths (Fig. 1c, d). Specifically, albedo tends to decrease with increasing snow grain-size and declining solar zenith angle. In this study, we derived quantitative snow parameters (grain size, albedo reduction, and RFLS) from MODIS data in conjunction with the SNICAR and SBDART models. The specific workflow for retrieving RFLS from satellite data is shown in Fig. 2.

3.2.1. Retrieval of blue-sky albedo

MCD43 provides black-sky and white-sky albedo, which are defined as albedo in the absence of diffuse and direct component of solar irradiance. Accordingly, the actual spectral albedo for a land surface at wavelength λ (also called blue-sky albedo:

$\alpha_{MODIS,\lambda}^{blue-clear}$ under clear-sky condition can be calculated as follows:

$$\alpha_{MODIS,\lambda}^{blue-clear} = f_{dif,\lambda}^{clear} \cdot \alpha_{MODIS,\lambda}^{white-sky} + (1 - f_{dif,\lambda}^{clear}) \cdot \alpha_{MODIS,\lambda}^{black-sky} \quad (1)$$

where $\alpha_{MODIS,\lambda}^{white-sky}$ and $\alpha_{MODIS,\lambda}^{black-sky}$ are MODIS-derived values for white-sky and black-sky albedo, respectively, and $f_{dif,\lambda}^{clear}$ is the ratio of diffuse radiation to the total solar radiation under clear-sky (Lewis and Barnsley, 1994). The latter is calculated as follows:

$$f_{dif,\lambda}^{clear} = \frac{E_{dif}^{clear}(\lambda; \varphi)}{E_{dif}^{clear}(\lambda; \varphi) + E_{dir}^{clear}(\lambda; \varphi) \cdot \cos \theta} = \frac{E_{atf}(\lambda; \varphi)}{E_{atf}(\lambda; \varphi) + E_{atf}(\lambda; \varphi)} \quad (2)$$

where φ is latitude, and $E_{dif}^{clear}(\lambda; \varphi)$ and $E_{dir}^{clear}(\lambda; \varphi)$ denote diffuse and

direct spectral solar ~~radiation~~irradiance, respectively, derived from the SBDART model under clear-sky condition. β represents local solar zenith angle, which is obtained using the topographic correction method (Teillet et al., 1982; Negi and Kokhanovsky, 2011):

$$\cos \beta = \cos \theta_0 \cos \theta_T + \sin \theta_0 \sin \theta_T \cos(\phi_0 - \phi_T) \quad (3)$$

for which θ_0 represents the solar zenith angle for a horizontal surface, ϕ_0 is the solar azimuth angle, and θ_T and ϕ_T denote slope inclination and aspect, respectively.

Similarly, we can derive the blue-sky albedo for cloudy-sky condition ($\alpha_{MODIS,\lambda}^{blue-cloudy}$).

Then, we used cloud fraction (f_{cloud}) from CERES to weight clear-sky albedo and cloudy-sky albedo to obtain actual all-sky albedo ($\alpha_{MODIS,\lambda}^{all}$):

$$\alpha_{MODIS,\lambda}^{all} = f_{cloud} \cdot \alpha_{MODIS,\lambda}^{blue-cloudy} + (1 - f_{cloud}) \cdot \alpha_{MODIS,\lambda}^{blue-clear} \quad (4)$$

3.2.2. Retrieval of snow cover and albedo values

As shown in Fig. 2, the snow-covered area is mapped according to the actual all-sky~~blue-sky~~ albedo ($\alpha_{MODIS,\lambda}^{all}$ ~~$\alpha_{MODIS,\lambda}^{blue-sky}$~~) in band 4 (band center ~555 nm: $\alpha_{blue-sky,\lambda}(\lambda_{VIS})$) and the Normalized Difference Snow Index (NDSI), both of which are required to exceed 0.6 (Negi and Kokhanovsky, 2011).~~NDSI is calculated as follows (Dozier and Marks, 1987; Hall et al., 1995):~~

$$1 \quad \text{NDSI} = \frac{\alpha_{\text{blue-sky},\lambda}(\lambda_{\text{VIS}}) - \alpha_{\text{blue-sky},\lambda}(\lambda_{\text{SWIR}})}{\alpha_{\text{blue-sky},\lambda}(\lambda_{\text{VIS}}) + \alpha_{\text{blue-sky},\lambda}(\lambda_{\text{SWIR}})} \quad (3)$$

2 where $\alpha_{\text{blue-sky},\lambda}(\lambda_{\text{SWIR}})$ is $\alpha_{\text{blue-sky},\lambda}$ in band 6 (band center 1640 nm).

3 According to the MODIS Snow Products Collection 6 User Guide
4 (<http://nsidc.org/data>), the Fractional Snow Cover (FSC) can be calculated as follows:

$$5 \quad FSC = -0.01 + 1.45 \cdot \text{NDSI} \quad (45)$$

6 Accordingly, the identified snow-covered area (ISCA) has an FSC value of >86% but
7 not always 100%. Therefore, the MODIS-derived albedo for a particular ISCA is a
8 combination of values representing both snow and the snow-free underlying surface.

9 Following Pu et al. (2019), the snow albedo ($\alpha_{\text{snow},\lambda}^{\text{MODISall}}$) can be distinguished from the
10 mixed albedo by the equation:

$$\begin{aligned} 11 \quad & \alpha_{\text{snow},\lambda}^{\text{all}} \alpha_{\text{MODIS},\lambda}^{\text{all}} \alpha_{\text{blue-sky},\lambda} \\ 12 \quad & = \frac{E_{\text{all-sky},\lambda} E_{\text{A}} \cdot FSC \cdot \alpha_{\text{snow},\lambda}^{\text{all}} \alpha_{\text{snow},\lambda}^{\text{MODISall}} + E_{\text{all-sky},\lambda} E_{\text{A}} \cdot (1 - FSC) \cdot \alpha_{\text{underlying},\lambda}}{E_{\text{all-sky},\lambda} E_{\text{A}}} \\ 13 \quad & = FSC \cdot \alpha_{\text{snow},\lambda}^{\text{all}} \alpha_{\text{MODIS},\lambda}^{\text{MODISall}} + (1 - FSC) \cdot \alpha_{\text{underlying},\lambda} \\ 14 \quad & (56) \end{aligned}$$

$$\begin{aligned} 15 \quad & \alpha_{\text{snow},\lambda}^{\text{all}} \alpha_{\text{snow},\lambda}^{\text{MODIS}} = \frac{\alpha_{\text{MODIS},\lambda}^{\text{all}} \alpha_{\text{blue-sky},\lambda} - (1 - FSC) \cdot \alpha_{\text{underlying},\lambda}}{FSC} \\ 16 \quad & \text{---} (67) \end{aligned}$$

17 where $E_{\text{all-sky},\lambda} E_{\text{A}}$ is total solar radiation irradiance under all-sky condition, a linear
18 combination of direct/diffuse competent of solar irradiance irradiation under clear-sky
19 and cloudy-sky using similar strategy via Eq. (1)-(4). $\alpha_{\text{underlying},\lambda}$ represents the

albedo of the underlying surface and was obtained from Siegmund and Menz (2005).

As depicted in Fig. 3b, vegetation and bare soil are the main types of underlying surface in the ISCA.

3.2.3. Retrieval of snow grain size

The snow optical-equivalent grain size (R_{eff}) is retrieved by fitting SNICAR-simulated snow albedo to MODIS-derived snow albedo at 1240 nm (the central wavelength of MODIS band 5), following the protocol of Nolin and Dozier (2000). This retrieval method is not influenced by liquid water and water vapor and has been employed widely in previous studies (e.g., Painter et al., 2013; Seidel et al, 2016). Both Nolin and Dozier (2000) and Pu et al. (2019) reported that the retrieved R_{eff} compares favorably with ground-based measurements of snow grain size. In this study, we chose to exclude the ISCA, where MODIS-derived snow albedo at 1240 nm is <0.3 , to avoid misrepresenting R_{eff} (Tedesco et al., 2007).

3.2.4. Retrieval of snow albedo reduction and RFLS

The ~~instantaneous~~, spectrally integrated reduction in snow albedo due to LAPs ($\Delta\alpha_{MODIS,insnoon}^{LAPs}$) is estimated for local-noon and ~~clearall~~-sky conditions, using solar ~~radiation~~irradiance—and the difference between MODIS-derived spectral snow albedo ($\alpha_{snow,\lambda}^{MODISall}$) and simulated pure snow albedo ($\alpha_{snow,\lambda}^{mdl}$). Because MODIS provides only

four VIS bands, we fitted snow albedo data obtained via MODIS to a continuous 300–
~~1300–2500~~ nm spectrum ($\alpha_{snow,\lambda}^{MODIS}$ with a 10 nm interval) following the method provided
 by Pu et al. (2019). Thereafter, the broadband albedo reduction due to LAPs retrieved
 from MODIS ($\Delta\alpha_{MODIS,noon}^{LAPs}$) $\Delta\alpha_{MODIS,ins}^{LAPs}$ can be calculated as follows:

$$\Delta\alpha_{MODIS,noon}^{LAPs} = \frac{\sum_{\lambda=300nm}^{\lambda=2500nm} (\alpha_{snow,\lambda}^{mdl} - \alpha_{snow,\lambda}^{MODIS}) \cdot E_{all-sky,\lambda} \cdot \Delta\lambda}{\sum_{\lambda=300nm}^{\lambda=2500nm} E_{all-sky,\lambda} \cdot \Delta\lambda} \quad (8)$$

$$\Delta\alpha_{MODIS,ins}^{LAPs} = \frac{\sum_{\lambda=300nm}^{\lambda=1300nm} (\alpha_{snow,\lambda}^{mdl} - \alpha_{snow,\lambda}^{MODIS}) \cdot (E_{atm,\lambda} \cdot \cos\beta + E_{atf,\lambda}) \cdot \Delta\lambda}{\sum_{\lambda=300nm}^{\lambda=1300nm} (E_{atm,\lambda} \cdot \cos\beta + E_{atf,\lambda}) \cdot \Delta\lambda} \quad (7)$$

where $\alpha_{snow,\lambda}^{mdl}$ is the pure snow albedo simulated by SNICAR using MODIS-derived
 R_{eff} and ERA-Interim snow depth data, $\alpha_{snow,\lambda}^{MODIS}$ is the continuous snow albedo
 derived from MODIS retrievals, and $\Delta\lambda$ is 10 nm. ~~Finally, β represents local solar
 zenith angle, which is obtained using the topographic correction method (Teillet et al.,
 1982; Negi and Kokhanovsky, 2011):~~

$$\cos\beta = \cos\theta_g \cos\theta_T + \sin\theta_g \sin\theta_T \cos(\phi_g - \phi_T) \quad (8)$$

~~for which θ_g represents the solar zenith angle for a horizontal surface, ϕ_g is the solar
 azimuth angle, and θ_T and ϕ_T denote slope inclination and aspect, respectively.~~

Following Miller et al. (2016), we assumed that the properties for snow and LAPs
 remain invariable throughout the day. Based on calculated $\alpha_{snow,\lambda}^{mdl}$ and $\alpha_{snow,\lambda}^{MODIS}$ at
 noon, the diurnal variation of pure and polluted snow albedo can be simulated by
 SNICAR from sunrise to sunset. Then, daily-average snow albedo reduction
 ($\Delta\alpha_{MODIS,daily}^{LAPs}$) can be derived by integrating the diurnal snow albedo reduction, which
 is weighted by simultaneous solar irradiance from SBDART. Similarly, we used

measurements of LAPs in contaminated snow to calculate the ~~instantaneous,~~
~~in-situ~~ reduction in snow albedo ($\Delta\alpha_{in-situ,insdaily}^{LAPs}$). To derive a correction factor for
MODIS retrievals, we applied a similar validation strategy to that of Zhu et al. (2017):

$$c = \frac{1}{n} \sum_{i=1}^n \left(\frac{\Delta\alpha_{MODIS,insdaily}^{LAPs}}{\Delta\alpha_{in-situ,dailyins}^{LAPs}} \right) \quad (9)$$

where c is the correction factor for $\Delta\alpha_{MODIS,dailyins}^{LAPs}$ and n is the number of the
respective ~~in-situ~~ measurements. Accordingly, the corrected albedo reduction
($\Delta\alpha_{MODIS,corrected}^{LAPs}$) is calculated as follows:

$$\Delta\alpha_{MODIS,corrected}^{LAPs} = \frac{1}{c} \cdot \Delta\alpha_{MODIS,dailyins}^{LAPs} \quad (10)$$

3.2.5. Retrieval of RFLS

The ~~daily-average~~~~instantaneous~~, spectrally integrated RFLS ($RF_{MODIS,insdaily}^{LAPs}$) is
calculated for ~~noon and clear~~all-sky conditions as follows:

$$RF_{MODIS,daily}^{LAPs} = \Delta\alpha_{MODIS,corrected}^{LAPs} \cdot SW_{all-sky} \quad (11)$$

$$RF_{MODIS,ins}^{LAPs} = \Delta\alpha_{MODIS,corrected}^{LAPs} \cdot \sum_{\lambda=300nm}^{\lambda=1300nm} (E_{air,\lambda} \cdot \cos\beta + E_{diff,\lambda}) \cdot \Delta\lambda \quad (11)$$

~~We assumed that the properties for snow and LAPs remain invariable throughout the
day and that the average daily RFLS ($RF_{MODIS,daily}^{LAPs}$) can be expressed as follows:~~

$$RF_{MODIS,daily}^{LAPs} = \Delta\alpha_{MODIS,corrected}^{LAPs} \cdot (SW_{air} \cdot \cos\beta + SW_{diff}) \quad (12)$$

where $SW_{dirall-sky}$ and SW_{diff} represent the average-daily ~~direct and diffuse~~total

downward shortwave fluxes, ~~respectively~~, obtained from CERES under ~~clearall~~-sky conditions.

3.2.56. Attribution of spatial variability in snow albedo reductions and radiative forcing

As demonstrated above, reductions in snow albedo and RFLS are dependent primarily on LAP content, R_{eff} , snow depth (SD), solar zenith angle, surface topography, and solar ~~radiation~~irradiance, the latter three of which can be categorized as the geographic factor (G). We used an impurity index (I_{LAPs}) to represent the LAP content of the snowpack (Di Mauro et al., 2015; Pu et al., 2019), following the equation:

$$I_{LAPs} = \frac{\ln(\alpha_{snow,band4}^{MODISall})}{\ln(\alpha_{snow,band5}^{MODISall})} \quad (4312)$$

where $\alpha_{snow,band4}^{MODISall}$ and $\alpha_{snow,band5}^{MODISall}$ are the MODIS-derived snow albedo values for bands 4 and 5, respectively. We then calculated $\Delta\alpha_{MODIS,corrected}^{LAPs}$ as follows:

$$\Delta\alpha_{MODIS,corrected}^{LAPs} = f(I_{LAPs}, R_{eff}, SD, G) \quad (4413)$$

~~Values for R_{eff} , SD , and G were kept spatially constant as the averages $\overline{R_{eff}}$, \overline{SD} , and \overline{G} , with \overline{G} requiring spatially constant values for the solar zenith angle, surface topography, and solar radiation parameters. As a result, The~~ spatial variability in snow albedo reduction due to I_{LAPs} can be expressed as

$$\Delta\alpha_{MODIS,corrected}^{LAPs}(I_{LAPs}) = f(I_{LAPs}, \overline{R_{eff}}, \overline{SD}, \overline{G}) \quad (4514)$$

where $\overline{R_{eff}}$, \overline{SD} , \overline{G} indicate spatial-mean values of R_{eff} , SD , and G , with \overline{G}

requiring spatially constant values for the solar zenith angle, surface topography, and solar irradiance parameters. The following three equations were applied in a similar manner:

$$\Delta\alpha_{MODIS,corrected}^{LAPs}(R_{eff}) = f(\overline{I_{LAPs}}, \overline{R_{eff}}, \overline{SD}, \overline{G}) \quad (1615)$$

$$\Delta\alpha_{MODIS,corrected}^{LAPs}(SD) = f(\overline{I_{LAPs}}, \overline{R_{eff}}, SD, \overline{G}) \quad (1716)$$

$$\Delta\alpha_{MODIS,corrected}^{LAPs}(G) = f(\overline{I_{LAPs}}, \overline{R_{eff}}, \overline{SD}, G) \quad (1817)$$

We then fitted $\Delta\alpha_{MODIS,corrected}^{LAPs}$ through multiple linear regression:

$$\Delta\alpha_{MODIS}^{LAPs,fit} = a \cdot \Delta\alpha_{MODIS,corrected}^{LAPs}(I_{LAPs}) + b \cdot \Delta\alpha_{MODIS,corrected}^{LAPs}(R_{eff}) + c \cdot \Delta\alpha_{MODIS,corrected}^{LAPs}(SD) + d \cdot \Delta\alpha_{MODIS,corrected}^{LAPs}(G) \quad (1918)$$

where $\Delta\alpha_{MODIS}^{LAPs,fit}$ is the fitted snow albedo reduction and a, b, c, and d denote the regression coefficients. Figure S3a illustrates how $\Delta\alpha_{MODIS}^{LAPs,fit}$ can explain 9899% of the variance in $\Delta\alpha_{MODIS,corrected}^{LAPs}$. Therefore, the attribution of spatial variance in $\Delta\alpha_{MODIS,corrected}^{LAPs}$ can be replaced with $\Delta\alpha_{MODIS}^{LAPs,fit}$, enabling Eq. (1918) to be written as follows:

$$\begin{aligned} \Delta\alpha_{MODIS}^{LAPs,fit} - \overline{\Delta\alpha_{MODIS}^{LAPs,fit}} &= a \cdot (\Delta\alpha_{MODIS,corrected}^{LAPs}(I_{LAPs}) - \overline{\Delta\alpha_{MODIS,corrected}^{LAPs}(I_{LAPs})}) + b \cdot (\Delta\alpha_{MODIS,corrected}^{LAPs}(R_{eff}) - \overline{\Delta\alpha_{MODIS,corrected}^{LAPs}(R_{eff})}) \\ &+ c \cdot (\Delta\alpha_{MODIS,corrected}^{LAPs}(SD) - \overline{\Delta\alpha_{MODIS,corrected}^{LAPs}(SD)}) + d \cdot (\Delta\alpha_{MODIS,corrected}^{LAPs}(G) - \overline{\Delta\alpha_{MODIS,corrected}^{LAPs}(G)}) \end{aligned} \quad (2019)$$

where $\Delta\alpha_{MODIS}^{LAPs,fit} - \overline{\Delta\alpha_{MODIS}^{LAPs,fit}}$ is the snow albedo reduction anomaly
 $(\Delta\alpha_{MODIS,anomaly}^{LAPs,fit})$. Then, Eq. (19) can be written as and

$$\Delta\alpha_{MODIS,anomaly}^{LAPs,fit} = a \cdot \Delta\alpha_{MODIS,corrected,anomaly}^{LAPs}(I_{LAPs}) + b \cdot \Delta\alpha_{MODIS,corrected,anomaly}^{LAPs}(R_{eff}) + c \cdot \Delta\alpha_{MODIS,corrected,anomaly}^{LAPs}(SD) + d \cdot \Delta\alpha_{MODIS,corrected,anomaly}^{LAPs}(G). \quad (220)$$

According to Huang and Yi (1991) and Pu et al. (2019), the fractional contribution of
 LAP content to the variability in snow albedo reduction ($R_{\Delta\alpha}^{LAPs}$) can be calculated as:

$$R_{\Delta\alpha}^{LAPs} = \frac{1}{m} \sum_{j=1}^m \frac{(a \cdot \Delta\alpha_{MODIS,corrected,anomaly}^{LAPs}(I_{LAPs})_j)^2}{K_j} \quad (221)$$

$$K_j = (a \cdot \Delta\alpha_{MODIS,corrected,anomaly}^{LAPs}(I_{LAPs})_j)^2 + (b \cdot \Delta\alpha_{MODIS,corrected,anomaly}^{LAPs}(R_{eff})_j)^2 + (c \cdot \Delta\alpha_{MODIS,corrected,anomaly}^{LAPs}(SD)_j)^2 + (d \cdot \Delta\alpha_{MODIS,corrected,anomaly}^{LAPs}(G)_j)^2 \quad (222)$$

where m denotes the length of the data set. Values for $R_{\Delta\alpha}^{R_{eff}}$, $R_{\Delta\alpha}^{SD}$, and $R_{\Delta\alpha}^G$ can be
 derived in the same way. Similarly, we can obtain the fractional contribution for daily
 radiative forcing (R_{RF}^{LAPs} , $R_{RF}^{R_{eff}}$, R_{RF}^{SD} , and R_{RF}^G).

4. Results

4.1. Study area

Figure 3a depicts the ISCA employed in this study. Most are located ~~between $\geq 40^{\circ}\text{N}$~~
~~and 55°N~~ in Eurasia ~~and~~, North America, ~~—~~ and the Arctic, which are dominated by
grassland, shrublands and bare-soil surfaces (Fig. 3b). Several mid-high-latitude
regions that typically support a deep snowpack, including southern Russia, western
Europe, and eastern ~~North America~~US, are not identified by MODIS as ISCA due to
the broad distributions of forest ~~and shrubland~~ in those areas (Fig. 3b). This pattern is
supported by Bond et al. (2006), who demonstrated that, under such vegetated
conditions, LAPs in snow exert a relatively minor influence on radiative forcing. ~~In the~~
~~Arctic, where the polar night renders satellite-mounted sensors unable to detect~~
~~radiation, only a small part of southern Greenland can be identified as snow-covered~~
~~during January and February. On the other hand, the snowpack over midlatitude~~
~~mountains at such a coarse resolution ($0.05^{\circ} \times 0.05^{\circ}$) is too low to identify ISCA snow-~~
~~covered area. Moreover~~In addition, midlatitude mountains are characterized as
complex terrain, which will lead to high biases in radiative forcing retrieval at the coarse
resolution in spite of topographic correction. Therefore, we didn't report the results over
midlatitude mountains in this study.

As illustrated in Fig. 3a, ISCA can be separated into four general regions according to
geographical distribution and pollution conditions (~~Fig. 4a~~Fig. S2a, b): northeastern
China (NEC), Eurasia (EUA), North America (NA), and the Arctic. The following
analysis of snow albedo reduction and RFLS only concerns ISCA ~~during the January–~~
~~February–December–May study period and~~ the periods of the results are mainly in

~~W~~winter for midlatitudess due to snow melting and in ~~S~~spring for the Arctic due to polar night.

4.2. Global characteristics

Previous studies have highlighted the dominant role of BC in light absorption by snow (Wang et al., 2013b; Dang et al., 2017). The spatial distribution of BC emissions density for the Northern Hemisphere in ~~January–February~~December–May is shown in ~~Fig. 4a~~Fig. S2a. Emissions density exhibits a strong spatial inhomogeneity, ranging from $<10^{-1}$ to $>10^4$ g km⁻² month⁻¹ over ISCA. The highest values occur in NEC, where is considerably higher than~~the regional average~~ EUA of 10750 g km⁻² month⁻¹ is~~considerably higher than values for EUA (5643 g km⁻² month⁻¹) and NA (761 g km⁻² month⁻¹), and the lowest values occur in the Arctic (average 76 g km⁻² month⁻¹).~~ The wet and dry deposition of BC constitute the primary mechanisms for BC accumulation in snow. As shown in Fig. ~~S42~~b, the distribution of BC deposition (i.e., the sum of dry and wet deposition) is similar to BC emissions density, with the highest ~~(3.26 10⁻¹² kg m⁻² s⁻¹)~~ and lowest ~~(1.21 10⁻¹³ kg m⁻² s⁻¹)~~ regional averages corresponding to NEC and the Arctic, respectively. ~~Both NA and EUA return intermediate deposition values, with regional averages of 5.75 10⁻¹³ kg m⁻² s⁻¹ and 1.78 10⁻¹² kg m⁻² s⁻¹, respectively.~~ Together, these data indicate that the NEC snowpack is heavily polluted, and thus RFLS-snow albedo reduction is likely to be

1 highest, while the Arctic snowpack is the least contaminated.

2 In addition to LAP content, the physical properties of the snowpack, such as depth and
3 grain size, also impact snow albedo (Fig. 1). As depicted in Fig. ~~4e~~4a, the average
4 snowpack in ~~NEC-EUA~~ (0.~~19-15~~ m thick) is thinner than in both NA (0.~~26-24~~ m) and
5 ~~EUA-NEC~~ (0.~~21-19~~ m), implying a greater impact of snow depth on snow albedo and
6 radiative forcing in ~~NECEUA~~. The greatest snow depths occur in the Arctic (>1 m) and
7 can be considered semi-infinite, meaning that the impact of depth on albedo and
8 radiative forcing is negligible. Figure ~~4d-4b~~ shows the spatial distribution of MODIS-
9 derived snow grain radius (R_{eff}). In contrast to BC emissions density, BC deposition,
10 and snow depth, R_{eff} exhibits minor spatial variability, with regional average values
11 for NEC, EUA, NA, and the Arctic of ~~235-237~~ μm , 227 μm , ~~252-237~~ μm , and ~~255-215~~
12 μm , respectably. These values align with the findings of several previous studies
13 (Painter et al., 2013; Seidel et al, 2016; Pu et al., 2019) and imply that the contribution
14 of R_{eff} to spatial variability in snow albedo reduction and radiative forcing is
15 negligible.

16 According to Eq. (~~1011~~)~~and (11)~~, local solar ~~radiation~~radiances ~~—~~is an important factor
17 for determining RFLS. Figure ~~4e, f~~c depicts the ~~January-February-December-May~~
18 averaged ~~surface-direct-and-diffuse~~total downward surface shortwave flux~~solar~~
19 ~~irradiance, respectively,~~—under ~~clear~~all-sky conditions. Average solar radiances
20 flux~~direct radiation~~ values for EUA (~~138 W m⁻²~~) and NA (~~147 W m⁻²~~) are comparable
21 to one another but high relative to NEC (~~87 W m⁻²~~), which lies at a generally higher

latitude ($>40^\circ$). The lowest values occur in the Arctic (9 W m^{-2}) due to that region's extreme latitude. The Arctic goes through the polar night during winter, so that the radiative effect of LAPs in the Arctic mainly appears in spring. Figure S2d shows the March-May averaged downward surface shortwave flux~~radiance~~~~irradiance~~. As can be seen that the ~~averaged solar radiance~~ values in the Arctic in March-May are higher than ~~that those~~ in midlatitudes in December-MayFebruary (Figure S2c). We note that snow albedo reduction and radiative forcing are only calculated over the period ~~of when snow-~~ covered area was mapped, which implies that the RFLS will be higher in the Arctic than midlatitudes ~~of for~~ the same snow albedo reduction.

~~For diffuse radiation, average fluxes for NEC, EUA, NA, and the Arctic are 32 W m^{-2} , 46 W m^{-2} , 36 W m^{-2} , and 4 W m^{-2} , respectively. In summary, these data indicate a smaller radiative forcing in the Arctic than in the other three regions.~~

4.3. Corrections based on ~~in~~-in-situ observations

Albedo reduction calculated using in-situ observed LAPs~~In situ observations of snow albedo reduction~~ ($\Delta\alpha_{in-situ,ins}^{LAPs,daily}$) were used to quantitatively correct MODIS retrievals through comparison with MODIS-retrieved snow albedo reduction ($\Delta\alpha_{MODIS,daily}^{LAPs,ins}$). Figure ~~S2-S4~~ displays scatterplots of the ratios of $\Delta\alpha_{MODIS,daily}^{LAPs,ins}$ to $\Delta\alpha_{in-situ,daily}^{LAPs,ins}$ ($r_{in-situ}^{MODIS}$) for each sampling sites (Ye et al., 2012; Wang et al., 2013b, 2017; Doherty et al., 2010; 2014). Briefly, for NA~~and~~, EUA, and the Arctic

1 where the snowpack is relatively ~~pure~~clean, the values for $r_{in-situ}^{MODIS}$ mostly range
 2 between ~~1-2~~ and ~~1210~~. In contrast, the heavily polluted snowpack in NEC returns
 3 $r_{in-situ}^{MODIS}$ values ranging from 0.5 to 2.5, indicating a negative correlation between the
 4 biases of $\Delta\alpha_{MODIS,ins}^{LAPs}$ and snow contamination, and thus supporting the findings
 5 of previous studies (Painter et al., 2012a; Pu et al., 2019). To improve the quality of
 6 MODIS retrievals, we developed the correction factors ~~c_{clean}~~ for ~~the relatively pure~~
 7 ~~snowpack conditions observed in the EUA, NA, and the Arctic and~~ ~~$c_{polluted}$~~ for the
 8 ~~impure conditions found in NEC~~different regions. According to Eq. (910), the
 9 correction factors values for NEC, EUA, NA, Canadian Arctic, Russian Arctic and
 10 Greenland are 1.6, 4.1, 4.1, 4.4, 5.4 and 6.0 ~~c_{clean} and $c_{polluted}$ are 5.6 and 1.1,~~
 11 respectively. Hereafter, our analyses are based on the corrected MODIS retrievals.

12 Figure 5 compares the corrected MODIS retrievals to measurement-based results, and
 13 the mean absolute error (MAE) and root mean square error (RMSE) of
 14 $\Delta\alpha_{MODIS,corrected}^{LAPs}$ relative to $\Delta\alpha_{in-situ,daily}^{LAPs}$ are given in Table S1. ~~For clean snow,~~
 15 ~~the mean absolute error (MAE) of $\Delta\alpha_{MODIS,corrected}^{LAPs}$ relative to $\Delta\alpha_{in-situ,ins}^{LAPs}$ is~~
 16 ~~0.0096, with a root mean square error (RMSE) of 0.0129, corresponding to respective~~
 17 ~~radiative forcing MAE and RMSE values of 3.0 W m^{-2} and 3.8 W m^{-2} for $RF_{MODIS,ins}^{LAPs}$~~
 18 ~~and 0.95 W m^{-2} and 1.2 W m^{-2} for $RF_{MODIS,daily}^{LAPs}$.~~ For polluted snow conditions, the
 19 MAE and RMSE are 0.0501 and 0.0622 for albedo reduction, respectively, with
 20 respective radiative forcing MAE and RMSE values of 14 W m^{-2} and 18 W m^{-2} for
 21 ~~$RF_{MODIS,ins}^{LAPs}$ and 4.4 W m^{-2} and 5.5 W m^{-2} for $RF_{MODIS,daily}^{LAPs}$.~~

Together, these results imply that the corrected MODIS retrievals are plausible. Nevertheless, we note that the correction used in this study is spatially rough due to the low density of ~~in-in~~-situ measurements, ~~and thus~~ that both the uncertainty and bias are non-negligible. To address this issue, we presented further discussion about the accuracy of radiative forcing retrievals (see Sect. 4.5). ~~As a result, we~~ We also conducted a comprehensive series of comparisons between the MODIS-derived retrievals and values provided via surface measurements, model simulations, and remote sensing (see Sect. 5). We concluded that further field-based measurements of snow albedo are required to improve the quality of satellite retrievals.

4.4. Spatial distributions of snow albedo reduction and radiative forcing

Figure 6a shows the spatial distributions ~~and statistics~~ of MODIS-based ~~and ground-based~~ albedo reduction and daily radiative forcing, and statistics are shown in Figure 6b and Table 1. ~~$\Delta\alpha_{MODIS,corrected}^{LAPs}$, $RF_{MODIS,ins}^{LAPs}$, and $RF_{MODIS,daily}^{LAPs}$ retrievals.~~ On average, $\Delta\alpha_{MODIS,corrected}^{LAPs}$, ~~$RF_{MODIS,ins}^{LAPs}$~~ , and $RF_{MODIS,daily}^{LAPs}$ provide respective values of 0.021 and ~~2.90-0.0246, 5.9~~ $W\ m^{-2}$, ~~and 1.7~~ $W\ m^{-2}$ for Northern Hemisphere ISCA. The highest $\Delta\alpha_{MODIS,corrected}^{LAPs}$ occurs in NEC, where the regional average of ~~~0.1669-11~~ exceeds those of EUA (~~~0.02100.031~~) and NA (~~~0.01810.027~~) by a factor of ~~~8-93-4~~. This feature reflects the relatively high rate of ~~winter-time~~ emissions over NEC, which

results in the highest level of BC deposition over ISCA (Fig. 4a Fig. S2a–, b). In contrast,
 being located far from major sources of pollution, the relatively clean Arctic snowpack
 returns the lowest $\Delta\alpha_{MODIS,corrected}^{LAPs}$ (~ 0.0123016) of the entire Northern Hemisphere.
 Consistent with snow albedo reduction, the highest regional-average daily radiative
 forcing ($RF_{MODIS,daily}^{LAPs}$) occurs in NEC, with ~~respective $RF_{MODIS,ms}^{LAPs}$ and~~
 ~~$RF_{MODIS,daily}^{LAPs}$~~ values of $\sim 36.12 \text{ W m}^{-2}$ ~~and $\sim 11 \text{ W m}^{-2}$~~ , and the lowest regional average
 occurs in the Arctic, with ~~$RF_{MODIS,ms}^{LAPs}$ and $RF_{MODIS,daily}^{LAPs}$~~ values of $\sim 1.12.6 \text{ W m}^{-2}$
~~and $\sim 0.29 \text{ W m}^{-2}$, respectively. As well as receiving the lowest levels of pollution, the~~
~~relatively low winter time surface solar radiation also contributes to the Arctic returning~~
~~the smallest radiative forcing (Fig. 4e–f).~~ Regional-average radiative forcing for NA
 and EUA are both intermediate, with ~~$RF_{MODIS,ms}^{LAPs}$ ($RF_{MODIS,daily}^{LAPs}$)~~ values of $\sim 3.1 \text{ W}$
 ~~m^{-2} and $\sim 3.5 \text{ W m}^{-2}$~~ $\sim 4.8 \text{ W m}^{-2}$ ($\sim 1.4 \text{ W m}^{-2}$) and $\sim 5.3 \text{ W m}^{-2}$ ($\sim 1.5 \text{ W m}^{-2}$),
 respectively. ~~Furthermore, because NA and EUA experience similar pollution~~
~~conditions and are located at similar latitudes, both regions exhibit comparable radiative~~
~~forcing.~~
 On a regional level, NEC $\Delta\alpha_{MODIS,corrected}^{LAPs}$ falls primarily within the range ~ 0.077 –
 0.14 ~~~ 0.1177 – 0.2157~~ , and intra-regional variability is relatively small due to pervasive
 heavy pollution (Fig. 4S2). Compared to snow albedo reduction, the radiative forcing
 for NEC exhibits a slightly greater spatial variability due to latitude-dependent
 differences in the flux of surface solar ~~radiation~~ radiances, with ~~$RF_{MODIS,ms}^{LAPs}$~~
~~($RF_{MODIS,daily}^{LAPs}$)~~ ranging from $\sim 7.2 \text{ W m}^{-2}$ to ~ 17 – 24 W m^{-2} to $\sim 53 \text{ W m}^{-2}$ ($\sim 6.9 \text{ W m}^{-2}$

1 ~~to -16 W m^{-2}~~). In NA, where the principal ISCA are located in southern Canada, the
 2 western US, and Central America Plains, $\Delta\alpha_{MODIS,corrected}^{LAPs}$ and $RF_{MODIS,daily}^{LAPs}$ tends
 3 to range between $\sim 0.014\text{--}0.046$ and $\sim 1.3\text{--}7.0 \text{ W m}^{-2}$, respectively. ~~~ 0.0071 and ~ 0.0309 .~~
 4 ~~The Central America Plains exhibit the highest value of $\Delta\alpha_{MODIS,corrected}^{LAPs}$ (~ 0.045),~~
 5 ~~with corresponding $RF_{MODIS,ins}^{LAPs}$ and $RF_{MODIS,daily}^{LAPs}$ values of 14 W m^{-2} and 3.9 W~~
 6 ~~m^{-2} , respectively. This region also displays a clear gradient in~~
 7 ~~$RF_{MODIS,ins}^{LAPs}$ ($RF_{MODIS,daily}^{LAPs}$), with values increasing from $<5 \text{ W m}^{-2}$ ($<1 \text{ W m}^{-2}$) in the~~
 8 ~~northwest to $>15 \text{ W m}^{-2}$ ($>4 \text{ W m}^{-2}$) in the southeast, in line with previously reported~~
 9 ~~observational data (Doherty et al., 2014).~~
 10 In EUA, $\Delta\alpha_{MODIS,corrected}^{LAPs}$, ~~$RF_{MODIS,ins}^{LAPs}$~~ and $RF_{MODIS,daily}^{LAPs}$ fall largely within the
 11 respective ranges of $\sim 0.017\text{--}0.049$ and $\sim 1.6\text{--}8.4 \text{ W m}^{-2}$. ~~$\sim 0.0097\text{--}0.0352$, $\sim 2.4\text{--}9.9 \text{ W}$~~
 12 ~~m^{-2} , and $\sim 0.69\text{--}2.9 \text{ W m}^{-2}$. The Middle East returns relatively high values for~~
 13 ~~$\Delta\alpha_{MODIS,corrected}^{LAPs}$ (>0.04), $RF_{MODIS,ins}^{LAPs}$ ($>12 \text{ W m}^{-2}$), and $RF_{MODIS,daily}^{LAPs}$ ($>4 \text{ W m}^{-2}$),~~
 14 ~~likely due to the combined effects of elevated dust fluxes (Solomos et al., 2017) and~~
 15 ~~high solar insolation at these low latitudes. Similar to the Middle East, Central Asia and~~
 16 ~~Mongolia northwestern China also exhibits~~ relatively high values for
 17 $\Delta\alpha_{MODIS,corrected}^{LAPs}$ (>0.03504), ~~$RF_{MODIS,ins}^{LAPs}$ ($>11 \text{ W m}^{-2}$)~~, and $RF_{MODIS,daily}^{LAPs}$ ($>3.2 \text{ W}$
 18 m^{-2}), while this pattern likely reflects the influence of anthropogenic BC in addition to
 19 natural dust (Pu et al., 2017; Zhou et al., 2019) (Fig. 4a Fig. S2a–b). ~~In contrast, Europe~~
 20 ~~and Russia return the relatively low $\Delta\alpha_{MODIS,corrected}^{LAPs}$ (<0.03), with a~~
 21 ~~$RF_{MODIS,ins}^{LAPs}$ ($RF_{MODIS,daily}^{LAPs}$) value of $<10 \text{ W m}^{-2}$ ($<3 \text{ W m}^{-2}$), reflecting the generally~~

low concentration of LAPs in this region. Finally, in the Arctic, where ISCA comprise only a small part of southern Greenland (see Sect. 4.1), respective $\Delta\alpha_{MODIS,corrected}^{LAPs}$, $RF_{MODIS,ms}^{LAPs}$, and $RF_{MODIS,daily}^{LAPs}$ values fall within the ranges ~ 0.0018 – 0.038 , ~ 0.18 – 3.8 $W\ m^{-2}$, and ~ 0.046 – 0.98 $W\ m^{-2}$.

In the Arctic, $\Delta\alpha_{MODIS,corrected}^{LAPs}$ and $RF_{MODIS,daily}^{LAPs}$ both present quite large intra-regional variabilities from ~ 0.0028 to ~ 0.046 and ~ 0.48 to ~ 6.6 $W\ m^{-2}$. Greenland has the cleanest snow with $\Delta\alpha_{MODIS,corrected}^{LAPs}$ and $RF_{MODIS,daily}^{LAPs}$ of ~ 0.011 – 0.023 and ~ 0.40 – 3.3 $W\ m^{-2}$. In Canadian Arctic, $\Delta\alpha_{MODIS,corrected}^{LAPs}$ and $RF_{MODIS,daily}^{LAPs}$ are mainly in a range of ~ 0.012 – 0.055 and ~ 0.59 – 6.1 $W\ m^{-2}$. In addition, the relatively high values are found around the edge of ISCA over west of Canadian Arctic. The possible reason is that these areas are suffering from faster snow melting compared with rest of Canadian Arctic in spring, which is characterized by higher snow grain size (Fig. 4b). Hence, more LAPs are accumulated in the surface snow resulting in higher snow albedo reduction. In Russian Arctic, $\Delta\alpha_{MODIS,corrected}^{LAPs}$ and $RF_{MODIS,daily}^{LAPs}$ present a significant altitude-dependent trend of ~ 0.012 – 0.048 and ~ 1.0 – 7.3 $W\ m^{-2}$. The snow albedo reduction in eastern Siberia are quite high and comparable with the values in midlatitudes. Moreover, benefiting from the higher solar radiances in eastern Siberia in Spring (Figure S2d) than that in midlatitudes in Winter-Spring (Figure 4c and Fig. S2c), $RF_{MODIS,daily}^{LAPs}$ in eastern Siberia are higher than parts of midlatitudes. Even different with the findings in previous modeling studies (e.g.

Flanner et al., 2007; 2009), the results seem to be comparable with the limited ground-based estimates (Figure. SXXX3). The serious biomass burning in eastern Siberia in Spring may be responsible for such high values (Warneke et al., 2010; Hegg et al., 2009). Overall, the Arctic spatial pattern of $\Delta\alpha_{MODIS,corrected}^{LAPs}$ and $RF_{MODIS,daily}^{LAPs}$ in our study is consistent with the previous studies based on field experiments (Dang et al., 2017) and model simulation (Flanner et al., 2007). Nevertheless, we note that readers should be cautious ~~for~~about our reported high values in Russian Arctic and more field experiments are necessary for validating the results.

As mentioned above, the assumption of semi-infinite snowpack will trigger an overestimate for radiative forcing when snow depth is not thick enough. Figure 7 shows the spatial distribution of the ratio of retrieved radiative forcing using semi-infinite snow to radiative forcing using ERA-Interim snow depth. As can be seen that semi-infinite snowpack assumption will lead to an overestimate of up to ~25% in midlatitude areas, where snow depth is thin. In contrast, the influence of snow depth on radiative forcing is negligible in the Arctic, where snow is thick enough to become semi-infinite snowpack. These results demonstrated the important impact of snow depth on radiative forcing retrievals, which must be considered to reduce the overestimate for the following study.

4.5. Accuracy discussion

In spite of the rigorous processes for radiative forcing retrieval ~~and in situ correction~~, the uncertainty is still existed. For example, light-absorbing particles in the atmosphere

will reduce the accuracy of MODIS surface reflectance retrieval, even ~~that~~ although the atmospheric correction has been conducted. In addition, previous study pointed out a high scatter when converting NDSI to FSC using Eq. (5), which will induce bias in snow albedo retrieval (Rittger et al., 2013; Riggs et al., 2016). Furthermore, the method for snow grain size retrieval is only based on a single MODIS band at 1.24 μm , which could lead to higher uncertainties. Above all, all of these factors will result in a non-negligible uncertainty for radiative forcing retrieval, which needs to be further discussed.

To account for ~~address~~ this issue, we consider that the accuracy of atmospheric correction is typically $\pm (0.005 + 0.05 \times \text{reflectance})$ under conditions that AOD is less than 5.0 and solar zenith angle is less than 75° according to the MODIS Surface Reflectance User's Guide (Collection 6, <https://modis.gsfc.nasa.gov/data/dataproduct/mod09.php>). In addition, the bias for FSC calculation ~~used~~ is assumed as 10% according to Riggs et al. (2016). The bias for snow grain size retrieval ~~used~~ is assumed as 30% according to the studies of Pu et al. (2019) and Wang et al. (2017). Figure 8 shows the overall uncertainty of radiative forcing retrieval due to all these factors while Figure S6 show the uncertainty caused by each factor. In general, the positive (negative) uncertainty falls in a range of 15%~108% (-106%~-20%), with ~~a~~ Atmospheric correction and FSC calculation ~~by~~ing higher uncertainties than snow grains size retrieval. The highest uncertainty occurs in the Arctic ~~while~~ the lowest uncertainty occurs in NEC. Furthermore, the uncertainty,

which further shows a negative correlation with retrieved radiative forcing and snow pollution condition. The results indirectly demonstrated the reasonability of the different correction factors performed in different regions. For example, the value of 1.6 used in NEC suggests that the correction approach works well for heavily polluted snow, while the value of 6.0 used in Greenland for relatively clean snow suggests that the method becomes not accurate enough.s

It worth noting that the uncertainties from these factors could not fully explain the high correction factor in clean snow. There are four probable reasons: (1) the rough snow surface and uncertainties of vegetation and soil reflectance can effectively influence radiative forcing retrieval; (2) MODIS cannot proceed with a continuous spectral measurement of a continuous variable forcing like what LAPs afford to snow albedo due to the variably spaced and discrete bands of MODIS, which prevents a more quantitative retrieval and thus results in a non-negligible uncertainty in radiative forcing retrieval (Painter et al., 2012); (3) We use the retrieved radiative forcing in a pixel size of $0.05^\circ \times 0.05^\circ$ to compare with the in-situ radiative forcing calculated from the measured BC_{equiv} concentration with the sample site located in the center of the pixel.

However, such a comparison may not be true at some sites due to the inhomogeneous spatial distribution of LAP contents, which will influence radiative forcing retrieval; (4) In-situ measurements also have uncertainties, which may cause a high bias for snow albedo reduction in clean snow. For example, a 10% bias for $50 \text{ ng g}^{-1} \text{ BC}$ can result in an 8% bias for snow albedo reduction.

4.56. Attribution to the spatial variability of snow albedo reduction and radiative forcing

Here, we address the attributions to the spatial variability of snow albedo reduction and radiative forcing. As discussed in Sect. 3.2.65, the spatial variability in snow albedo reduction and radiative forcing are largely dependent on LAP content, snow grain radius, snow depth, and the geographic factor. Figure 79 illustrates the fractional contributions of each factor within the study regions. For the Northern Hemisphere ISCA as a whole, LAPs (I_{LAPs}) is the greatest contributor (~~57.6~~84.3%) to snow albedo reduction, followed by SD (~~38.1~~13.7); R_{eff} and G have only a minor influence (~~2.7~~1.9% and ≤ 1.6 %, respectively) (Fig. 7a9a). This result confirms that the concentration of LAPs in the snowpack plays a fundamental role in spatial variability of snow albedo reduction.

LAPs also constitute the dominant contributors to snow albedo reduction on a regional scale, accounting for ~~96.0%~~76.2% of the Arctic signal and ~~56.7%~~54.4% in EUA and ~~49.9% in NA~~, and are the second largest contributor in ~~both~~ NEC (~~43.7~~40.3%) ~~and NA~~ (~~48.1%~~). The contribution of SD is greatest in NEC (~~51.6~~56.3%) ~~and NA~~ (~~49.8%~~), with slightly lower values in EUA (40.3%) and NA (48.8%), reflecting the significant spatial variability in SD across these regions. In the Arctic, the snowpack is sufficiently thick to be considered a homogeneous, semi-infinite snowpack and thus the contribution of SD is negligible. In contrast, R_{eff} makes only minor contributions in

1 NEC (~~3.9~~3.3%), NA (~~1.4~~3%), ~~and~~ EUA (~~3.3~~2.8%) ~~and the Arctic (1.4%).but is an~~
2 ~~important factor in the Arctic (22%).~~ Finally, G makes the smallest contribution to
3 snow albedo reduction (~~<2~~1%), both on regional and global scales.

4 On a hemispheric scale, the greatest contributors to radiative forcing are LAP content
5 (~~37.2~~70.0%) and G (~~34.6~~22.3%), followed by SD (~~27.9~~7.6%). As with snow albedo
6 reduction, R_{eff} plays only a minor role (~~0.2~~%). ~~The influence of G on~~Our data
7 ~~indicate that~~ spatial variability in radiative forcing is ~~highly dependent on G , a pattern~~
8 ~~that we~~ attributed to the high degree of variability in latitude-dependent solar
9 ~~radiation~~radiances among ISCA.

10 On a regional scale, the respective contributions of LAP content, G , and SD are also
11 comparable among the four study areas, accounting for ~~34.1%, 11.1%, and 52.0%~~27.4%,
12 ~~37%, and 34%~~ of radiative forcing in NEC, ~~39.2%, 13.9%, and 46.4%~~24.9%, 38%, and
13 ~~36.8%~~ in NA, and ~~48.0%, 19.3%, and 31.6%~~35.6%, 35.2%, and 27.2% in EUA. The
14 Arctic radiative forcing is dominated by LAPs (~~52.8~~85.6%) and G (~~46.4~~12.7%).

15 In summary, LAPs play a dominant role in the spatial variability of snow albedo
16 reduction and radiative forcing. Our results also highlight the significant contribution
17 of SD to snow albedo reduction and G to radiative forcing.

19 4.6. Comparisons with model simulations

20 To investigate the global distribution and variance of RFLS, previous studies have

tended to rely on Earth system models with minimal cross-checking from ~~in~~-in-situ measurements or remote sensing observations (Qian et al., 2015; Skiles et al., 2018). In this study, we compared MODIS retrievals with ~~two model-based estimates~~ CESM2 to improve our understanding of the magnitude of RFLS on a global scale. ~~Flanner et al. (2009) simulated springtime RFLS for the Northern Hemisphere by applying a Global Climate Model (GCM) coupled with a SNICAR model, the results of which are presented in Fig. 8a and Fig. S5a.~~

~~Figure 8b depicts the direct comparison of our MODIS retrievals ($RF_{MODIS,daily}^{LAPs}$) to the simulations of Flanner et al. (2009) (RF_{GCM}). In general, $RF_{MODIS,daily}^{LAPs}$ and RF_{GCM} are of the same magnitude and both fall in the range 0.10–4.6 W m⁻². The MAE for RF_{GCM} against $RF_{MODIS,daily}^{LAPs}$ is 1.6 W m⁻². Regionally, the average $RF_{MODIS,daily}^{LAPs}$ in NEC (NA) is 11 W m⁻² (1.4 W m⁻²), a value that is higher by a factor of 2.5 (2.0) than the RF_{GCM} value of 4.2 W m⁻² (0.69 W m⁻²). In contrast, $RF_{MODIS,daily}^{LAPs}$ (0.29 W m⁻²) for the Arctic is systematically lower than RF_{GCM} value (1.1 W m⁻²) by a factor of 3.9. For EUA, average $RF_{MODIS,daily}^{LAPs}$ (1.5 W m⁻²) and RF_{GCM} (1.9 W m⁻²) are comparable, while correlations between $RF_{MODIS,daily}^{LAPs}$ and RF_{GCM} for NA, NEC, and the Arctic are all significant at the 99 % confidence level ($R^2 = 0.36, 0.43, \text{ and } 0.72$, respectively).~~

Employing ~~ensemble-average~~ snow BC concentrations from CESM2 ~~and CESM2-WACCM~~, we also calculated ~~January–February~~ December–May daily radiative forcing ($RF_{CESM2CMIP6}$) for the Northern Hemisphere ISCA during the period 2003–2014 (Fig. ~~9a10a~~). Statistics are presented in Fig. ~~S75b~~. Briefly, $RF_{CESM2CMIP6}$ exhibits strong

1 spatial inhomogeneity, with values ranging from $0.068\text{--}20\text{ W m}^{-2}$ to $5.64\text{--}6\text{ W m}^{-2}$. The
 2 highest regional average in $RF_{CESM2CMIP6}$ occurs in NEC ($\geq 5\text{--}10\text{ W m}^{-2}$) and the
 3 lowest in the Arctic ($\leq 0.2\text{--}5\text{ W m}^{-2}$), consistent with $RF_{MODIS,daily}^{LAPs}$.
 4 Figure 109b depicts the comparison of $RF_{MODIS,daily}^{LAPs}$ and $RF_{CMIP6CESM2}$, ~~for which~~
 5 ~~the MAE of RF_{CMIP6} to $RF_{MODIS,daily}^{LAPs}$ is 0.90 W m^{-2} .~~ In NEC, $RF_{CMIP6CESM2}$
 6 (8.415 W m^{-2}) compares well with $RF_{MODIS,daily}^{LAPs}$ (10.602 W m^{-2}), with a significant
 7 correlation at the 99% confidence level ($R^2 = 0.43$). For EUA, RF_{CESM2} (3.8 W m^{-2})
 8 is similar to $RF_{MODIS,daily}^{LAPs}$ (3.5 W m^{-2}). For NA and EUA, $RF_{CMIP6CESM2}$ ($0.691.2\text{ W}$
 9 m^{-2} and $3.81.6\text{ W m}^{-2}$, respectively) are is lower than $RF_{MODIS,daily}^{LAPs}$ ($1.43.1\text{ W m}^{-2}$ and
 10 $1.53.5\text{ W m}^{-2}$, respectively) and the spatial correlations between them are poor. In the
 11 Arctic,
 12 ~~RF_{CMIP6} is significantly correlated with $RF_{MODIS,daily}^{LAPs}$ at the 99% confidence level ($R^2 =$~~
 13 ~~0.80). However, $RF_{CMIP6CESM2} - RF_{CESM2}$ is correlated with $RF_{MODIS,daily}^{LAPs}$ at the 99%~~
 14 ~~confidence level. However, RF_{CESM2} ($0.151.7\text{ W m}^{-2}$) is lower than $RF_{MODIS,daily}^{LAPs}$~~
 15 ~~($0.292.6\text{ W m}^{-2}$) by a factor of 21.5 , an outcome that is contrary to the comparison~~
 16 ~~between RF_{GCM} and $RF_{MODIS,daily}^{LAPs}$.~~

17 Overall, the RFLS derived from our MODIS retrievals and modeling-based estimates
 18 exhibit a same magnitude over the Northern Hemisphere. In NEC, the MODIS- derived
 19 and model-derived estimates show good general agreement, indicating the satisfactory
 20 performance of Earth system modeling in this heavily polluted region. In ~~NA and~~ EUA,
 21 average radiative forcing values are comparable but the spatial correlation is relatively

poor, while MODIS retrievals for the Arctic are significantly ~~correlated with~~ higher than those simulations.

5. Discussion

In recent decades, there has been increasing scientific interest in snow LAPs due to their role in the climate system, and numerous studies have attempted to evaluate RFLS. In addition to making global-scale comparisons between our MODIS retrievals and model-based estimates, this study collects a comprehensive set of radiative forcing estimates, based on local-scale observations and remote sensing, to make quantitative regional- and global-scale comparisons and synthetically evaluate the magnitude of RFLS (~~Fig. 10~~ Table 2). This approach also affords the opportunity to examine the MODIS retrievals used in our study.

~~For instantaneous RFLS, Pu et al. (2019) reported an average value for NEC of -45 W m^{-2} , based on high-resolution (500 m) MODIS retrievals (Fig. 10a), which compares well with our findings (-24 – -53 W m^{-2}). This agreement indicates that the coarse-resolution (0.05°) MODIS data used in this study are sufficient to establishing RFLS. In NA, Painter et al. (2012a) reported RFLS values of -100 – -250 W m^{-2} for the Upper Colorado River Basin, while Seidel et al. (2016) obtained values of 20 – 200 W m^{-2} in the Sierra Nevada and Rocky Mountain (Fig. 10a). For EUA, Di Mauro et al. (2015) estimated a maximum RFLS of 153 W m^{-2} in the European Alps (Fig. 10a). In the Arctic,~~

Nagorski et al. (2019) reported a maximum RFLS for Alaska of $>4 \text{ W m}^{-2}$ in May and 87 W m^{-2} in June (Fig. 10a), while Ganey et al. (2017) provided a microbe-LAP-induced noontime radiative forcing of $>20 \text{ W m}^{-2}$ (Fig. 10a). We note that the findings of previous studies are approximately one order of magnitude higher than our results in NA, EUA, and the Arctic. We attribute this partly to the fact that those earlier studies focused on a local-scale estimates for sites with high LAP loadings, whereas our study provides regional-scale estimates.

Relative to estimates of instantaneous RFLS, which are comparatively rare, average-daily RFLS has been paid more attention climatologically. Figure 10b shows the calculated average-daily RFLS based on *in situ* measurements and remote sensing.

Dang et al. (2017) reported RFLS values of $7\text{--}18 \text{ W m}^{-2}$, $0.6\text{--}1.9 \text{ W m}^{-2}$, and $0.1\text{--}0.8 \text{ W m}^{-2}$ for northern China, North America, and the Arctic, respectively, which only focused on the period of January-March, and therefore are smaller than we note are comparable with our own retrievals. In NA, Sterle et al. (2013) estimated a daily-averaged RFLS of $\sim 2.5\text{--}40$

W m^{-2} for the eastern Sierra Nevada in February-May, 2009, while Miller et al. (2016) reported a daily RFLS of $\sim 35\text{--}86$ ($37\text{--}100$) 4 W m^{-2} based on in-situ measurements (remote sensing) in the San Juan Mountains in May 2010. Both values are higher than our estimate ($\sim 1.43.1 \text{ W m}^{-2}$), potentially due to the significant dust deposition in those areas.

In addition, we also collected Figure 10e shows the average-daily RFLS simulated by

regional and/or global climate models ([Table 2](#)). For NEC, Zhao et al. (2014) and Qian et al. (2014) reported values of 10 W m^{-2} [in January-February](#) and 5–10 W m^{-2} [in April](#), respectively. In NA, [Qian et al. \(2009\)](#) ~~the latter study also~~ provided an estimate of ~~23~~–7 W m^{-2} for the central Rockies and southern Alberta [in March](#) ~~(Qian et al., 2014)~~, while Oaida et al. (2015) reported an average RFLS of 16 W m^{-2} over the western US [in spring](#). ~~In EUA, Flanner et al. (2014) concluded that a RFLS of 0.1–1 W m^{-2} was caused by the deposition of volcanic ash in snow.~~ Finally, Qian et al. (2014) and Qi et al. (2017) estimated RFLS values of <0.3 W m^{-2} and 0.024–0.39 W m^{-2} for the Arctic [in April](#), respectively. We consider our retrievals for NEC, ~~EUA, and the Arctic~~ to be comparable with these regional model simulations, despite some disparity. However, we note that our result ~~for NA~~ is significantly lower than those of previous studies [in NA, but higher in the Arctic](#).

[On a global scale, Hansen and Nazarenko \(2004\) reported the RFLS is 0.3 \$\text{W m}^{-2}\$, while Flanner et al. \(2007\) showed a RFLS of ~0.05 \$\text{W m}^{-2}\$.](#) For the North Hemisphere as a whole, Bond et al. (2013) estimated a climate forcing of 0.13 W m^{-2} , ~~while Hansen and Nazarenko (2004) and Wang et al. (2014a) reported RFLS values of 0.3 W m^{-2} and 0.45 W m^{-2} , respectively.~~ Each of these previous values is significantly lower than our retrieval (~~~1.7~~[2.9](#) W m^{-2}). [However, those studies included all areas regardless of snow covered throughout the whole year, while our results are only for Northern Hemisphere ISCA from December to May.](#) ~~We attribute this disparity to the inclusion in those studies of low-LAP boreal forests, which contribute very little to overall radiative forcing yet~~

exhibit a high degree of uncertainty. Skiles et al. (2018) also concluded that modeled RFLS might be biased if the snow-covered area itself is not accurately represented.

Overall, we consider our MODIS-based retrievals to be physical realistic on both regional and global scales, although we note a number of differences between our results and those generated by different methods. On the other hand, while ~~in~~-in-situ measurements are the most precise, their spatial coverage is restricted by logistical limitations and the extreme environments involved. Conversely, models can provide broad perspectives of climatic impacts yet are typically undermined by large uncertainty. Therefore, we argue that remote sensing provides a powerful technique, with high spatial and temporal resolutions, that can bridge the gap between ~~in~~-in-situ measurements and climate models and reduce the uncertainties associated with the latter. Further retrieval of remote-sensing data, including the use of multiple satellites and sensors, is therefore warranted to exploit this opportunity fully. We also indicate the fact that parts of central EUA, ~~such as Middle East, are characterized by high dust deposition, and Russian Arctic,~~ however, studies are barely performed but desired. Finally, we note that ~~in~~-in-situ observations remain limited, and more field campaigns are needed to constrain remote sensing retrievals and modeling simulations.

6. Conclusion

We presented a global-scale evaluation of the daily radiative forcing of LAPs in the Northern Hemisphere snowpack (RFLS), estimated from remote-sensing data. The

1 satellite-retrieved RFLS also has implications for expanding the value of limited ~~in in-~~
2 situ measurements, which can provide valuable information for climate models and
3 help optimize model simulations.

4 Based on the corrected snow albedo reduction ($\Delta\alpha_{MODIS,corrected}^{LAPs}$), we ~~used the~~
5 ~~SBDART model to~~ calculated ~~instantaneous RFLS ($RF_{MODIS,ms}^{LAPs}$) and~~ average-daily
6 RFLS ($RF_{MODIS,daily}^{LAPs}$) during ~~January February~~December-May for the period 2003–
7 2018. For the identified snow covered area over Northern Hemisphere as a whole,
8 average $\Delta\alpha_{MODIS,corrected}^{LAPs}$ is ~~~ 0.0246021~~ , ~~$RF_{MODIS,ms}^{LAPs}$ is ~ 5.9 W m⁻²~~, and
9 $RF_{MODIS,daily}^{LAPs}$ is ~~$\sim 1.72.9$~~ W m⁻². We also observed distinct spatial variability in snow

10 albedo reduction and RFLS. The highest regional-average $\Delta\alpha_{MODIS,corrected}^{LAPs}$
11 (~~~ 0.166911~~), ~~and~~ $RF_{MODIS,daily}^{LAPs}$ (~~$\sim 11-12$ W m⁻²~~), ~~and~~ $RF_{MODIS,ms}^{LAPs}$ (~~~ 36 W m⁻²~~)
12 occur in northeastern China, while the lowest regional averages of ~~~ 0.0123016~~ and,
13 ~~$\sim 0.292.6$ W m⁻²~~, ~~and~~ ~~~ 1.1 W m⁻²~~, respectively, are observed in the Arctic. Moreover,
14 we indicated that the semi-infinite assumption could overestimates up to $\sim 25\%$ of RFLS,
15 especially for thin and patchy snow, such as midlatitudes in Eurasia and NA. In addition,
16 if the ground-based corrections were not considered, the total uncertainty of RFLS
17 retrievals is in the range of $15\%\sim 108\%$ ($-106\%\sim -20\%$) due to atmospheric correction,
18 snow cover fraction calculation and snow grain size retrieval.~~sed from atmospheric~~
19 ~~correction, snow cover fraction calculation and snow grain size retrieval, which fall~~
20 ~~in a range of $15\%\sim 108\%$ ($-106\%\sim -20\%$) if ground-based corrections were not~~
21 ~~conducted. with the positive (negative) values fall in a range of $15\%\sim 108\%$ ($-106\%\sim -20\%$)~~

~~when take into account uncertainty of atmospheric correction, snow cover fraction (FSC) calculation and snow grain size retrieval.~~

Following this assessment, we made quantitative attributions of the spatial variability in snow albedo reduction and radiative forcing. Our results indicate that the LAP content is the largest contributor (~~57.6~~84.3%) to spatial variance in snow albedo reduction, followed by snow depth (~~38.4~~13.7%), whereas snow grain size (~~2.7~~1.9%) and the geographic factor G (~~1.6~~<1%) are only minor contributors on a Northern Hemispheric scale. LAP content and G account for ~~37.2~~70.0% and ~~34.6~~22.3% of the spatial variability of radiative forcing, respectively, following by SD (~~27.9~~7.6%) over Northern Hemisphere.

Retrieved RFLS values are compared spatially with the model-derived estimates of the ~~Global Climate Model (GCM) and the Coupled Model Intercomparison Project (CMIP Phase 6)~~CESM2. Our results indicate that MODIS retrievals ~~provide~~ show the same magnitude with modeled estimates for Northern Hemisphere. However, although the Earth system models perform well in NEC, there remain large uncertainties in the Arctic. To evaluate and examine the MODIS retrievals synthetically, we then compared the retrieved RFLS to previously published estimates, including local-scale observations, remote sensing retrievals, and regional- and global-scale model simulations. The results of this evaluation suggest that MODIS retrievals are generally realistic, despite a number of important differences among the various methods.

1 Finally, we urge the community to expand the ground-based measurements of the global
2 snowpack, particularly in those regions currently lacking ~~in~~in-situ observations. Such
3 development would help further constrain and improve satellite-based retrievals in the
4 future. We propose that climate models ~~which could be validated~~ ed and developed by
5 ~~incorporating~~ these refined remote sensing retrievals should be able to capture the
6 RFLS more accurately, thereby providing more reliable estimates of the future impacts
7 of global climate change. _____

1

2

3 **Data availability.**

4 MODIS data can be found at <https://earthdata.nasa.gov/> (last access: 20 January 2019).

5 CERES data can be found from NASA's Clouds and the Earth's Radiant Energy System

6 at <https://ceres.larc.nasa.gov> (last access: 12 April 2019). Shuttle Radar Topography

7 Mission (SRTM) digital elevation data are provided by the US Geological Survey at

8 <https://www.usgs.gov/> (last access: 9 December 2018). Snow depth can be found from

9 ERA-Interim at <https://www.ecmwf.int> (last access: 15 January 2019). BC emission

10 data can be found at <http://inventory.pku.edu.cn> (last access: 5 June 2019). BC

11 deposition data can be found at <https://gmao.gsfc.nasa.gov/reanalysis/MERRA-2/> (last

12 access: 5 June 2019). CMIP6 data can be found at <https://esgf-node.llnl.gov/> (last access:

13 15 July 2019). Surface measurement datasets are from Wang et al. (2013, 2017), Ye et

14 al. (2012) and Doherty et al. (2010, 2014). Springtime radiative forcing due to LAPs in

15 snow is derived from a GCM run by Flanner et al. (2007)._____

1

2 **Author contributions.**

3 PW and WX designed the study and evolved the overarching research goals and aims.

4 CJC carried the study out and wrote the first draft with contributions from all co-authors.

5 CJC and STL applied formal techniques such as statistical, mathematical and

6 computational to analyze study data. ZY prepared input data and managed activities to

7 annotate, scrub data and maintain research data. WDY completed the implementation

8 of the computer code and supporting algorithms used for the calculations in this study.

9 PW and WX assumed oversight and leadership responsibility for the research activity

10 planning and execution. All authors contributed to the improvement of results and

11 revised the final paper._____

1

2 **Competing interests.**

3 The authors declare that they have no conflict of interest.

4 **Acknowledgments**

5 This research was supported jointly by the National Key R&D Program of China
6 (~~2019YFA0606800~~2019YFA0606801), the National Natural Science Foundation of
7 China (grants 41975157, 41775144, and 41875091), the China Postdoctoral Science
8 Foundation (2020M673530).

1

2

3 **References**

4 Bair, E. H., Rittger, K., Skiles, S. M., and Dozier, J.: An Examination of Snow Albedo
5 Estimates From MODIS and Their Impact on Snow Water Equivalent Reconstruction,
6 Water Resources Research, 10.1029/2019wr024810, 2019.

7 Barnett, T. P., Adam, J. C., and Lettenmaier, D. P.: Potential impacts of a warming
8 climate on water availability in snow-dominated regions, Nature, 438, 303-309,
9 10.1038/nature04141, 2005.

10 Berrisford, P., Kållberg, P., Kobayashi, S., Dee, D., Uppala, S., Simmons, A. J., Poli, P.,
11 and Sato, H.: Atmospheric conservation properties in ERA-Interim, Quarterly Journal
12 of the Royal Meteorological Society, 137, 1381-1399, 10.1002/qj.864, 2011.

13 Bian, H., Colarco, P. R., Chin, M., Chen, G., Rodriguez, J. M., Liang, Q., Blake, D.,
14 Chu, D. A., da Silva, A., Darmenov, A. S., Diskin, G., Fuelberg, H. E., Huey, G., Kondo,
15 Y., Nielsen, J. E., Pan, X., and Wisthaler, A.: Source attributions of pollution to the
16 Western Arctic during the NASA ARCTAS field campaign, Atmospheric Chemistry
17 and Physics, 13, 4707-4721, 10.5194/acp-13-4707-2013, 2013.

18 Bond, T. C., Habib, G., and Bergstrom, R. W.: Limitations in the enhancement of visible
19 light absorption due to mixing state, Journal of Geophysical Research, 111,
20 10.1029/2006jd007315, 2006.

1 Bond, T. C., Doherty, S. J., Fahey, D. W., Forster, P. M., Berntsen, T., DeAngelo, B. J.,
 2 Flanner, M. G., Ghan, S., Kärcher, B., Koch, D., Kinne, S., Kondo, Y., Quinn, P. K.,
 3 Sarofim, M. C., Schultz, M. G., Schulz, M., Venkataraman, C., Zhang, H., Zhang, S.,
 4 Bellouin, N., Guttikunda, S. K., Hopke, P. K., Jacobson, M. Z., Kaiser, J. W., Klimont,
 5 Z., Lohmann, U., Schwarz, J. P., Shindell, D., Storelvmo, T., Warren, S. G., and Zender,
 6 C. S.: Bounding the role of black carbon in the climate system: A scientific assessment,
 7 Journal of Geophysical Research: Atmospheres, 118, 5380-5552, 10.1002/jgrd.50171,
 8 2013.

9 Brandt, R. E., Warren, S. G., and Clarke, A. D.: A controlled snowmaking experiment
 10 testing the relation between black carbon content and reduction of snow albedo, Journal
 11 of Geophysical Research, 116, 10.1029/2010jd015330, 2011.

12 Brown, R. D., and Mote, P. W.: The Response of Northern Hemisphere Snow Cover to
 13 a Changing Climate, Journal of Climate, 22, 2124-2145, 10.1175/2008jcli2665.1, 2009.

14 Brun, E., Vionnet, V., Boone, A., Decharme, B., Peings, Y., Valette, R., Karbou, F., and
 15 Morin, S.: Simulation of Northern Eurasian Local Snow Depth, Mass, and Density
 16 Using a Detailed Snowpack Model and Meteorological Reanalyses, Journal of
 17 Hydrometeorology, 14, 203-219, 10.1175/jhm-d-12-012.1, 2013.

18 Bryant, A. C., Painter, T. H., Deems, J. S., and Bender, S. M.: Impact of dust radiative
 19 forcing in snow on accuracy of operational runoff prediction in the Upper Colorado
 20 River Basin, Geophysical Research Letters, 40, 3945-3949, 10.1002/grl.50773, 2013.

1 Chin, M., Ginoux, P., Kinne, S., Torres, O., Holben, B. N., Duncan, B. N., Martin, R.
2 V., Logan, J. A., Higurashi, A., and Nakajima, T.: Tropospheric Aerosol Optical
3 Thickness from the GOCART Model and Comparisons with Satellite and Sun
4 Photometer Measurements, *Journal of the Atmospheric Sciences*, 59, 461-483,
5 10.1175/1520-0469(2002)059<0461:taotft>2.0.co;2, 2002.

6 Colarco, P., da Silva, A., Chin, M., and Diehl, T.: Online simulations of global aerosol
7 distributions in the NASA GEOS-4 model and comparisons to satellite and ground-
8 based aerosol optical depth, *Journal of Geophysical Research*, 115,
9 10.1029/2009jd012820, 2010.

10 Colombo, R., Garzonio, R., Di Mauro, B., Dumont, M., Tuzet, F., Cogliati, S., Pozzi,
11 G., Maltese, A., and Cremonese, E.: Introducing Thermal Inertia for Monitoring
12 Snowmelt Processes With Remote Sensing, *Geophysical Research Letters*, 46, 4308-
13 4319, 10.1029/2019gl082193, 2019.

14 Danabasoglu, G., Lamarque, J. F., Bacmeister, J., Bailey, D. A., DuVivier, A. K.,
15 Edwards, J., Emmons, L. K., Fasullo, J., Garcia, R., Gettelman, A., Hannay, C., Holland,
16 M. M., Large, W. G., Lauritzen, P. H., Lawrence, D. M., Lenaerts, J. T. M., Lindsay, K.,
17 Lipscomb, W. H., Mills, M. J., Neale, R., Oleson, K. W., Otto-Bliesner, B., Phillips, A.
18 S., Sacks, W., Tilmes, S., Kampenhout, L., Vertenstein, M., Bertini, A., Dennis, J., Deser,
19 C., Fischer, C., Fox-Kemper, B., Kay, J. E., Kinnison, D., Kushner, P. J., Larson, V. E.,
20 Long, M. C., Mickelson, S., Moore, J. K., Nienhouse, E., Polvani, L., Rasch, P. J., and
21 Strand, W. G.: The Community Earth System Model Version 2 (CESM2), *Journal of*

1 [Advances in Modeling Earth Systems, 12, 10.1029/2019ms001916, 2020.](#)

2 Dang, C., Brandt, R. E., and Warren, S. G.: Parameterizations for narrowband and
3 broadband albedo of pure snow and snow containing mineral dust and black carbon,
4 Journal of Geophysical Research: Atmospheres, 120, 5446-5468,
5 10.1002/2014jd022646, 2015.

6 Dang, C., Warren, S. G., Fu, Q., Doherty, S. J., Sturm, M., and Su, J.: Measurements of
7 light-absorbing particles in snow across the Arctic, North America, and China: Effects
8 on surface albedo, J Geophys Res-Atmos, 122, 10149-10168, 2017.

9 Dee, D. P., Uppala, S. M., Simmons, A. J., Berrisford, P., Poli, P., Kobayashi, S., Andrae,
10 U., Balmaseda, M. A., Balsamo, G., Bauer, P., Bechtold, P., Beljaars, A. C. M., van de
11 Berg, L., Bidlot, J., Bormann, N., Delsol, C., Dragani, R., Fuentes, M., Geer, A. J.,
12 Haimberger, L., Healy, S. B., Hersbach, H., Hólm, E. V., Isaksen, L., Kållberg, P.,
13 Köhler, M., Matricardi, M., McNally, A. P., Monge-Sanz, B. M., Morcrette, J. J., Park,
14 B. K., Peubey, C., de Rosnay, P., Tavolato, C., Thépaut, J. N., and Vitart, F.: The ERA-
15 Interim reanalysis: configuration and performance of the data assimilation system,
16 Quarterly Journal of the Royal Meteorological Society, 137, 553-597, 10.1002/qj.828,
17 2011.

18 Deems, J. S., Painter, T. H., Barsugli, J. J., Belnap, J., and Udall, B.: Combined impacts
19 of current and future dust deposition and regional warming on Colorado River Basin
20 snow dynamics and hydrology, Hydrology and Earth System Sciences, 17, 4401-4413,

1 10.5194/hess-17-4401-2013, 2013.

2 Di Mauro, B., Fava, F., Ferrero, L., Garzonio, R., Baccolo, G., Delmonte, B., and
3 Colombo, R.: Mineral dust impact on snow radiative properties in the European Alps
4 combining ground, UAV, and satellite observations, *Journal of Geophysical Research:*
5 *Atmospheres*, 120, 6080-6097, 10.1002/2015jd023287, 2015.

6 Di Mauro, B., Baccolo, G., Garzonio, R., Giardino, C., Massabò, D., Piazzalunga, A.,
7 Rossini, M., and Colombo, R.: Impact of impurities and cryoconite on the optical
8 properties of the Morteratsch Glacier (Swiss Alps), *The Cryosphere*, 11, 2393-2409,
9 10.5194/tc-11-2393-2017, 2017.

10 Di Mauro, B., Garzonio, R., Rossini, M., Filippa, G., Pogliotti, P., Galvagno, M., Morra
11 di Cella, U., Migliavacca, M., Baccolo, G., Clemenza, M., Delmonte, B., Maggi, V.,
12 Dumont, M., Tuzet, F., Lafaysse, M., Morin, S., Cremonese, E., and Colombo, R.:
13 Saharan dust events in the European Alps: role in snowmelt and geochemical
14 characterization, *The Cryosphere*, 13, 1147-1165, 10.5194/tc-13-1147-2019, 2019.

15 Doelling, D. R., Loeb, N. G., Keyes, D. F., Nordeen, M. L., Morstad, D., Nguyen, C.,
16 Wielicki, B. A., Young, D. F., and Sun, M.: Geostationary Enhanced Temporal
17 Interpolation for CERES Flux Products, *Journal of Atmospheric and Oceanic*
18 *Technology*, 30, 1072-1090, 10.1175/jtech-d-12-00136.1, 2013.

19 Doherty, S. J., Warren, S. G., Grenfell, T. C., Clarke, A. D., and Brandt, R. E.: Light-
20 absorbing impurities in Arctic snow, *Atmospheric Chemistry and Physics*, 10, 11647-

1 11680, 10.5194/acp-10-11647-2010, 2010.

2 Doherty, S. J., Dang, C., Hegg, D. A., Zhang, R., and Warren, S. G.: Black carbon and
3 other light-absorbing particles in snow of central North America, *Journal of*
4 *Geophysical Research: Atmospheres*, 119, 12,807-812,831, 10.1002/2014jd022350,
5 2014.

6 Dozier, J., and Marks, D.: Snow Mapping and Classification from Landsat Thematic
7 Mapper Data, *Annals of Glaciology*, 9, 97-103,
8 <https://doi.org/10.3189/S026030550000046X>, 1987.

9 Drusch, M., Vasiljevic, D., and Viterbo, P.: ECMWF's Global Snow Analysis:
10 Assessment and Revision Based on Satellite Observations, *Journal of Applied*
11 *Meteorology*, 43, 1282-1294, 10.1175/1520-0450(2004)043<1282:egsaaa>2.0.co;2,
12 2004.

13 Eyring, V., Bony, S., Meehl, G. A., Senior, C. A., Stevens, B., Stouffer, R. J., and Taylor,
14 K. E.: Overview of the Coupled Model Intercomparison Project Phase 6 (CMIP6)
15 experimental design and organization, *Geosci Model Dev*, 9, 1937-1958, 10.5194/gmd-
16 9-1937-2016, 2016.

17 Flanner, M. G., Zender, C. S., Randerson, J. T., and Rasch, P. J.: Present-day climate
18 forcing and response from black carbon in snow, *Journal of Geophysical Research*, 112,
19 10.1029/2006jd008003, 2007.

20 Flanner, M. G., Zender, C. S., Hess, P. G., Mahowald, N. M., Painter, T. H., Ramanathan,

1 V., and Rasch, P. J.: Springtime warming and reduced snow cover from carbonaceous
2 particles, *Atmospheric Chemistry and Physics*, 9, 2481-2497, 10.5194/acp-9-2481-
3 2009, 2009.

4 Flanner, M. G., Shell, K. M., Barlage, M., Perovich, D. K., and Tschudi, M. A.:
5 Radiative forcing and albedo feedback from the Northern Hemisphere cryosphere
6 between 1979 and 2008, *Nature Geoscience*, 4, 151-155, 10.1038/ngeo1062, 2011.

7 Flanner, M. G., Gardner, A. S., Eckhardt, S., Stohl, A., and Perket, J.: Aerosol radiative
8 forcing from the 2010 Eyjafjallajökull volcanic eruptions, *Journal of Geophysical*
9 *Research: Atmospheres*, 119, 9481-9491, 10.1002/2014jd021977, 2014.

10 Fu, Y., Zhu, J., Yang, Y., Yuan, R., Liu, G., Xian, T., and Liu, P.: Grid-cell aerosol direct
11 shortwave radiative forcing calculated using the SBDART model with MODIS and
12 AERONET observations: An application in winter and summer in eastern China,
13 *Advances in Atmospheric Sciences*, 34, 952-964, 10.1007/s00376-017-6226-z, 2017.

14 Ganey, G. Q., Loso, M. G., Burgess, A. B., and Dial, R. J.: The role of microbes in
15 snowmelt and radiative forcing on an Alaskan icefield, *Nature Geoscience*, 10, 754-759,
16 10.1038/ngeo3027, 2017.

17 Grell, G. A., Peckham, S. E., Schmitz, R., McKeen, S. A., Frost, G., Skamarock, W. C.,
18 and Eder, B.: Fully coupled “online” chemistry within the WRF model, *Atmospheric*
19 *Environment*, 39, 6957-6975, 10.1016/j.atmosenv.2005.04.027, 2005.

20 Grenfell, T. C., Doherty, S. J., Clarke, A. D., and Warren, S. G.: Light absorption from

- 1 [particulate impurities in snow and ice determined by spectrophotometric analysis of](#)
2 [filters, Appl Opt, 50, 2037-2048, 10.1364/AO.50.002037, 2011.](#)
- 3 Hadley, O. L., and Kirchstetter, T. W.: Black-carbon reduction of snow albedo, Nature
4 Climate Change, 2, 437-440, 10.1038/nclimate1433, 2012.
- 5 Hall, A., and Qu, X.: Using the current seasonal cycle to constrain snow albedo
6 feedback in future climate change, Geophysical Research Letters, 33,
7 10.1029/2005gl025127, 2006.
- 8 Hall, D. K., Riggs, G. A., and Salomonson, V. V.: Development of methods for mapping
9 global snow cover using moderate resolution imaging spectroradiometer data, Remote
10 Sensing of Environment, 54, 127-140, 10.1016/0034-4257(95)00137-p, 1995.
- 11 Hansen, J., and Nazarenko, L.: Soot climate forcing via snow and ice albedos, P Natl
12 Acad Sci USA, 101, 423-428, 2004.
- 13 [Hegg, D. A., Warren, S. G., Grenfell, T. C., Doherty, S. J., Larson, T. V., and Clarke, A.](#)
14 [D.: Source attribution of black carbon in Arctic snow, Environ Sci Technol, 43, 4016-](#)
15 [4021, 10.1021/es803623f, 2009.](#)
- 16 Huang, J. P. and Yi, Y. H.: Inversion of a nonlinear dynamic-model from the observation,
17 Sci. China Chem., 34, 1246–1246, 1991.
- 18 Huang, J., Fu, Q., Zhang, W., Wang, X., Zhang, R., Ye, H., and Warren, S. G.: Dust and
19 Black Carbon in Seasonal Snow Across Northern China, Bulletin of the American
20 Meteorological Society, 92, 175-181, 10.1175/2010bams3064.1, 2011.

1 Kaspari, S., Painter, T. H., Gysel, M., Skiles, S. M., and Schwikowski, M.: Seasonal
2 and elevational variations of black carbon and dust in snow and ice in the Solu-Khumbu,
3 Nepal and estimated radiative forcings, *Atmospheric Chemistry and Physics*, 14, 8089-
4 8103, 10.5194/acp-14-8089-2014, 2014.

5 Kaspari, S., McKenzie Skiles, S., Delaney, I., Dixon, D., and Painter, T. H.: Accelerated
6 glacier melt on Snow Dome, Mount Olympus, Washington, USA, due to deposition of
7 black carbon and mineral dust from wildfire, *Journal of Geophysical Research:*
8 *Atmospheres*, 120, 2793-2807, 10.1002/2014jd022676, 2015.

9 Lee, L. A., Reddington, C. L., and Carslaw, K. S.: On the relationship between aerosol
10 model uncertainty and radiative forcing uncertainty, *Proc Natl Acad Sci U S A*, 113,
11 5820-5827, 10.1073/pnas.1507050113, 2016.

12 Lewis, P., and Barnsley, M.: Influence of the sky radiance distribution on various
13 formulations of the earth surface albedo, 6th International Symposium on Physical
14 Measurements and Signatures in Remote Sensing, ISPRS, 1994, 707-715,

15 Liou, K. N., Takano, Y., He, C., Yang, P., Leung, L. R., Gu, Y., and Lee, W. L.:
16 Stochastic parameterization for light absorption by internally mixed BC/dust in snow
17 grains for application to climate models, *Journal of Geophysical Research:*
18 *Atmospheres*, 119, 7616-7632, 10.1002/2014jd021665, 2014.

19 Loeb, N. G., Doelling, D. R., Wang, H., Su, W., Nguyen, C., Corbett, J. G., Liang, L.,
20 Mitrescu, C., Rose, F. G., and Kato, S.: Clouds and the Earth's Radiant Energy System

1 (CERES) Energy Balanced and Filled (EBAF) Top-of-Atmosphere (TOA) Edition-4.0
2 Data Product, *Journal of Climate*, 31, 895-918, 10.1175/jcli-d-17-0208.1, 2018.

3 Meinander, O., Kazadzis, S., Arola, A., Riihelä, A., Räisänen, P., Kivi, R., Kontu, A.,
4 Kouznetsov, R., Sofiev, M., Svensson, J., Suokanerva, H., Aaltonen, V., Manninen, T.,
5 Roujean, J. L., and Hautecoeur, O.: Spectral albedo of seasonal snow during intensive
6 melt period at Sodankylä, beyond the Arctic Circle, *Atmospheric Chemistry and*
7 *Physics*, 13, 3793-3810, 10.5194/acp-13-3793-2013, 2013.

8 Miller, S. D., Wang, F., Burgess, A. B., Skiles, S. M., Rogers, M., and Painter, T. H.:
9 Satellite-Based Estimation of Temporally Resolved Dust Radiative Forcing in Snow
10 Cover, *Journal of Hydrometeorology*, 17, 1999-2011, 2016.

11 Nagorski, S. A., Kaspari, S. D., Hood, E., Fellman, J. B., and Skiles, S. M.: Radiative
12 Forcing by Dust and Black Carbon on the Juneau Icefield, Alaska, *Journal of*
13 *Geophysical Research: Atmospheres*, 124, 3943-3959, 10.1029/2018jd029411, 2019.

14 Negi, H. S., and Kokhanovsky, A.: Retrieval of snow grain size and albedo of western
15 Himalayan snow cover using satellite data, *The Cryosphere*, 5, 831-847, 10.5194/tc-5-
16 831-2011, 2011.

17 Nolin, A. W., and Dozier, J.: Estimating snow grain size using AVIRIS data, *Remote*
18 *Sensing of Environment*, 44, 231-238, 10.1016/0034-4257(93)90018-s, 1993.

19 Nolin, A. W., and Dozier, J.: A Hyperspectral Method for Remotely Sensing the Grain
20 Size of Snow, *Remote Sensing of Environment*, 74, 207-216, 10.1016/s0034-

1 4257(00)00111-5, 2000.

2 Nowottnick, E., Colarco, P., Ferrare, R., Chen, G., Ismail, S., Anderson, B., and Browell,
3 E.: Online simulations of mineral dust aerosol distributions: Comparisons to NAMMA
4 observations and sensitivity to dust emission parameterization, *Journal of Geophysical*
5 *Research*, 115, 10.1029/2009jd012692, 2010.

6 Nowottnick, E., Colarco, P., da Silva, A., Hlavka, D., and McGill, M.: The fate of
7 saharan dust across the atlantic and implications for a central american dust barrier,
8 *Atmospheric Chemistry and Physics*, 11, 8415-8431, 10.5194/acp-11-8415-2011, 2011.

9 Oaida, C. M., Xue, Y., Flanner, M. G., Skiles, S. M., De Sales, F., and Painter, T. H.:
10 Improving snow albedo processes in WRF/SSiB regional climate model to assess
11 impact of dust and black carbon in snow on surface energy balance and hydrology over
12 western U.S, *Journal of Geophysical Research: Atmospheres*, 120, 3228-3248,
13 10.1002/2014jd022444, 2015.

14 Painter, T. H., Roberts, D. A., Green, R. O., and Dozier, J.: The Effect of Grain Size on
15 Spectral Mixture Analysis of Snow-Covered Area from AVIRIS Data, *Remote Sensing*
16 *of Environment*, 65, 320-332, 10.1016/s0034-4257(98)00041-8, 1998.

17 Painter, T. H., Barrett, A. P., Landry, C. C., Neff, J. C., Cassidy, M. P., Lawrence, C. R.,
18 McBride, K. E., and Farmer, G. L.: Impact of disturbed desert soils on duration of
19 mountain snow cover, *Geophysical Research Letters*, 34, 10.1029/2007gl030284, 2007.

20 Painter, T. H., Rittger, K., McKenzie, C., Slaughter, P., Davis, R. E., and Dozier, J.:

1 Retrieval of subpixel snow covered area, grain size, and albedo from MODIS, Remote
2 Sensing of Environment, 113, 868-879, 10.1016/j.rse.2009.01.001, 2009.

3 Painter, T. H., Deems, J. S., Belnap, J., Hamlet, A. F., Landry, C. C., and Udall, B.:
4 Response of Colorado River runoff to dust radiative forcing in snow, Proc Natl Acad
5 Sci U S A, 107, 17125-17130, 10.1073/pnas.0913139107, 2010.

6 Painter, T. H., Bryant, A. C., and Skiles, S. M.: Radiative forcing by light absorbing
7 impurities in snow from MODIS surface reflectance data, Geophysical Research
8 Letters, 39, n/a-n/a, 10.1029/2012gl052457, 2012a.

9 Painter, T. H., Skiles, S. M., Deems, J. S., Bryant, A. C., and Landry, C. C.: Dust
10 radiative forcing in snow of the Upper Colorado River Basin: 1. A 6 year record of
11 energy balance, ~~radiation~~radiances, and dust concentrations, Water Resources Research,
12 48, 10.1029/2012wr011985, 2012b.

13 Painter, T. H., Seidel, F. C., Bryant, A. C., McKenzie Skiles, S., and Rittger, K.: Imaging
14 spectroscopy of albedo and radiative forcing by light-absorbing impurities in mountain
15 snow, Journal of Geophysical Research: Atmospheres, 118, 9511-9523,
16 10.1002/jgrd.50520, 2013.

17 Pu, W., Wang, X., Wei, H., Zhou, Y., Shi, J., Hu, Z., Jin, H., and Chen, Q.: Properties
18 of black carbon and other insoluble light-absorbing particles in seasonal snow of
19 northwestern China, The Cryosphere, 11, 1213-1233, 10.5194/tc-11-1213-2017, 2017.

20 Pu, W., Cui, J., Shi, T., Zhang, X., He, C., and Wang, X.: The remote sensing of radiative

1 forcing by light-absorbing particles (LAPs) in seasonal snow over northeastern China,
2 Atmospheric Chemistry and Physics, 19, 9949-9968, 10.5194/acp-19-9949-2019, 2019.

3 Qi, L., Li, Q., Henze, D. K., Tseng, H.-L., and He, C.: Sources of springtime surface
4 black carbon in the Arctic: an adjoint analysis for April 2008, Atmospheric Chemistry
5 and Physics, 17, 9697-9716, 10.5194/acp-17-9697-2017, 2017.

6 Qian, Y., Gustafson, W. I., Leung, L. R., and Ghan, S. J.: Effects of soot-induced snow
7 albedo change on snowpack and hydrological cycle in western United States based on
8 Weather Research and Forecasting chemistry and regional climate simulations, Journal
9 of Geophysical Research, 114, 10.1029/2008jd011039, 2009.

10 Qian, Y., Flanner, M. G., Leung, L. R., and Wang, W.: Sensitivity studies on the impacts
11 of Tibetan Plateau snowpack pollution on the Asian hydrological cycle and monsoon
12 climate, Atmospheric Chemistry and Physics, 11, 1929-1948, 10.5194/acp-11-1929-
13 2011, 2011.

14 Qian, Y., Wang, H., Zhang, R., Flanner, M. G., and Rasch, P. J.: A sensitivity study on
15 modeling black carbon in snow and its radiative forcing over the Arctic and Northern
16 China, Environmental Research Letters, 9, 064001, 10.1088/1748-9326/9/6/064001,
17 2014.

18 Qian, Y., Yasunari, T. J., Doherty, S. J., Flanner, M. G., Lau, W. K. M., Ming, J., Wang,
19 H., Wang, M., Warren, S. G., and Zhang, R.: Light-absorbing particles in snow and ice:
20 Measurement and modeling of climatic and hydrological impact, Advances in

1 Atmospheric Sciences, 32, 64-91, 10.1007/s00376-014-0010-0, 2015.

2 Ramanathan, V., and Carmichael, G.: Global and regional climate changes due to black
3 carbon, Nature Geoscience, 1, 221-227, 10.1038/ngeo156, 2008.

4 Randles, C. A., da Silva, A. M., Buchard, V., Colarco, P. R., Darmenov, A., Govindaraju,
5 R., Smirnov, A., Holben, B., Ferrare, R., Hair, J., Shinozuka, Y., and Flynn, C. J.: The
6 MERRA-2 Aerosol Reanalysis, 1980 Onward. Part I: System Description and Data
7 Assimilation Evaluation, Journal of Climate, 30, 6823-6850, 10.1175/jcli-d-16-0609.1,
8 2017.

9 Ricchiazzi, P., Yang, S., Gautier, C., and Sowle, D.: SBDART: A Research and Teaching
10 Software Tool for Plane-Parallel Radiative Transfer in the Earth's Atmosphere, Bulletin
11 of the American Meteorological Society, 79, 2101-2114, 10.1175/1520-
12 0477(1998)079<2101:sarats>2.0.co;2, 1998.

13 [Riggs G A, Hall D K, Román M O. MODIS snow products collection 6 user guide.](#)
14 [National Snow and Ice Data Center: Boulder, CO, USA, 2016.](#)

15 Rittger, K., Painter, T. H., and Dozier, J.: Assessment of methods for mapping snow
16 cover from MODIS, Advances in Water Resources, 51, 367-
17 380,10.1016/j.advwatres.2012.03.002, 2013.

18 Sarangi, C., Qian, Y., Rittger, K., Bormann, K. J., Liu, Y., Wang, H., Wan, H., Lin, G.,
19 and Painter, T. H.: Impact of light-absorbing particles on snow albedo darkening and
20 associated radiative forcing over high-mountain Asia: high-resolution WRF-Chem

1 modeling and new satellite observations, *Atmospheric Chemistry and Physics*, 19,
2 7105-7128, 10.5194/acp-19-7105-2019, 2019.

3 Seidel, F. C., Rittger, K., Skiles, S. M., Molotch, N. P., and Painter, T. H.: Case study
4 of spatial and temporal variability of snow cover, grain size, albedo and radiative
5 forcing in the Sierra Nevada and Rocky Mountain snowpack derived from imaging
6 spectroscopy, *The Cryosphere*, 10, 1229-1244, 10.5194/tc-10-1229-2016, 2016.

7 Siegmund, A. and Menz, G.: Fernes nah gebracht–Satelliten-undLuftbildeinsatz zur
8 Analyse von Umweltveränderungen im Geographieunterricht, *Geographie und Schule*,
9 154, 2–10, 2005.

10 [Shi, T., Pu, W., Zhou, Y., Cui, J., Zhang, D., and Wang, X.: Albedo of Black Carbon-](#)
11 [Contaminated Snow Across Northwestern China and the Validation With Model](#)
12 [Simulation, *Journal of Geophysical Research: Atmospheres*, 125, e2019JD032065,](#)
13 [10.1029/2019JD032065, 2020.](#)

14 Skamarock, W. C., Klemp, J. B., Dudhia, J., Gill, D. O., Barker, D. M., Duda, M. G.,
15 Huang, X., Wang, W., and Powers, J. G.: A description of the advanced research WRF
16 version 3, NCAR Tech. Note, NCAR/TN-475+STR, 8 pp., Natl. Cent. for Atmos. Res.,
17 Boulder, Colo., 2008 (available at:
18 http://www.mmm.ucar.edu/wrf/users/docs/arw_v3.pdf)

19 Skiles, S. M., and Painter, T.: Daily evolution in dust and black carbon content, snow
20 grain size, and snow albedo during snowmelt, Rocky Mountains, Colorado, *J Glaciol*,

63, 118-132, 10.1017/jog.2016.125, 2016.

Skiles, S. M., Flanner, M., Cook, J. M., Dumont, M., and Painter, T. H.: Radiative forcing by light-absorbing particles in snow, *Nature Climate Change*, 8, 964-971, 10.1038/s41558-018-0296-5, 2018.

Solomos, S., Ansmann, A., Mamouri, R.-E., Binietoglou, I., Patlakas, P., Marinou, E., and Amiridis, V.: Remote sensing and modelling analysis of the extreme dust storm hitting the Middle East and eastern Mediterranean in September 2015, *Atmospheric Chemistry and Physics*, 17, 4063-4079, 10.5194/acp-17-4063-2017, 2017.

Stamnes, K., Tsay, S. C., Wiscombe, W., and Jayaweera, K.: Numerically stable algorithm for discrete-ordinate-method radiative transfer in multiple scattering and emitting layered media, *Appl Opt*, 27, 2502-2509, 10.1364/AO.27.002502, 1988.

Sterle, K. M., McConnell, J. R., Dozier, J., Edwards, R., and Flanner, M. G.: Retention and radiative forcing of black carbon in eastern Sierra Nevada snow, *The Cryosphere*, 7, 365-374, 10.5194/tc-7-365-2013, 2013.

Sturm, M., Holmgren, J., and Liston, G. E.: A Seasonal Snow Cover Classification System for Local to Global Applications, *Journal of Climate*, 8, 1261-1283, 10.1175/1520-0442(1995)008<1261:assccs>2.0.co;2, 1995.

Su, W., Corbett, J., Eitzen, Z., and Liang, L.: Next-generation angular distribution models for top-of-atmosphere radiative flux calculation from CERES instruments: validation, *Atmospheric Measurement Techniques*, 8, 3297-3313, 10.5194/amt-8-3297-

1 2015, 2015.

2 Tanré, D., Deroo, C., Duhaut, P., Herman, M., Morcrette, J. J., Perbos, J., and
3 Deschamps, P. Y.: Technical note Description of a computer code to simulate the
4 satellite signal in the solar spectrum: the 5S code, International Journal of Remote
5 Sensing, 11, 659-668, 10.1080/01431169008955048, 1990.

6 Tedesco, M., and Kokhanovsky, A. A.: The semi-analytical snow retrieval algorithm
7 and its application to MODIS data, Remote Sensing of Environment, 111, 228-241,
8 10.1016/j.rse.2007.02.036, 2007.

9 Teillet, P. M., Guindon, B., and Goodenough, D. G.: On the Slope-Aspect Correction
10 of Multispectral Scanner Data, Canadian Journal of Remote Sensing, 8, 84-106,
11 10.1080/07038992.1982.10855028, 1982.

12 Toon, O. B., McKay, C. P., Ackerman, T. P., and Santhanam, K.: Rapid calculation of
13 radiative heating rates and photodissociation rates in inhomogeneous multiple
14 scattering atmospheres, Journal of Geophysical Research, 94, 16287,
15 10.1029/JD094iD13p16287, 1989.

16 ~~Wang, H. L., Rasch, P. J., Easter, R. C., Singh, B., Zhang, R. D., Ma, P. L., Qian, Y.,~~
17 ~~Ghan, S. J., and Beagley, N.: Using an explicit emission tagging method in global~~
18 ~~modeling of source-receptor relationships for black carbon in the Arctic: Variations,~~
19 ~~sources, and transport pathways, J Geophys Res Atmos, 119, 12888-12909, 2014a.~~

20 Wang, R., Tao, S., Shen, H., Wang, X., Li, B., Shen, G., Wang, B., Li, W., Liu, X.,

1 Huang, Y., Zhang, Y., Lu, Y., and Ouyang, H.: Global emission of black carbon from
2 motor vehicles from 1960 to 2006, *Environ Sci Technol*, 46, 1278-1284,
3 10.1021/es2032218, 2012.

4 Wang, R., Tao, S., Ciais, P., Shen, H. Z., Huang, Y., Chen, H., Shen, G. F., Wang, B.,
5 Li, W., Zhang, Y. Y., Lu, Y., Zhu, D., Chen, Y. C., Liu, X. P., Wang, W. T., Wang, X. L.,
6 Liu, W. X., Li, B. G., and Piao, S. L.: High-resolution mapping of combustion processes
7 and implications for CO₂ emissions, *Atmospheric Chemistry and Physics*, 13, 5189-
8 5203, 10.5194/acp-13-5189-2013, 2013a.

9 Wang, R., Tao, S., Shen, H., Huang, Y., Chen, H., Balkanski, Y., Boucher, O., Ciais, P.,
10 Shen, G., Li, W., Zhang, Y., Chen, Y., Lin, N., Su, S., Li, B., Liu, J., and Liu, W.: Trend
11 in global black carbon emissions from 1960 to 2007, *Environ Sci Technol*, 48, 6780-
12 6787, 10.1021/es5021422, 2014^{ab}.

13 Wang, X., Doherty, S. J., and Huang, J.: Black carbon and other light-absorbing
14 impurities in snow across Northern China, *Journal of Geophysical Research:*
15 *Atmospheres*, 118, 1471-1492, 10.1029/2012jd018291, 2013b.

16 Wang, X., Pu, W., Ren, Y., Zhang, X., Zhang, X., Shi, J., Jin, H., Dai, M., and Chen, Q.:
17 Observations and model simulations of snow albedo reduction in seasonal snow due to
18 insoluble light-absorbing particles during 2014 Chinese survey, *Atmospheric*
19 *Chemistry and Physics*, 17, 2279-2296, 10.5194/acp-17-2279-2017, 2017.

20 Wang, X., Wei, H. L., Liu, J., Xu, B. Q., Wang, M., Ji, M. X., and Jin, H. C.: Quantifying

the light absorption and source attribution of insoluble light-absorbing particles on Tibetan Plateau glaciers between 2013 and 2015, Cryosphere, 13, 309-324, 10.5194/tc-13-309-2019, 2019.

Wang, X., Xu, B., and Ming, J.: An overview of the studies on black carbon and mineral dust deposition in snow and ice cores in East Asia, Journal of Meteorological Research, 28, 354-370, 10.1007/s13351-014-4005-7, 2014b.

Wang, X., Zhang, X., and Di, W.: Development of an improved two-sphere integration technique for quantifying black carbon concentrations in the atmosphere and seasonal snow, Atmospheric Measurement Techniques, 13, 39-52, 10.5194/amt-13-39-2020, 2020.

Warneke, C., Froyd, K. D., Brioude, J., Bahreini, R., Brock, C. A., Cozic, J., de Gouw, J. A., Fahey, D. W., Ferrare, R., Holloway, J. S., Middlebrook, A. M., Miller, L., Montzka, S., Schwarz, J. P., Sodemann, H., Spackman, J. R., and Stohl, A.: An important contribution to springtime Arctic aerosol from biomass burning in Russia, Geophysical Research Letters, 37, n/a-n/a, 10.1029/2009gl041816, 2010.

Warren, S. G.: Optical properties of snow, Reviews of Geophysics, 20, 67, 10.1029/RG020i001p00067, 1982.

Warren, S. G.: Impurities in Snow: Effects on Albedo and Snowmelt (Review), Annals of Glaciology, 5, 177-179, 10.3189/1984AoG5-1-177-179, 1984.

Warren, S. G., and Brandt, R. E.: Optical constants of ice from the ultraviolet to the

1 microwave: A revised compilation, Journal of Geophysical Research, 113,
2 10.1029/2007jd009744, 2008.

3 Warren, S. G.: Can black carbon in snow be detected by remote sensing?, Journal of
4 Geophysical Research: Atmospheres, 118, 779-786, 10.1029/2012jd018476, 2013.

5 Wiscombe, W. J., and Warren, S. G.: A Model for the Spectral Albedo of Snow. I: Pure
6 Snow, Journal of the Atmospheric Sciences, 37, 2712-2733, 10.1175/1520-
7 0469(1980)037<2712:amftsa>2.0.co;2, 1980.

8 Ye, H., Zhang, R., Shi, J., Huang, J., Warren, S. G., and Fu, Q.: Black carbon in seasonal
9 snow across northern Xinjiang in northwestern China, Environmental Research Letters,
10 7, 044002, 10.1088/1748-9326/7/4/044002, 2012.

11 Zhao, C., Hu, Z., Qian, Y., Ruby Leung, L., Huang, J., Huang, M., Jin, J., Flanner, M.
12 G., Zhang, R., Wang, H., Yan, H., Lu, Z., and Streets, D. G.: Simulating black carbon
13 and dust and their radiative forcing in seasonal snow: a case study over North China
14 with field campaign measurements, Atmospheric Chemistry and Physics, 14, 11475-
15 11491, 10.5194/acp-14-11475-2014, 2014.

16 Zhong, E., Li, Q., Sun, S., Chen, S., and Chen, W.: Analysis of euphotic depth in snow
17 with SNICAR transfer scheme, Atmospheric Science Letters, 18, 484-490,
18 10.1002/asl.792, 2017.

19 Zhou, Y., Wen, H., Liu, J., Pu, W., Chen, Q. C., and Wang, X.: The optical characteristics
20 and sources of chromophoric dissolved organic matter (CDOM) in seasonal snow of

1 [northwestern China, Cryosphere, 13, 157-175, 10.5194/tc-13-157-2019, 2019.](#)

2 Zhu, C., Kobayashi, H., Kanaya, Y., and Saito, M.: Size-dependent validation of
3 MODIS MCD64A1 burned area over six vegetation types in boreal Eurasia: Large
4 underestimation in croplands, Sci Rep, 7, 4181, 10.1038/s41598-017-03739-0, 2017.

5

6

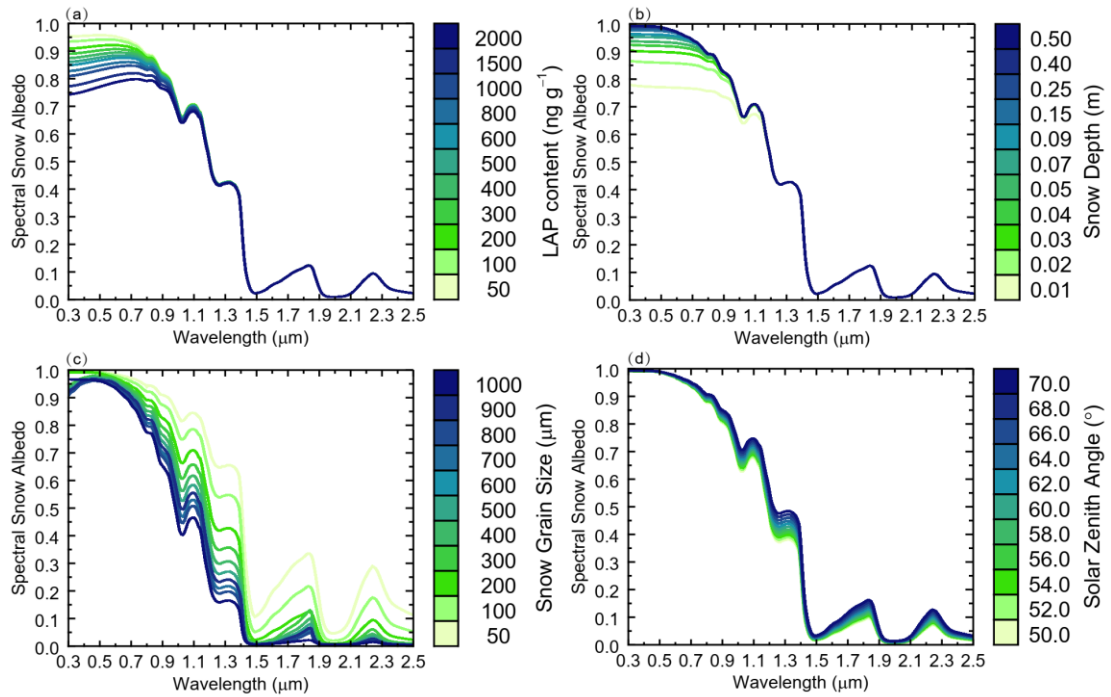
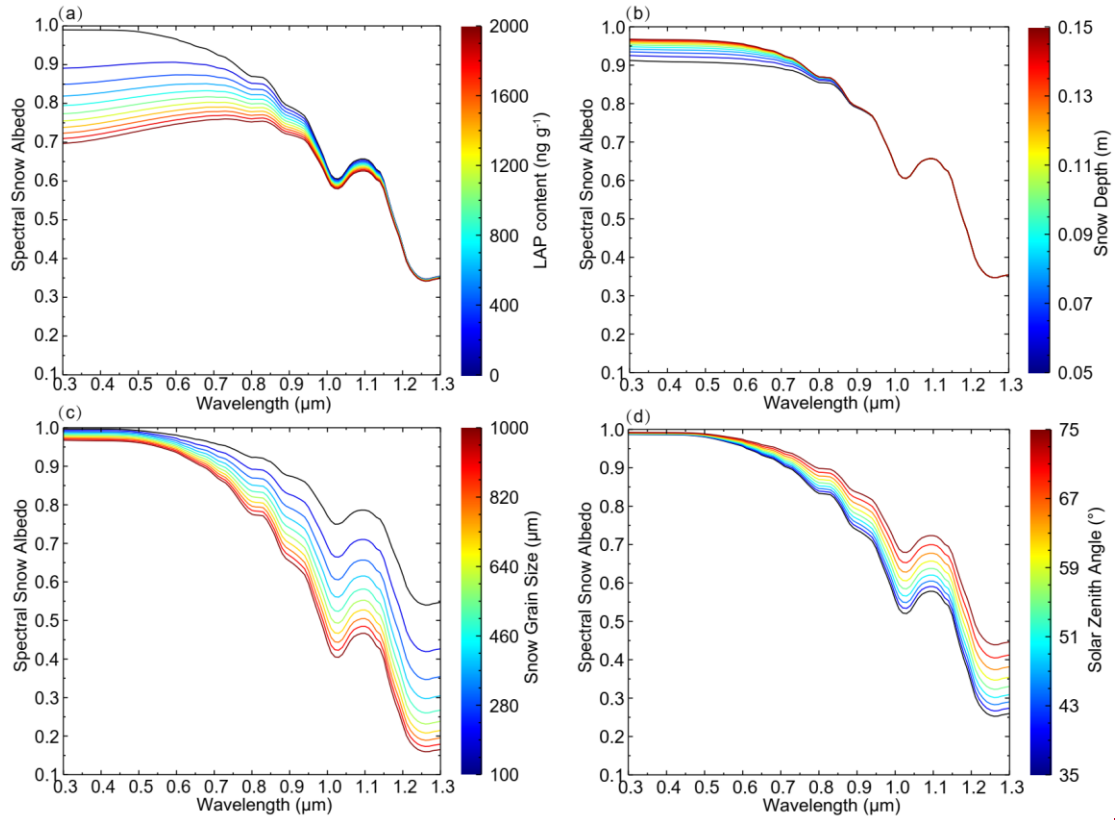
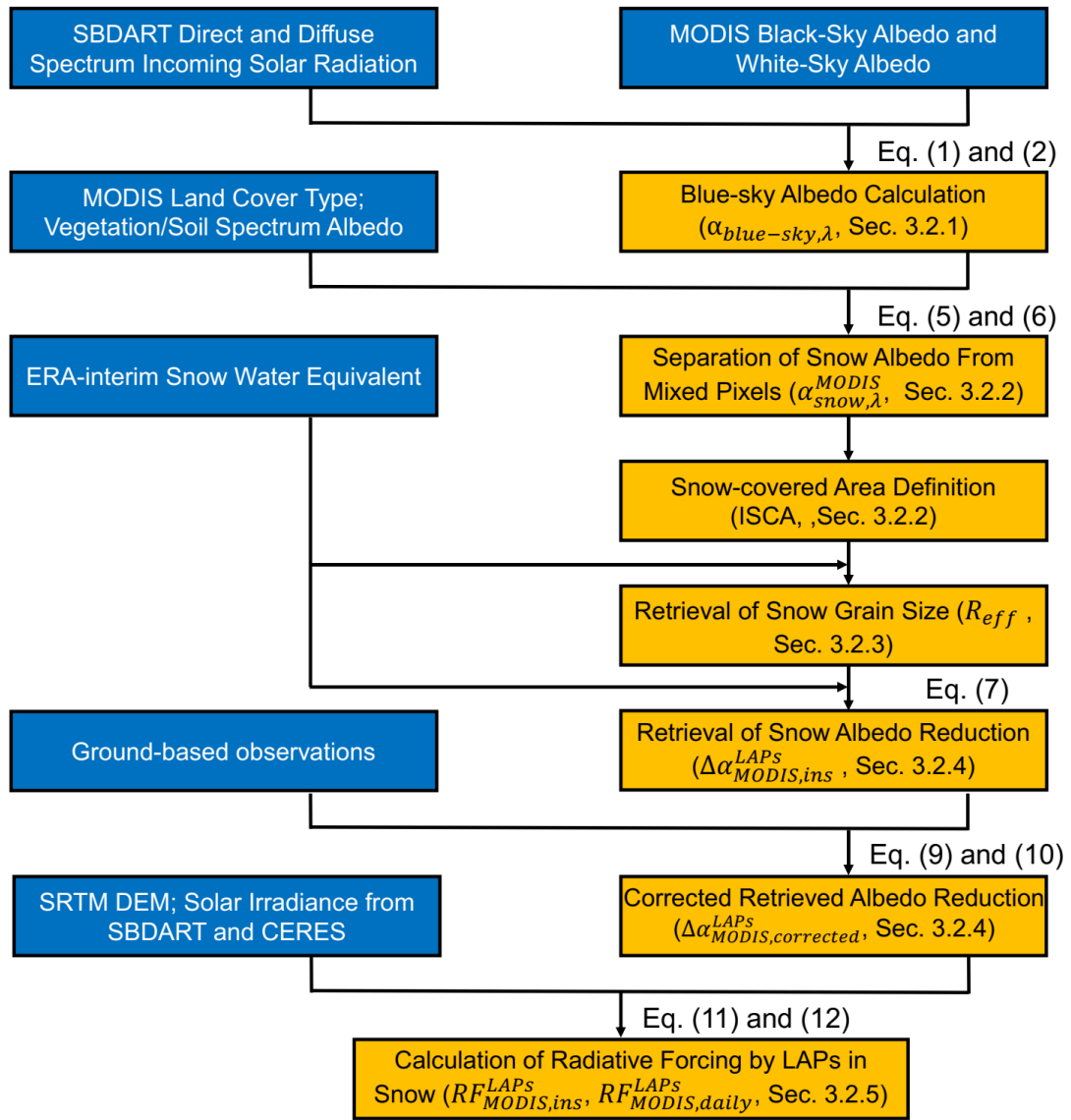


Figure 1. Variations in spectral snow albedo due to (a) LAP content (ng g^{-1}), (b) snow depth (m), (c) snow grain size (μm), and (d) solar zenith ~~angel~~angle (deg.).



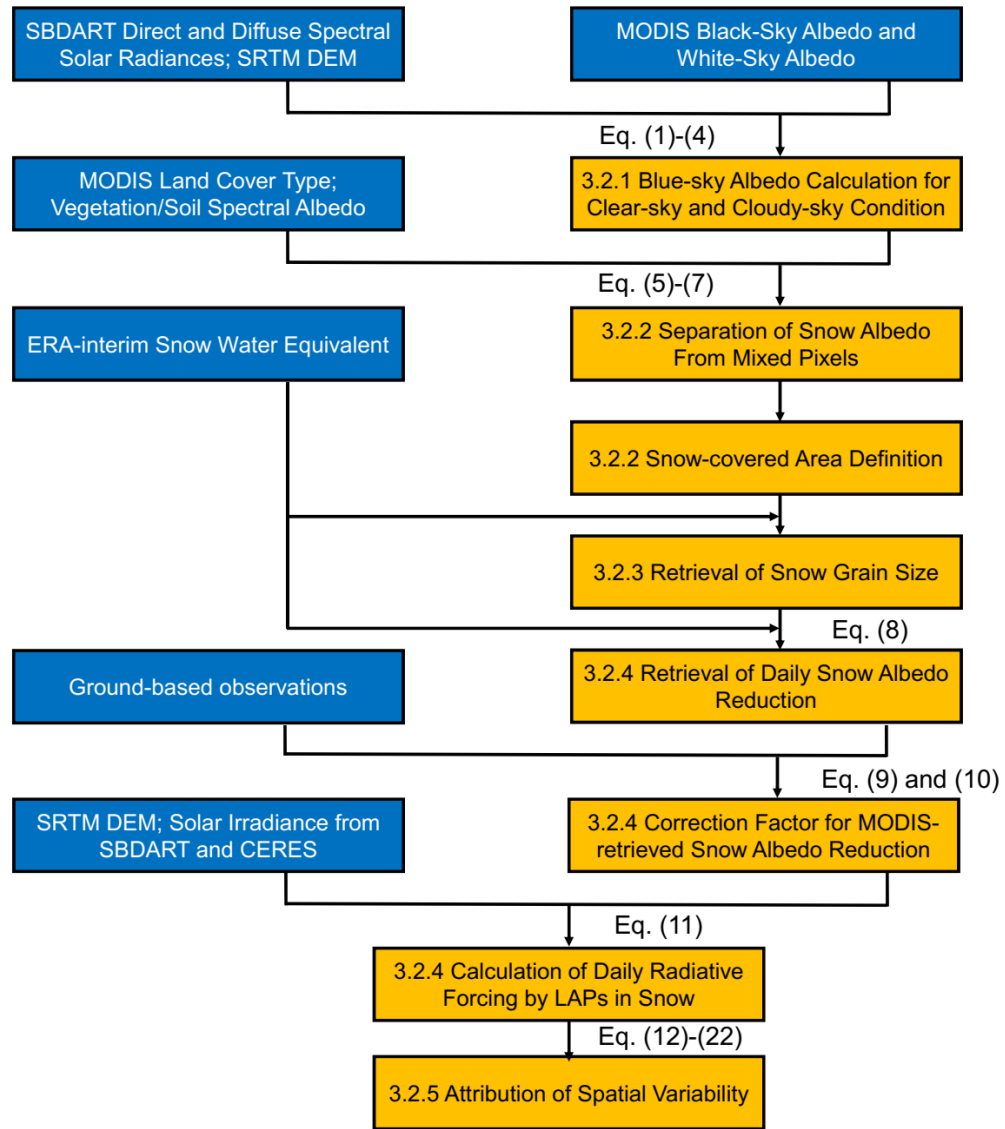
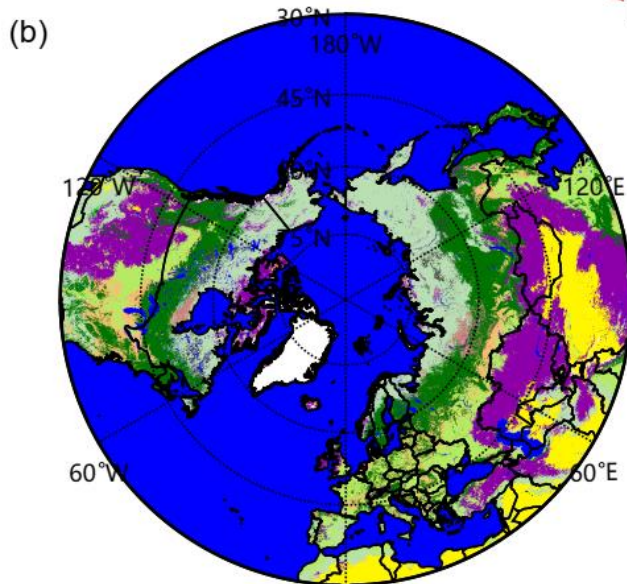
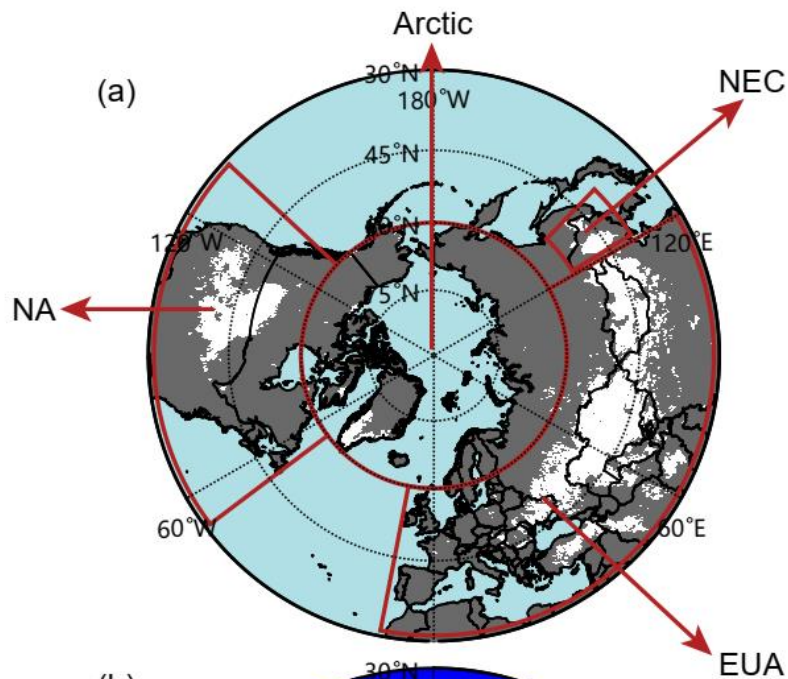
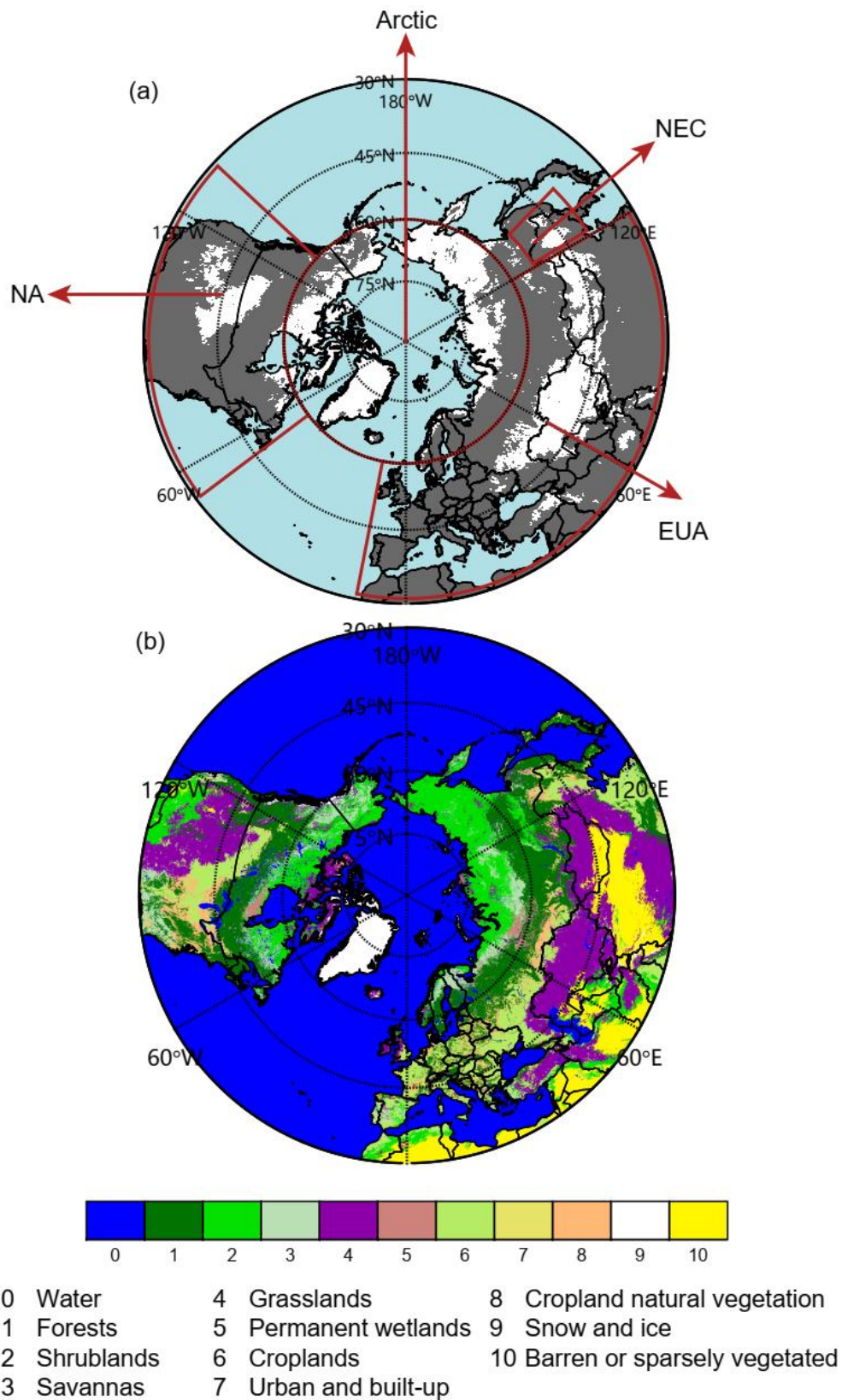


Figure 2. Workflow depicting the calculation and validation of radiative forcing of LAPs in snow: the blue boxes denote the external input data, while the orange boxes are used for calculations in this study.



- | | | |
|--------------|----------------------|---------------------------------|
| 0 Water | 4 Grasslands | 8 Cropland natural vegetation |
| 1 Forests | 5 Permanent wetlands | 9 Snow and ice |
| 2 Shrublands | 6 Croplands | 10 Barren or sparsely vegetated |
| 3 Savannas | 7 Urban and built-up | |



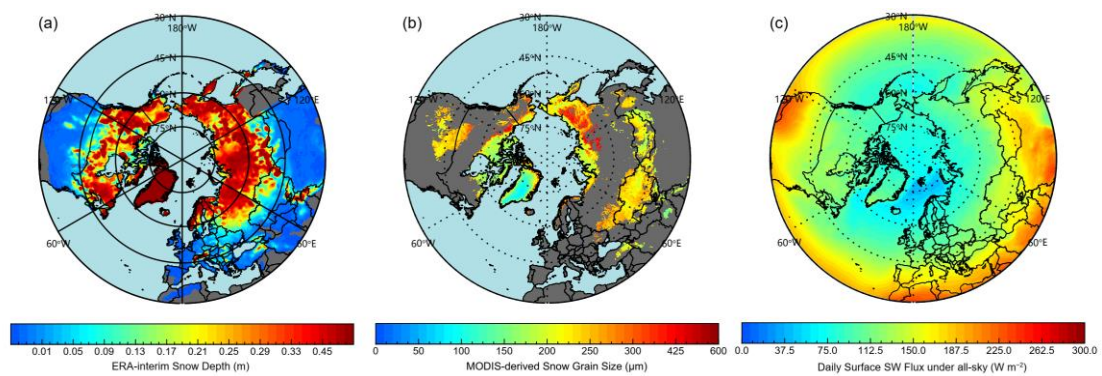
1

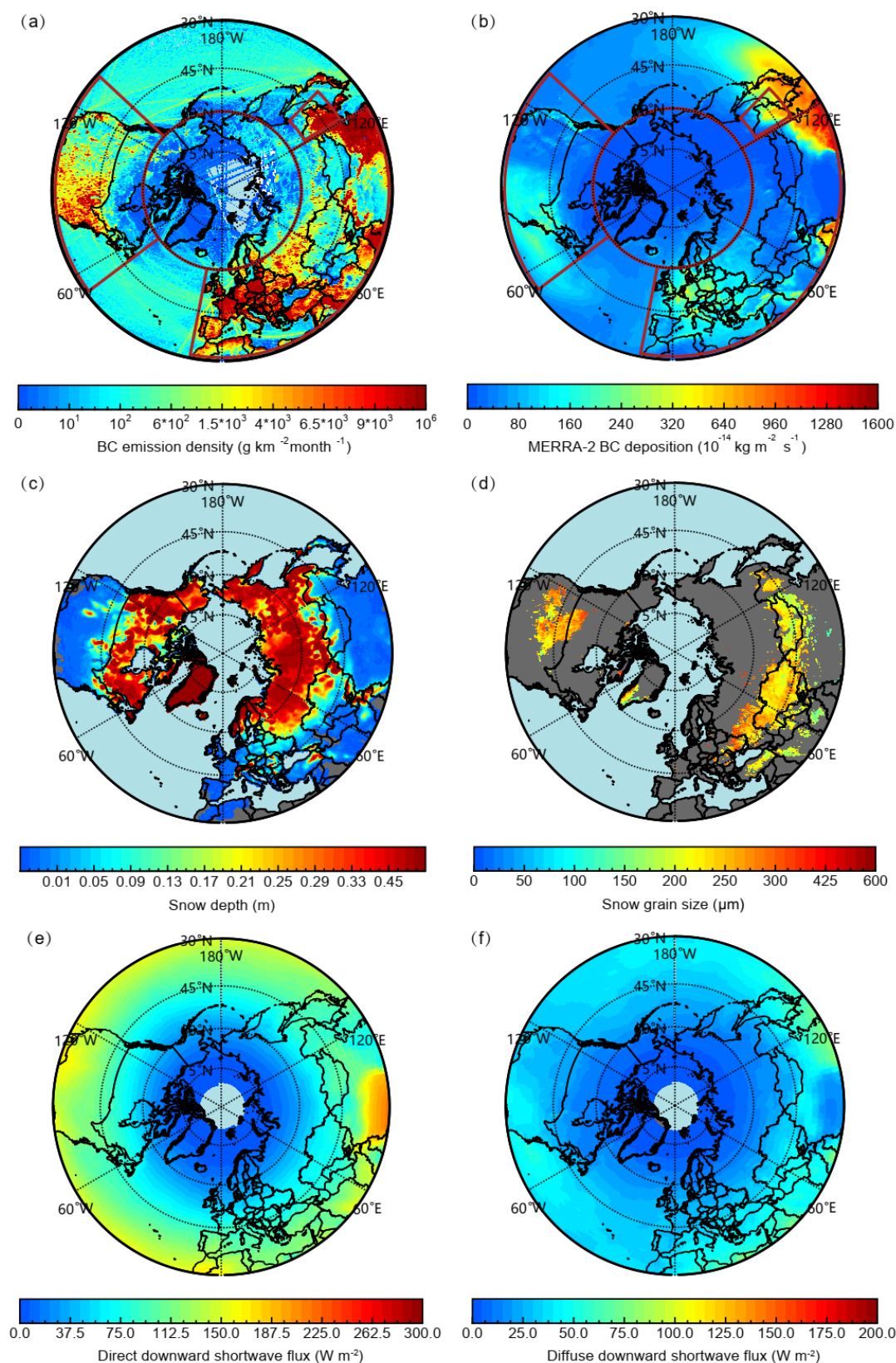
2 Figure 3. Spatial distributions of (a) identified snow-covered areas (ISCA) and (b) the different land-
 3 cover types, based on MODIS data, for the Northern Hemisphere. ISCA (white) can be separated

1 into northeastern China (NEC), Eurasia (EUA), North America (NA), and the Arctic. _____

1

2





1

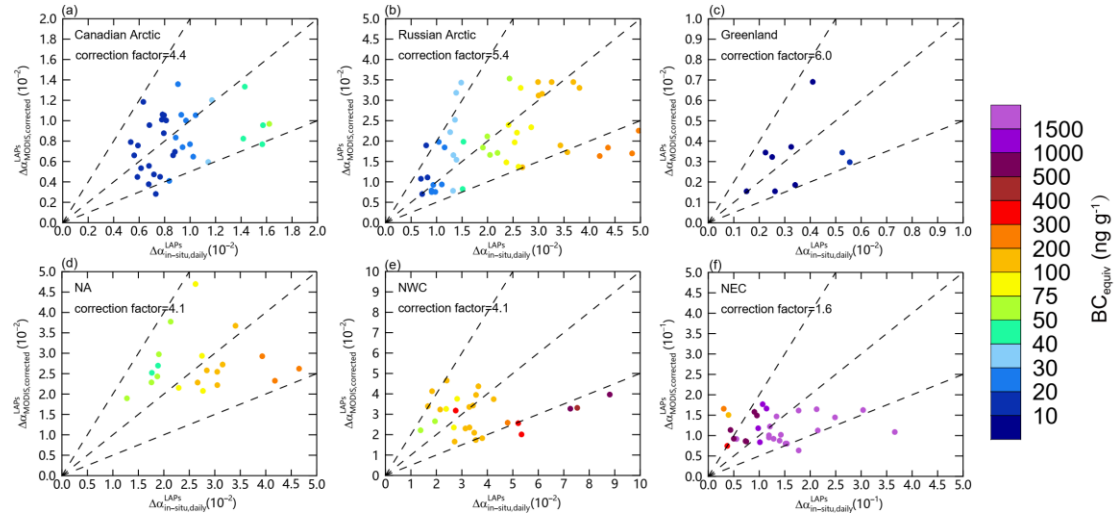
2 Figure 4. Spatial distributions of 2003-2018 averaged (a) ~~BC emissions density~~, (b) ~~BC deposition~~
 3 ~~from MERRA-2~~, (c) snow depth from ERA-interim, (d) snow grain size retrieved by MODIS, (e)

- 1 ~~direct and (fc) diffuse solar irradiance~~total downward shortwave flux at the surface ~~in~~during
- 2 ~~January-February-December-May~~ from CERES. _____

1 ~~BC emissions density is for the period 2003–2014 and employs data from the research group at~~
2 ~~Peking University, with additional data collected between 2003 and 2018.~~

3 _____

1



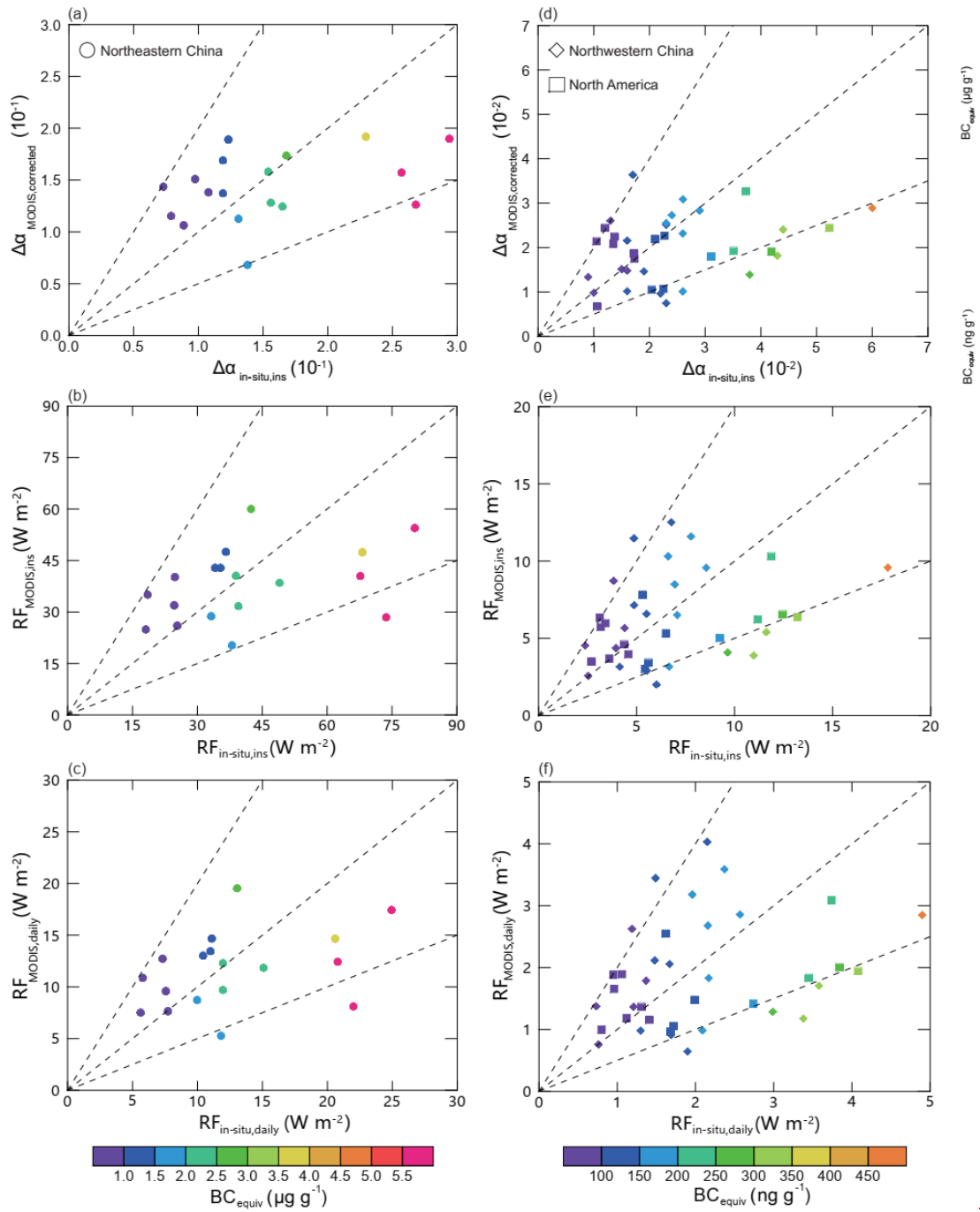
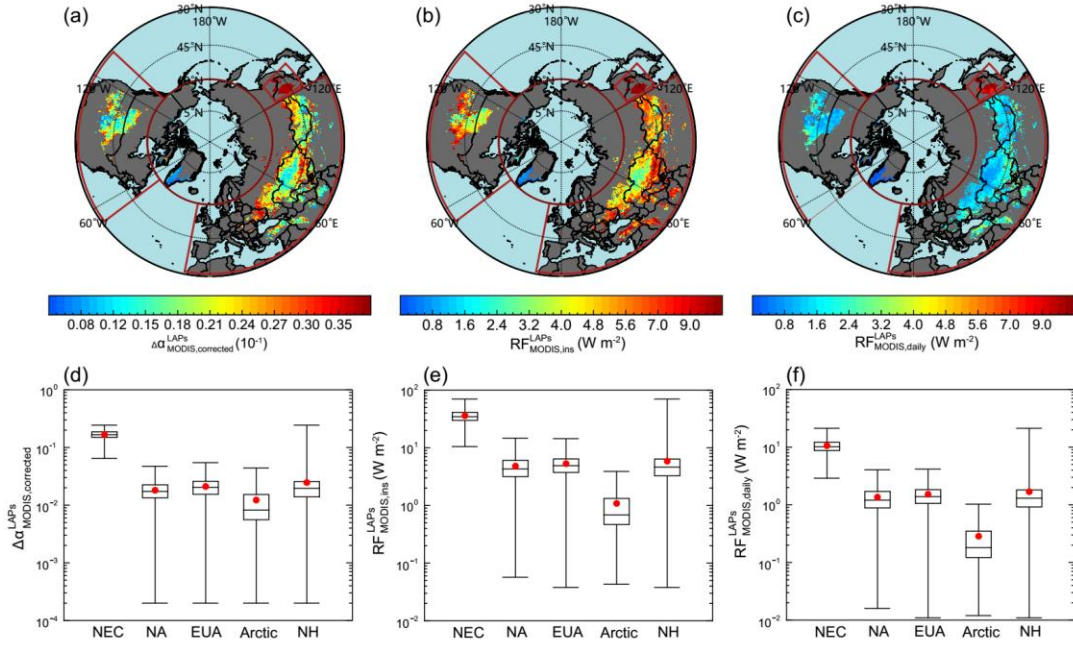
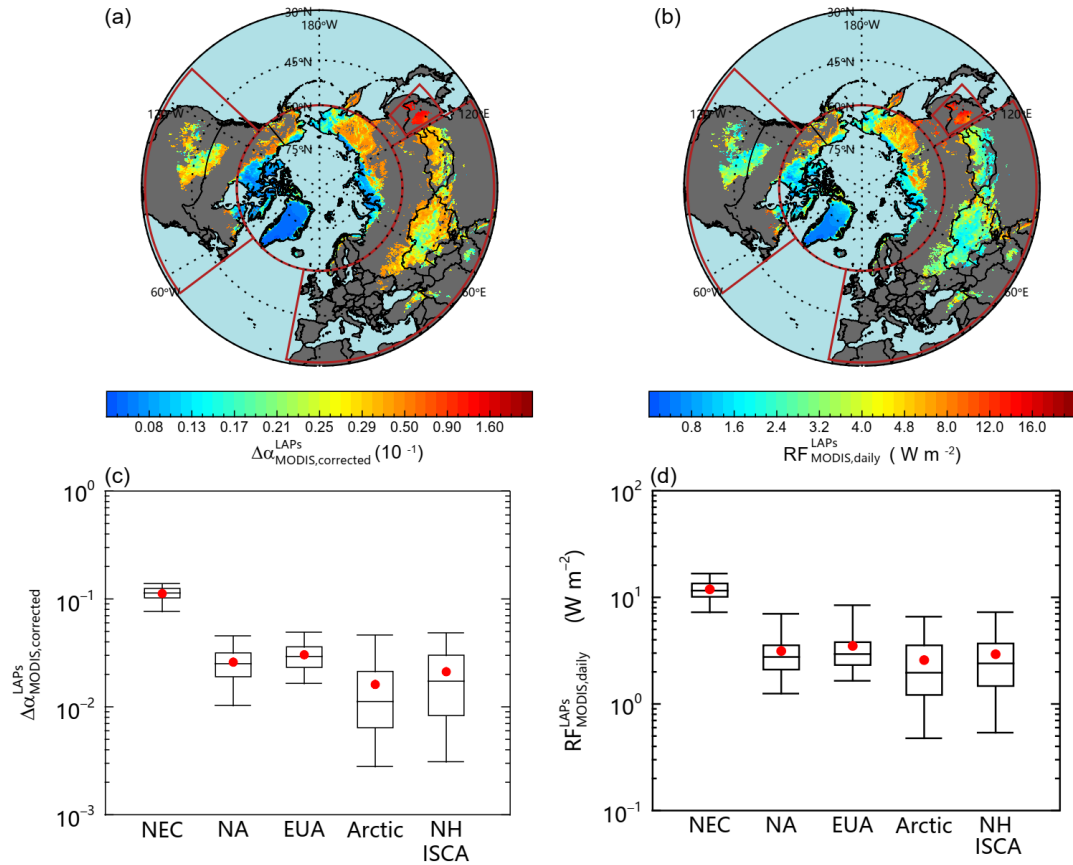


Figure 5. Scatterplots of (a) $\Delta\alpha_{MODIS,corrected}^{LAPs}$ versus $\Delta\alpha_{in-situ,ins}^{LAPs}$, (b) $RF_{MODIS,ins}$ versus $RF_{in-situ,ins}$, and (c) $RF_{MODIS,daily}$ versus $RF_{in-situ,daily}$ in heavily polluted regions. Panels (d)–(f) illustrate the same scatterplots as in (a)–(c) but for slightly polluted regions. Circles, diamonds, and squares represent the snow samples collected in Canadian Arctic, Russian Arctic, Greenland, NEC, NWC, and NA, respectively.

1



2

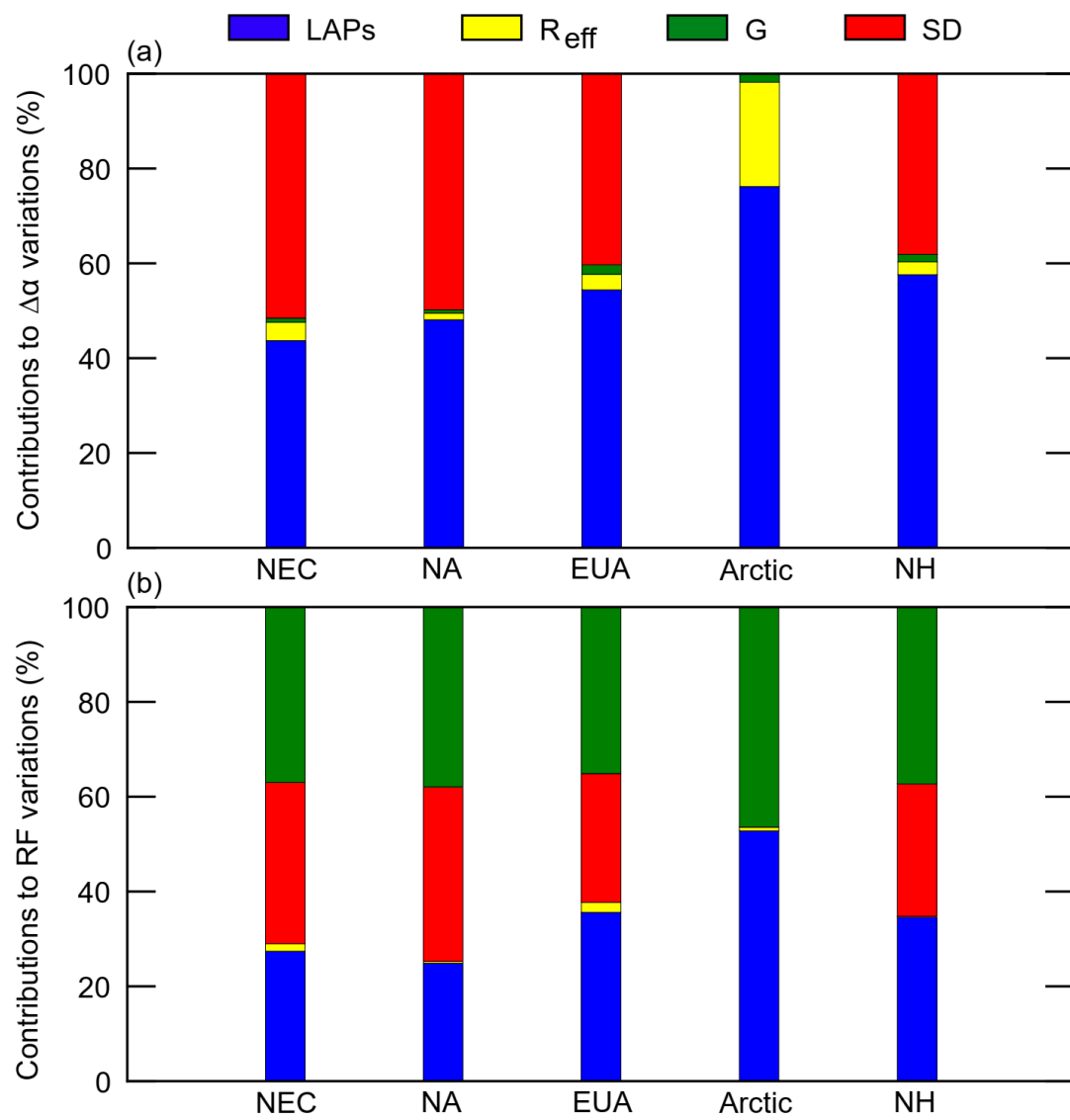


3

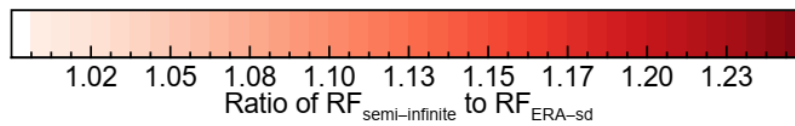
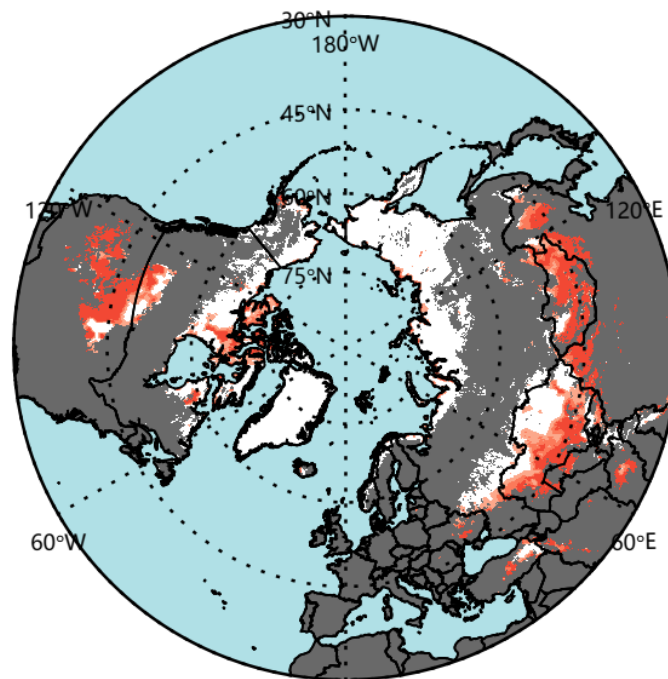
Figure 6. Spatial distributions of averaged (a) $\Delta\alpha_{MODIS,corrected}^{LAPS}$, (b) $RF_{MODIS,ins}^{LAPS}$, and (c) $RF_{MODIS,daily}^{LAPS}$ and statistics for regionally averaged (d) $\Delta\alpha_{MODIS,corrected}^{LAPS}$, (e) $RF_{MODIS,ins}^{LAPS}$ and (f) $RF_{MODIS,daily}^{LAPS}$.

1 for the Northern Hemisphere ISCA in ~~January-February~~December-May during the period 2003–
2 2018. The boxes denote the 25th and 75th quantiles, and the horizontal lines represent the 50th
3 quantiles (medians), the averages are shown as red dots; the whiskers denote the 5th and 95th
4 quantiles. _____

1



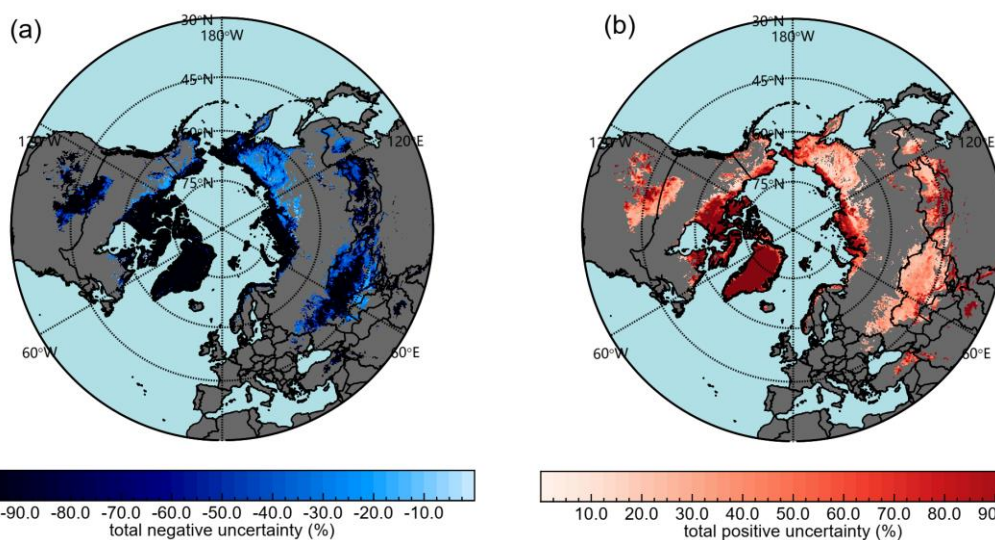
2



1

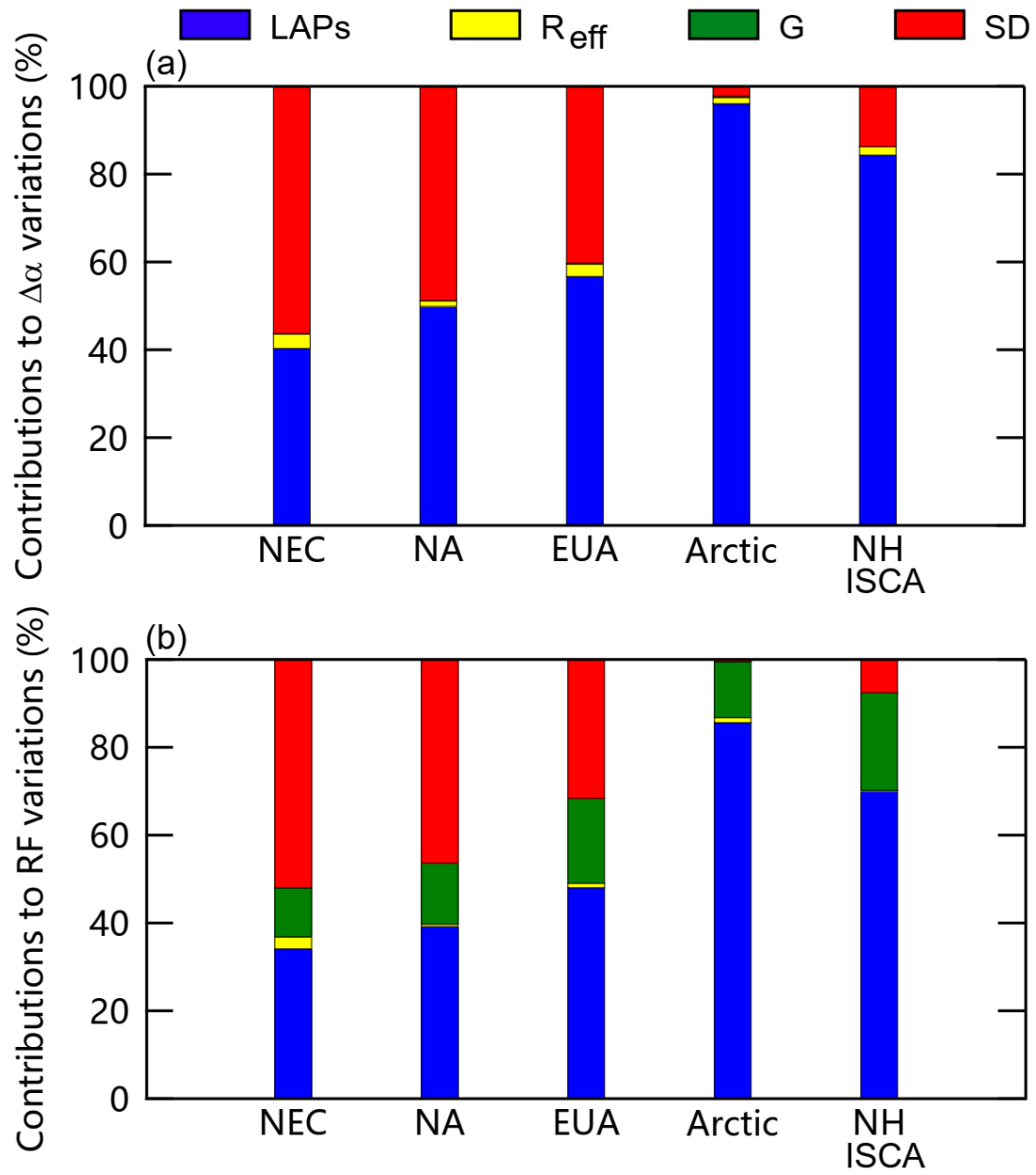
2 Figure 7. The spatial distribution of the ratio of retrieved radiative forcing using semi-infinite snow
 3 to radiative forcing using ERA-Interim snow depth.

1



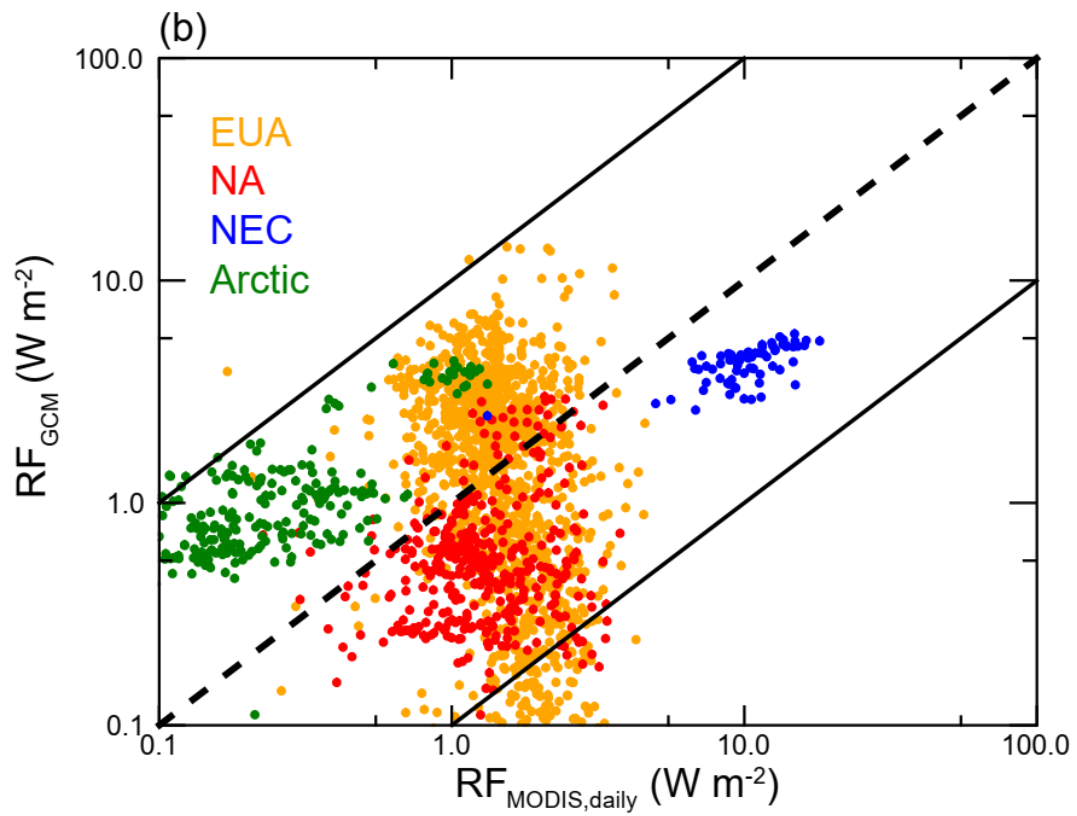
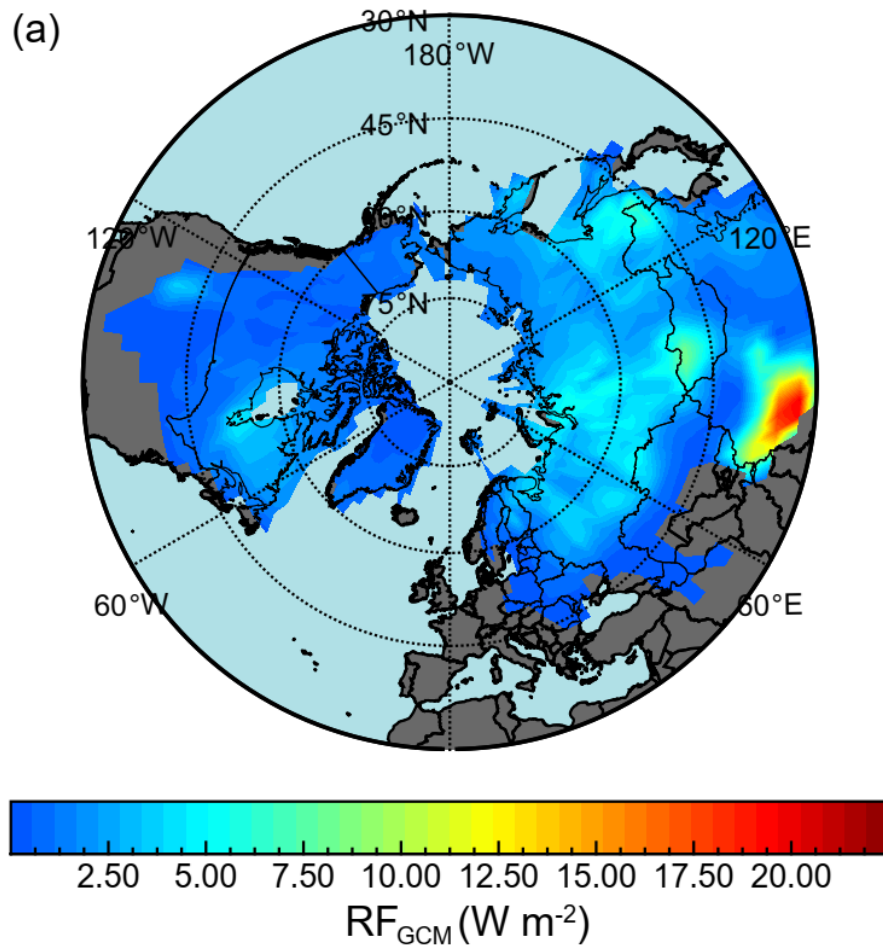
2

3 Figure 8. The overall uncertainty of radiative forcing retrieval due to ~~all about~~ atmospheric
 4 correction, MODIS-derived snow grain size retrieval and snow cover fraction calculation.



2

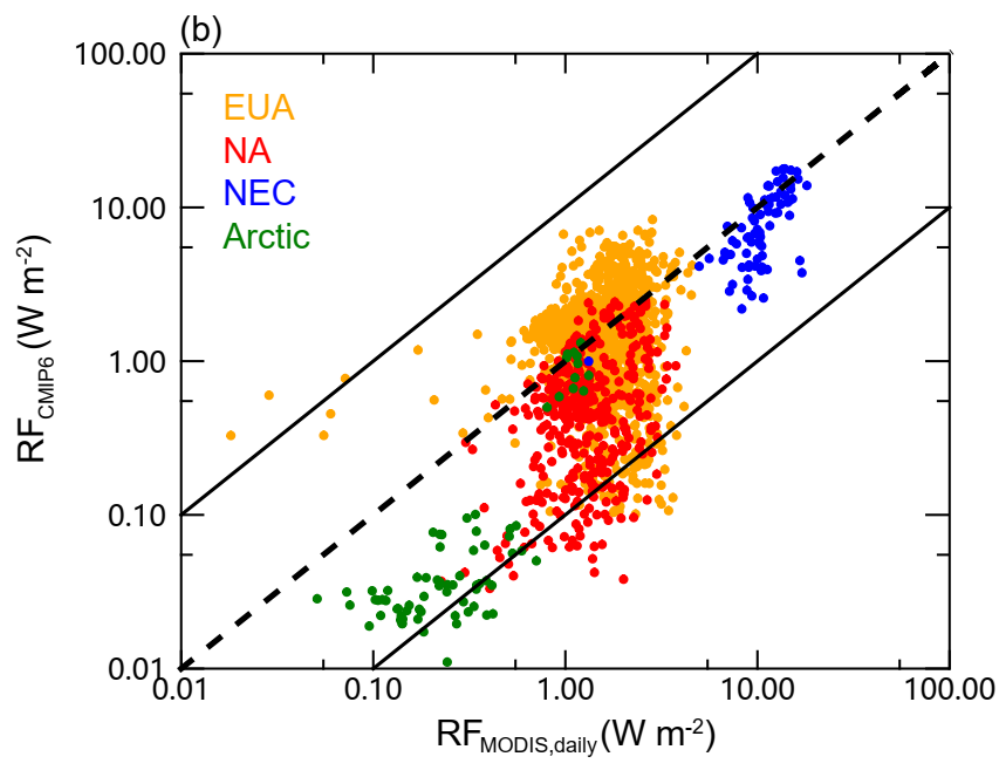
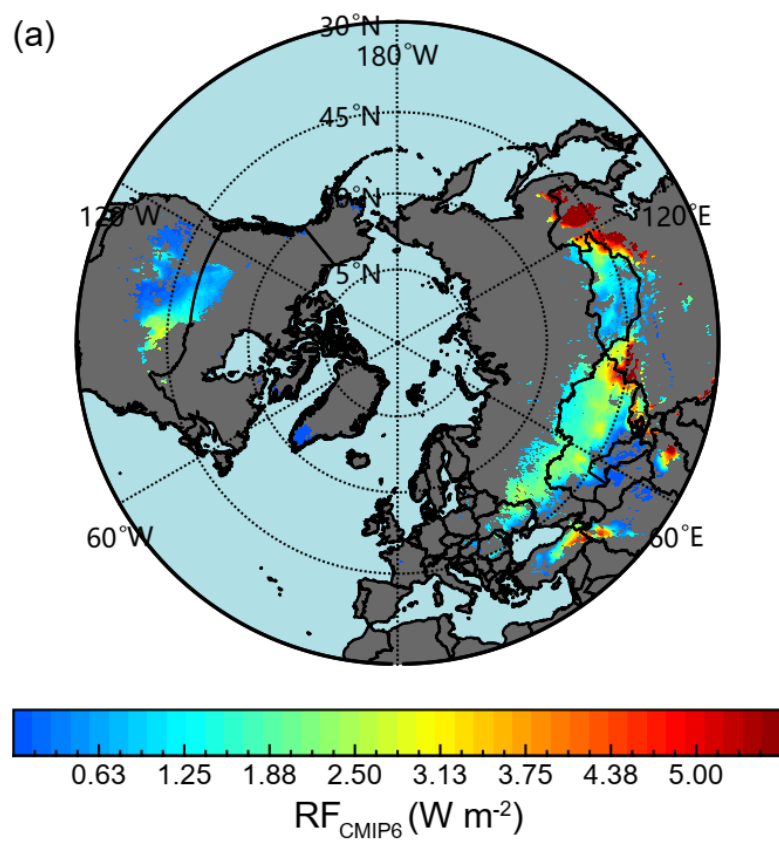
3 Figure 79. Fractional contributions of LAPs, snow grain size (R_{eff}), geographic factor (G), and
 4 snow depth (SD) to the spatial variations of (a) snow albedo reduction and (b) daily radiative forcing.



1 ~~Figure 8. Spatial distributions of (a) springtime radiative forcing (RF_{GCM}) due to LAPs in snow,~~
2 ~~derived from a GCM run by Flanner et al. (2007), and scatterplot of (b) $RF_{MODIS, daily}$ versus~~
3 ~~RF_{GCM} .~~

4 _____

1



2

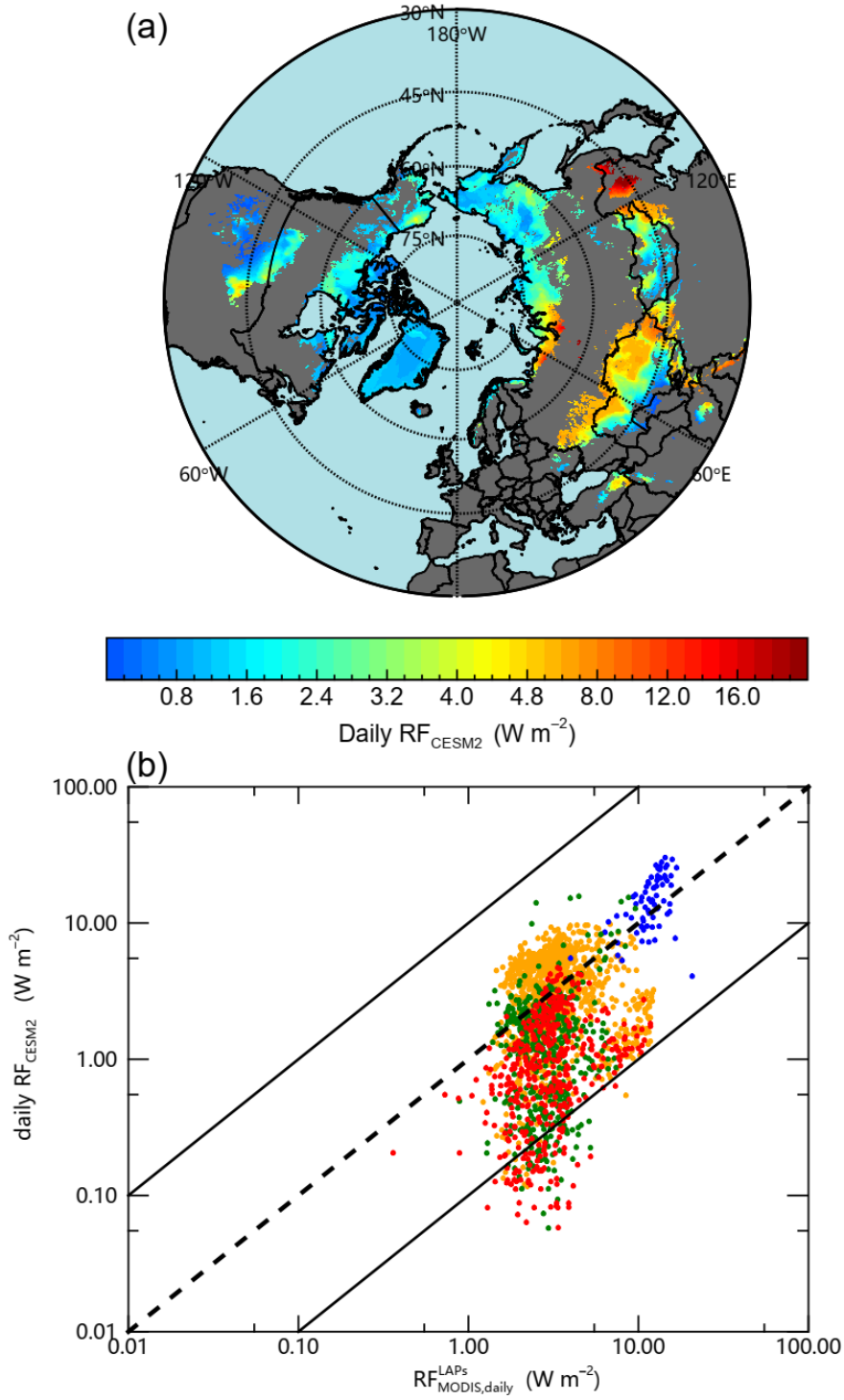


Figure 910. (a) Spatial distributions of average-daily radiative forcing ($RF_{\text{CMIP6CESM2}}$), based on the ~~CMIP6 ensemble average~~CESM2 soot content of snow in ~~January–February–December–May~~ for the period 2003–2014. (b) Scatterplot of $RF_{\text{MODIS,daily}}^{\text{LAPs}}$ versus $RF_{\text{CMIP6CESM2}}$.

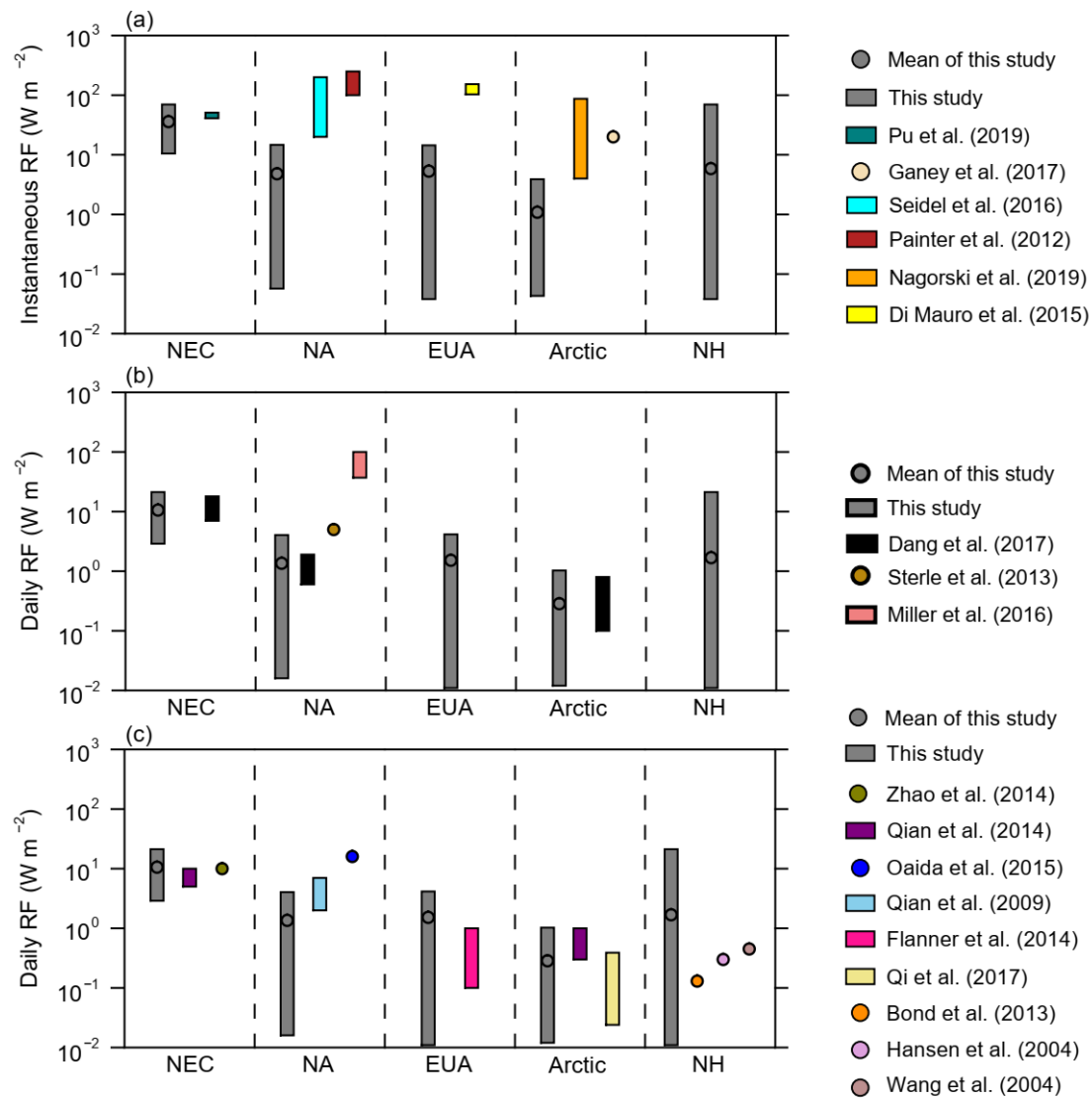
1 Table 1. Statistics for regionally averaged (5th and 95th quantiles) albedo reduction
 2 $(\Delta\alpha_{MODIS,corrected}^{LAPs})$ and daily radiative forcing ($RF_{MODIS,daily}^{LAPs}$, W m⁻²)

	<u>Northeastern China</u>	<u>EUA</u>	<u>NA</u>
<u>Albedo reduction ($\Delta\alpha_{MODIS,corrected}^{LAPs}$)</u>	<u>0.11 (0.077~0.14)</u>	<u>0.031 (0.017~0.049)</u>	<u>0.027 (0.014~0.04)</u>
<u>Daily radiative forcing ($RF_{MODIS,daily}^{LAPs}$, W m⁻²)</u>	<u>12 (7.2~17)</u>	<u>3.5 (1.6~8.4)</u>	<u>3.1 (1.3~7.0)</u>

3
4

- 1
- 2
- 3

1



2

3 **Figure 10** Table.2 Comparisons of radiative forcing due to LAPs in snow (this study) with
 4 observed and model-simulated values from previous studies.

Study	Region	Time period	Method	Radiative forcing (W m^{-2})
Miller et al. (2016)	San Juan Mountains	May, 2010	Remote sensing	~37-100
Sterle et al. (2013)	eastern Sierra Nevada	Feb to May, 2009	In-situ measurements	~2.5-40
Miller et al. (2016)	San Juan Mountains	May, 2010	In-situ measurements	35-86
Dang et al. (2017)	Northern China	Jan and Feb, 2010 and 2012	In-situ measurements	7-18

	<u>North America</u>	<u>Jan-Mar, 2013-2014</u>	<u>In-situ measurements</u>	<u>0.6–1.9</u>
	<u>The Arctic</u>	<u>Spring, 2005-2009</u>	<u>In-situ measurements</u>	<u>0.1–0.8</u>
<u>Hansen and Nazarenko (2004)</u>	<u>North Hemisphere</u>		<u>Model simulations</u>	<u>0.3</u>
<u>Qian et al. (2009)</u>	<u>western United States</u>	<u>Mar</u>	<u>Model simulations</u>	<u>~3-7</u>
<u>Bond et al. (2013)</u>	<u>Global</u>	<u>industrial era</u>	<u>Model simulations</u>	<u>0.13</u>
<u>Flanner et al. (2007)</u>	<u>Global</u>	<u>Annual 1998 (strong)</u>	<u>Model simulations</u>	<u>0.054</u>
		<u>Annual 2001(weak)</u>		<u>0.049</u>
<u>Qian et al. (2014)</u>	<u>Northeastern China</u>	<u>Apr</u>	<u>Model simulations</u>	<u>5-10</u>
	<u>North America</u>	<u>Apr</u>	<u>Model simulations</u>	<u>2-7</u>
	<u>The Arctic</u>	<u>Apr</u>	<u>Model simulations</u>	<u><0.3</u>
<u>Zhao et al. (2014)</u>	<u>Northeastern China</u>	<u>Jan and Feb, 2010</u>	<u>Model simulations</u>	<u>10</u>
<u>Oaida et al. (2015)</u>	<u>western US</u>	<u>Spring, 2009-2013</u>	<u>Model simulations</u>	<u>16</u>
<u>Qi et al. (2017)</u>	<u>The Arctic</u>	<u>Apr, 2008</u>	<u>Model simulations</u>	<u>0.024-0.39</u>
<u>This study</u>	<u>Northeastern China</u>	<u>Dec-May, 2003-2018</u>	<u>Remote sensing</u>	<u>12</u>
	<u>NA</u>			<u>3.1</u>
	<u>Canadian Arctic</u>			<u>2.6</u>
	<u>Russian Arctic</u>			<u>3.3</u>
	<u>Greenland</u>			<u>1.3</u>
	<u>EUA</u>			<u>3.5</u>

1

2

3

4

5

6

7

1

2